ISSN 1916-9698 (Print)
ISSN 1916-9701 (Online)

INTERNATIONAL JOURNAL OF CHEMISTRY

Vol. 6, No. 4 November 2014

CANADIAN CENTER OF SCIENCE AND EDUCATION

Editorial Board

Contents

International Journal of Chemistry; Vol. 6, No. 4; 2014
ISSN 1916-9698 E-ISSN 1916-9701
Published by Canadian Center of Science and Education

Characterization of Tar From Wood Pellet Production

Gurkaran S. Sarohia[1], Harpuneet S. Ghuman[1], Adrian K. James[1], Ronald W. Thring[1] & Guy L. Plourde[2]

[1] Department of Environmental Science and Engineering, University of Northern British Columbia, Prince George, British Columbia, Canada

[2] Department of Chemistry, University of Northern British Columbia, Prince George, British Columbia, Canada

Correspondence: Ronald W. Thring, Department of Environmental Science and Engineering, University of Northern British Columbia, Prince George, British Columbia, Canada. Tel: 1-250-960-5804. E-mail: thring@unbc.ca

Received: July 10, 2014 Accepted: August 8, 2014 Online Published: August 26, 2014

doi:10.5539/ijc.v6n4p1 URL: http://dx.doi.org/10.5539/ijc.v6n4p1

Abstract

In recent years, there has been an increased shift towards using renewable biomass as a source of energy generation. Wood pellets are widely used for energy production and are manufactured by densifying wood into pellets for increased energy efficiency. The manufacturing process of these pellets typically generates a tar-like byproduct resulting in increased production costs associated with waste disposal, equipment clean-up and handling operations. The current study focuses on characterization of this wood-based tar, which can create significant technological problems and environmental hazards. The tar was characterized by gas chromatography-mass spectrometry (GC-MS), thermogravimetric analysis (TGA), ^{1}H nuclear magnetic resonance spectroscopy (^{1}H-NMR), infrared spectroscopy (IR), solubility and moisture content. A total of 29 compounds were identified.

Keywords: wood, pellets, tar, distillation, gas chromatography, mass spectrometry, resin acids

1. Introduction

The generation of waste products by agricultural, industrial, commercial and domestic activities, make waste by-products an inevitable part of life. Due to an increase in environmental and sustainability issues, the treatment of such wastes is becoming of increasing importance. Today, recycling of waste by-products is preferred over their disposal due to the issues pertaining to landfills, water management and air quality. A report published by Environment Canada in 1991 stated that 30 million tons of solid waste were produced annually (Crowe & Ptacek, 2008). This waste has an enormous impact on water systems and therefore disposal has to be carefully monitored (Crowe & Ptacek, 2008). For these reasons, new methods of recycling and disposal need to be explored.

One such category of waste produced in significant quantity is wood tars. These tars are usually dark, thick flammable liquids that consist of a mixture of hydrocarbons, alcohols and other organic compounds (Milne, Evans, & Abatzoglou, 1998). Wood tars can cause many industrial problems such as blockages in engines, turbines and pipelines, causing machine failures and damaging engines (Hosoya, Kawamoto, & Saka, 2008; Devi, Ptasinski, & Janssen, 2003). Wood tars are produced in a variety of industrial processes and their compositions vary depending on the type of process, temperature of maturation and other factors (Blanco, Wu, Onwudili, & Williams, 2012).

Pellet production is a process that leads to the formation of wood tars. With the growing need for renewable fuels the demand for wood pellets is rapidly increasing across the world (Envirochem services INC., 2010). Furthermore, this growing demand has led to the construction of wood pellet plants in residue rich countries such as Canada (Scott, 2009). With the large forestry resource available in British Columbia, the province has seen rapid expansion in pellet manufacturing plants (Scott, 2009).

The wood pellets are made of waste material from lumber and sawmills. The production of wood pellets is composed of 5 stages: drying, milling, pressing, cooling and screening (Envirochem services INC., 2010; Scott, 2009). In the initial drying stage the wood chips which are high in moisture content (50-65%) need to be dried in order to reduce machine wear (Scott, 2009). This is normally done with rotary dryers using either a single-pass or multiple-pass technique (Envirochem services INC., 2010). During the drying stage volatile organic

compounds as well as condensable particulate matter (CPM) are often produced (Envirochem services INC., 2010). These CPM fractions which include sticky tars can cause machine failures by sticking to filters and blocking machinery (Envirochem Services Inc., 2010). In order to deal with the potential environmental and clean-up problems associated with the tar produced, knowledge of its physical and chemical characteristics is necessary. Furthermore, characterization of the tar might be useful in identifying economically beneficial chemicals such as poly aromatic hydrocarbons (PAH's), resin acids or other oxygenated compounds.

The present article describes the structural and chemical characterization of a by-product tar, produced at a pellet plant located in Northern British Columbia, Canada. Short path vacuum distillation was used to fractionate the tar into various fractions based on boiling points. Analytical techniques such as moisture analysis, gas chromatography-mass spectrometry (GC-MS), thermogravimetric analysis (TGA), infrared spectroscopy (IR) and proton nuclear magnetic resonance (^{1}H-NMR) were used in our analysis of the by-product tar.

2. Methods

2.1 Samples

The AR tar (as received tar) used for this study was obtained from the Pinnacle Pellet plant located near Quesnel, British Columbia, Canada. This plant produces pellets using sawdust obtained from coniferous wood sources. The AR tar was obtained from the condensate produced during the drying stage. The sample was collected in a plastic container which was stored in the dark at room temperature.

2.1.1 Fractionating Method

Short path distillation was used to thermally separate the compounds present based on their boiling points and was carried out under vacuum (Hickman, 1944). The low pressure used decreases the atmospheric boiling points of the compounds and forces them to distill at lower temperatures which help in the collection of heat sensitive as well as high boiling compounds.

The AR tar was stirred to ensure homogeneity and a sample (15.76 g) was distilled under vacuum (10^{-1} torr) in a Kugelrohr distillation apparatus purchased from Sigma Aldrich. The fractions were collected at 75 ^{o}C, 100 ^{o}C, 125 ^{o}C, 150 ^{o}C, 175 ^{o}C, 230 ^{o}C, > 230 ^{o}C and were labeled A, B, C, D, E, F, G respectively. After the specific temperature was reached, the temperature was held constant for a period of 30 minutes.

2.2 Analytical Techniques

The following techniques were used to identify the components from the fractionated tar samples: gas chromatography-mass spectrometry (GC-MS), thermogravimetric analysis (TGA), proton nuclear magnetic resonance spectroscopy (^{1}H-NMR), infrared spectroscopy (IR), solubility and moisture content.

2.2.1 Moisture Content Analysis

Approximately 1 g of AR tar was heated at 105 ^{o}C for a period of 72 hours. The moisture content was determined by difference of the initial and final weights. The analysis was repeated three times and the average is reported. This analysis assumes that only water escapes at this temperature and does not correct the data for potential mass changes due to volatile material.

2.2.2 Solubility

Approximately 5 g of the AR tar and 10 mL of the solvent being used for the analysis were placed in a pre-weighed 25 mL vial. The vial was set to shake at 300 rpm at a constant temperature of 25 ^{o}C. After 1 hour, the solvent was decanted and filtered through a Whatman 2 filter paper (55 mm, qualitative). The vial and the filter paper were air dried at room temperature for 72 hours. The solubility was measured by difference of the initial and final tar weights that was left on the filter paper and vial.

2.2.3 Thermogravimetric Analysis (TGA)

The thermal characteristics were determined using a TGA-50/50H Shimadzu thermogravimetric analyzer. The analyses were conducted using air at a flow rate of 50 mL/min, under atmospheric conditions. For each test, approximately 10 mg of the sample was heated from room temperature to 800 ^{o}C with a heating rate of 10 ^{o}C/min. The thermogravimetric (TGA) plot describes the weight loss of the sample with increasing temperature while the differential thermogravimetric (DTG) plot illustrates the derivative of the sample mass with time at a specific temperature.

2.2.4 Gas Chromatography-Mass Spectrometry (GC-MS)

The GC-MS instrumentation consisted of a Varian gas chromatograph equipped with a Saturn 2200 mass spectrometer. The separations were performed on a capillary column (30 m × 0.25 mm i.d., 0.25 micrometer;

Varian). The oven temperature was programmed from 50 to 100 °C at 15 °C/min and from 100 to 300 °C at 10 °C/min and finally held at 300 °C for 17 minutes. Splitless injections of 1 μL were performed at 300 °C with an autosampler (Varian). The mass spectrometer was operated in electron impact (EI) mode with a 40-650 m/z range.

2.2.5 Nuclear Magnetic Resonance Spectroscopy (^{1}H-NMR)

The tar samples were also analyzed by proton nuclear magnetic resonance spectroscopy to determine the presence of potential functional groups. The ^{1}H-NMR analysis was performed using a Bruker 300 Fourier NMR spectrometer (300 MHz). The samples were dissolved in deuterated chloroform ($CDCl_3$).

2.2.6 Fourier Transform Infrared Spectroscopy (FTIR)

The FTIR analysis was performed using a Perkin Elmer 2000 system to confirm the potential functional groups. The FTIR spectra were recorded within the region 4000 to 650 cm^{-1}. Spectra were recorded neat by placing each sample between 2 sodium chloride (NaCl) discs.

3. Results and Discussion

Identification of the compounds present in tars is usually achieved by GC-MS (Blanco et al., 2012; Jiang, Q. Wang, Y. Wang, Tong, & Xiao, 2007). Apart from GC-MS other techniques such as TGA and ^{1}H-NMR can also be used to complement GC-MS data. However, since these analytical techniques require that the samples be dissolved in a solvent, a solubility test using the following common solvents (pentane, toluene, methanol, ethanol, acetone, water) was performed. This solubility test demonstrated that the AR tar sample was not fully soluble in any of the solvents tested (see Table 1). Therefore, it was deemed necessary to carry out a fractionation of the AR tar in order to obtain material which would dissolve in common solvents.

3.1 Solubility

Table 1 shows the solubility of AR tar in each solvent. The solvents are listed in increasing order of polarity (Murov, 2014). Tar was found to be most soluble in acetone (0.412 g/mL) and least soluble in water (0.007 g/mL). The solubility of tar was comparable in toluene (0.296 g/mL) and ethanol (0.293 g/mL) whereas, tar was slightly less soluble in pentane (0.211 g/mL) and methanol (0.193 g/mL). With the buildup of tar in pellet producing machinery, the cleanup and removal of such waste is imperative. Based on the relatively low cost (Table 1) and low toxicity, ethanol may be a suitable solvent for cleanup at the pellet plant (NAFAA, 2001).

Table 1. The solubility analysis of AR tar in various solvents

Solvent	Solubility (g/mL)	Boiling Point (^{o}C)	Bulk cost of solvent ($/L) (ICIS 2013)
Pentane	0.211	36.1	-
Toluene	0.296	110.6	0.74-1.05
Methanol	0.193	64.7	0.25-0.67
Ethanol	0.293	78.4	0.56-1.03
Acetone	0.412	56.0	1.03-1.81
Water	0.00721	100.0	-

3.2 Moisture Analysis and Distillation

Short path distillation was used to fractionate the AR tar. Short path distillation thermally separates the compounds present based on their boiling points at low pressure (Hickman, 1994). Table 2 shows the wt % of the tar fractions obtained from distillation. The first four fractions (A-D) with boiling point up to 150 ^{o}C were considered to contain the volatile material. As seen in Table 2, the first fraction collected at 75 ^{o}C (fraction A) only represented < 1 % by weight of the AR tar, while fractions B (100 ^{o}C) and C (125 ^{o}C) consisted of ~ 6 % and ~ 12 %, respectively. The highest amounts of volatiles were obtained in Fraction D (150 ^{o}C) accounting for ~ 17 % of the sample weight. The higher boiling fractions E and F were darker in color and appeared to be more viscous. The last fraction collected at 230 ^{o}C accounted for ~ 10 % of the sample weight, leaving a char-like black solid behind. This solid contributed ~ 30 % to the overall weight of the sample. The unrecovered sample mass contributed ~ 19 % of the sample weight and could have been due to the presence of water and very

volatile compounds that did not condense in the distillation process.

Table 2. Recovered mass of various distillate fractions of wood tar[1]

Fraction[2]	Mass (g)	Yield (wt % of AR tar)	Physical observation
A	0.100	0.64	Yellow Liquid
B	0.871	5.56	Viscous yellow liquid
C	1.823	11.63	Yellow semi solid
D	2.643	16.86	Brown semi solid
E	0.900	5.74	Brown semi solid
F	1.570	10.02	Brown semi solid
G	4.708	30.03	Black char-like solid

[1]15.76 g of AR tar was used; [2] temperature range per fraction: A: up to 75 ^{o}C, B: 76-100 ^{o}C, C: 101-125 ^{o}C, D: 126-150 ^{o}C, E: 151-175 ^{o}C, F: 176-230 ^{o}C, G: > 230 ^{o}C.

3.3 Gas Chromatography-Mass Spectrometry (GC-MS)

Figure 1 shows gas chromatographs of the various fractions obtained after short path distillation of AR tar. As can be seen in Figure 1, many peaks overlap across the various fractions indicating that the short path distillation was unable to completely isolate the compounds into specific fractions. Tar, being a wood residue, potentially contains a large variety of compounds making it difficult to completely separate them into fractions based on boiling point alone. Therefore, simple distillation techniques do not appear to be able to completely fractionate compounds without overlaps. However, Figure 1 suggests that the fractionating technique used was able to provide for a small segregation between volatile and semi-volatile material since most compounds present in the low boiling fractions (A-D) are not found in the higher boiling fractions (E and F).

Table 3 shows the possible components present in each fraction of the tar. By correlating the GC-MS data to the NIST database (National Institute of Standards and Technology) a total of 29 compounds were identified. Low boiling point fractions A and B contained 15 out of the total 29 compounds identified. The compounds of these two fractions were mostly aldehydes, ketones, alkenes and aromatic in nature. Similar compounds were also identified to populate fraction C. Furthermore, fraction C (125 ^{o}C) appears to be the threshold point in the distillation process. Most compounds in the higher boiling fractions (D-F) are not found in the lower boiling fractions (A-B). The higher boiling fractions (D, E, and F) were composed mainly of carboxylic acids and were especially concentrated in resin acids such as abietic acid, palusteric acid, and pimaric acid. These resin acids are a complex mixture that mainly contains monocarboxylic acids of alkylated hydrophenanthrene structures (Hudy, 1959). Further isolation of the specific acids such as Abietic acid has been discussed in previous studies (Harris & Sanderson, 1948) since such resin acids could cause a problem in disposal of tar due to their toxicity to fish and microorganisms (Wang, Chen, Gao, Breuil, & Hiratsuka, 1995; Peng & Roberts, 2000; Villeneuve, Yagminas, Marino, & Becking, 1977).

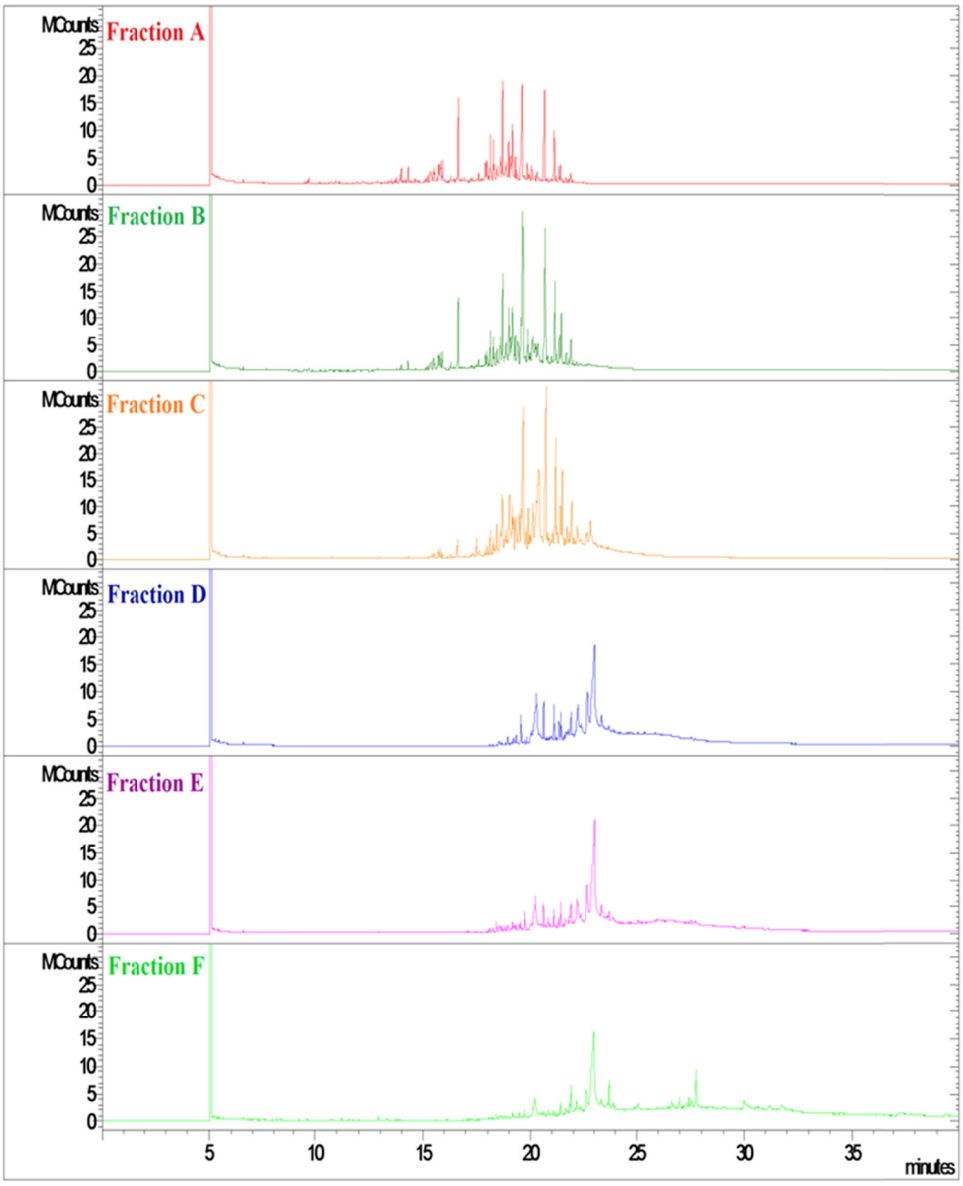

Figure 1. Gas chromatographs of various distillate fractions of wood tar

Table 3. Major components of various wood tar fractions identified using the NIST GC-MS library

Peak no.	Retention Time (min)	MW (g/mol)	Possible component	A	B	C	D	E	F
1	15.86	494	4-Norcaren-2-one,1,3,5-tri-tert-butyl-3-(3,5-di-tert-butyl-4-h	*					
2	15.944	234	1-Tetralone, 8-trimethylsilyloxy-	*					
3	16.665	219	2-Phenyl-6-vinylindolizine	*	*				
4	16.665	219	Androst-2,16-diene	*	*				
5	18.733	272	Naphthalene,decahydro-1,1,4a-trimethyl-6-methylene-5-(3-methyl	*	*	*			
6	18.878	410	6-Methyl-11,12-dioxatricyclo[7.2.1.0(1,6)]dodecan-5-ol-8-carbox		*				

7	18.99	266	1-Cyclohexene-1-carboxylic acid, 4-(1,5-dimethyl-3-oxohexyl)-,	*	*	*				
8	19.02	207	4-(Diethylaminomethyl)-2,5-dimethylphenol		*					
9	19.045	293	Benzothiazole, 2-(2,6-dimethyl-1-morpholyl)-6-nitro-			*				
10	19.077	290	1H-Naphtho[2,1-b]pyran, 3-ethenyldodecahydro-3,4a,7,7,10a-penta	*	*					
11	19.152	272	Phenanthrene, 7-ethenyl-1,2,3,4,4a,4b,5,6,7,9,10,10a-dodecahydro	*	*	*				
12	19.209	506	Olean-12-ene-3,16,21,22,23,28-hexol, (3.beta.,4.beta.,16.alpha)			*				
13	19.306	290	1H-Naphtho[2,1-b]pyran, 3-ethenyldodecahydro-3,4a,7,7,10a-penta	*	*	*				
14	19.62	290	1-Naphthalenepropanol, .alpha.-ethenyldecahydro-.alpha.,5,5,8a-	*	*	*	*			
15	19.466	282	1,2,3-Benzenetricarboxylic acid, 4-hydroxy-5-methyl-, trimethyl			*				
16	19.79	299	10-Formamido-10,11-dihydro-2,3-dimethoxydibenz (b,f)oxepin			*				
17	19.87	292	5.alpha.-Androstane, 1,3-dihydroxy-, (1.alpha.,3.alpha.)-		*	*				
18	20.095	398	28-Nor-17.alpha.(H)-hopane			*				
19	20.284	562	Oleic acid, eicosyl ester			*	*	*	*	
20	20.656	286	1-Phenanthrenecarboxaldehyde, 7-ethenyl-1,2,3,4,4a,4b,5,6,7,9,10	*	*	*	*			
21	21.032	288	Podocarp-7-en-3.beta.-ol, 13.beta.-methyl-13-vinyl-			*				
22	21.166	286	Retinol			*				
23	21.471	288	19-Hydroxy-3alpha,5-cyclo-5alpha-androstan-17-one			*				
24	22.186	302	Pimaric acid			*	*	*		
25	22.696	302	Paulstric acid				*	*	*	
26	22.873	300	1-Phenanthrenecarboxylic acid, 1,2,3,4,4a,9,10,10a-octahydro-1			*	*	*	*	
27	23.374	302	Abietic acid				*	*		
28	23.726	328	7-Oxodehydroabietic acid, methyl ester						*	
29	27.755	456	beta.-Sitosterol acetate						*	

3.4 Thermogravimetric Analysis (TGA)

Figure 2 and Table 4 show the thermal degradation of the tar in air at a constant heating rate. The derivative thermogravimetric analysis (drTGA) curve (Figure 2) shows three major mass losses that occur within the ranges 200-300 ^{o}C, 300-420 ^{o}C and 420-500 ^{o}C. The first volatile release occurs at 200-300 ^{o}C and the second volatile release occurs between 300-420 ^{o}C. The weight loss at temperature 200-300 ^{o}C was ~ 28 % while ~ 31 % weight loss was observed at temperature 300-420 ^{o}C. The final weight loss is observed at temperature of 420 ^{o}C and above contributing to ~ 35 %. The weight losses for temperatures over 380 ^{o}C contributed to ~ 47 % of the total weight. This weight loss can be attributed to some resin acids and char. This conclusion is based on the fact that the AR tar main wood source was coniferous in nature and other studies have reported the presence of resin acids in coniferous plants (Funk & Croteau, 1994). Furthermore, the boiling point of the resin acids is usually greater than 400 ^{o}C at atmospheric pressure and as such major mass loss after 400 ^{o}C can be attributed to the resin acids (CRC Handbook of Chemistry and Physics 2012-2013). As seen from Table 3 the GC-MS data also verifies the

presence of resin acids in the higher boiling tar fractions. These compounds are of wood origin, and have a high probability of being present in the tar, which is a by-product of a wood pellet manufacturing operation. Furthrmore, previous studies indicate that the char oxidation occurs at ~ 400 °C in lignocellulosic samples (Elder, Kush, & Hermann, 2011; Blasi, 2009). This indicates that char might be present in the sample. The residual black mass observed during distillation might be attributed to char.

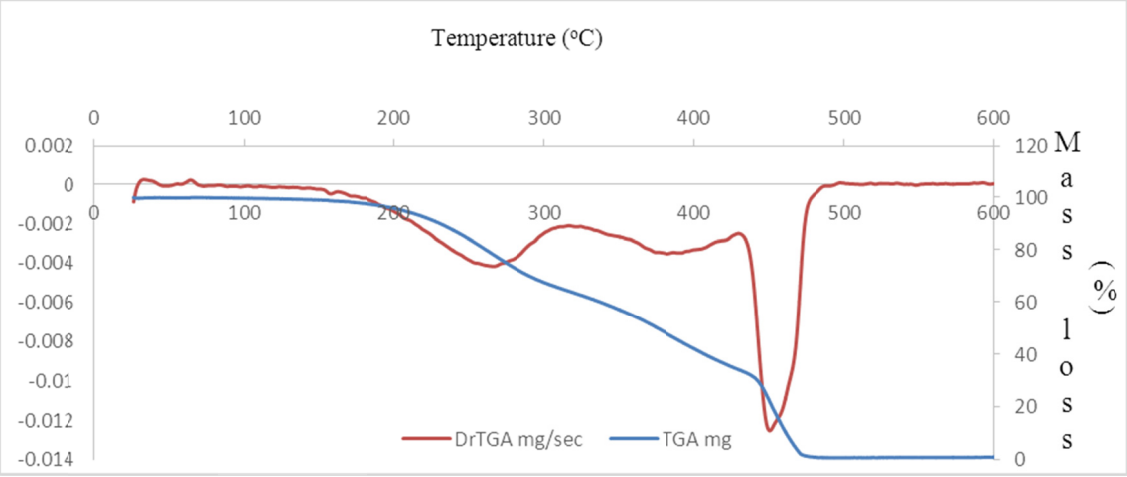

Figure 2. Thermogravimetric analysis curve with the derivative TGA of the wood tar

Table 4. Weight losses of the AR tar analyzed through thermogravimetric analysis.

Temperature (°C)	Wt loss (%)
<200	4.22
200-250	11.79
250-300	16.61
300-350	10.50
350-400	14.79
400-450	19.62
450-500	21.74

3.5 Nuclear Magnetic Resonance Spectroscopy (^{1}H-NMR)

The solution state ^{1}H-NMR spectrum of each distillate fraction (A-F) was obtained in 1 mL deuterated chloroform. The overlaid ^{1}H-NMR spectra of each distillate fraction are presented in Figure 3. The NMR spectra can be divided into 6 parts to identify the potential functional groups: aldehyde functional groups (10-9 ppm), aromatics (9-6.5 ppm), phenolics (6.5-5.5 ppm), olefinic (5.5-4.5 ppm), benzylic (4.5-3.3 ppm) and aliphatic (3.3-0.0 ppm). The listed NMR spectra were obtained from 0-10 ppm. As can been seen from Figure 3, the aldehyde proton (10-9 ppm) disappeared in the higher boiling fractions D, E and F, indicating that there were very few compounds containing the aldehyde functional group present in the higher boiling fractions. GC-MS and TGA showed that the higher boiling fractions were mostly composed of resin acids. Resin acids do not have any aldehyde functional groups present in their structures and only contain carboxylic acid protons (Fieser & Campbell, 1938; Morales, Birkholz, & Hrudy, 1992). Therefore, the NMR spectra agree with the data obtained from GC-MS and TGA. The NMR analysis also suggests the presence of more benzylic protons (4.5-3.3 ppm) in the lower boiling fractions (A-C) than in the high boiling ones (D-F). Once again this is also in agreement with the GC-MS data previously discussed (Table 3). Furthermore, all fractions contain aromatic protons (7.0-7.5 ppm) while the low boiling fractions A-D appears to contain more olefinic protons (4.5-6.0 ppm), also confirming our results from the GC-MS analysis.

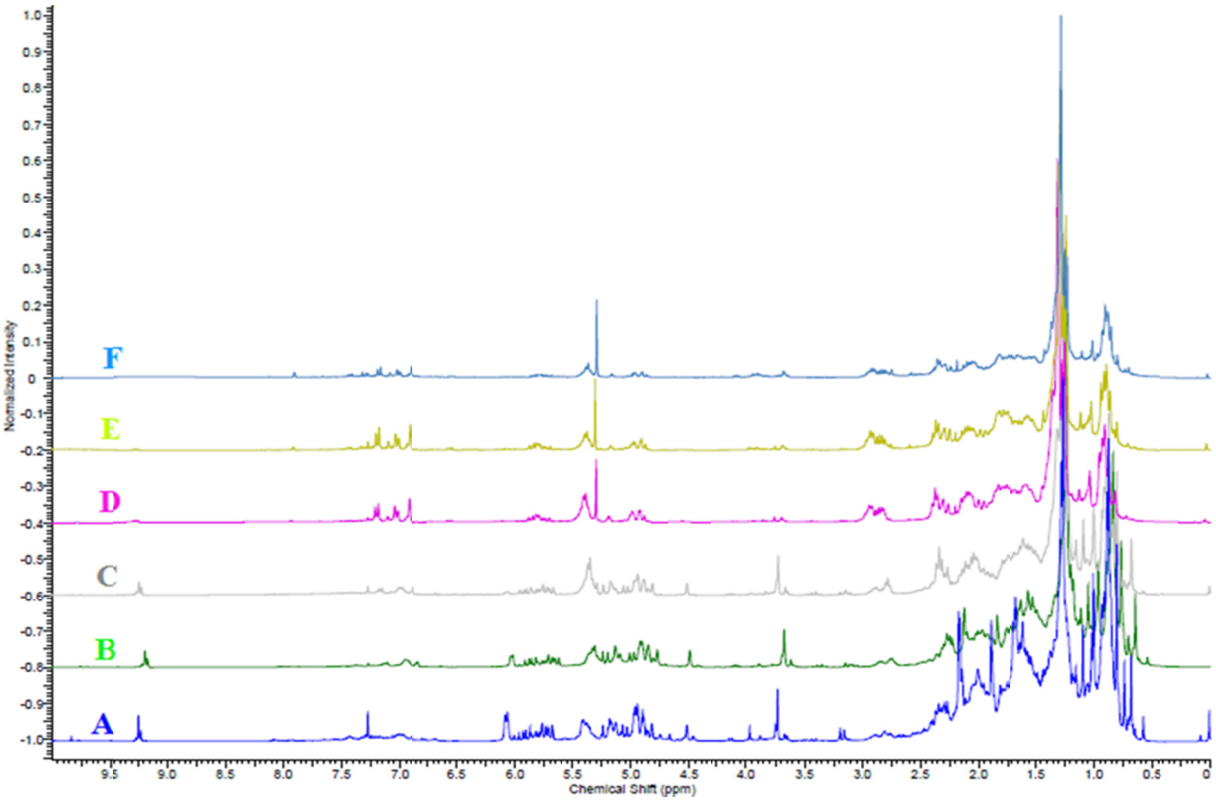

Figure 3. ^{1}H-NMR spectra of various distillate fractions of wood tar

3.6 Fourier Transform Infrared Spectroscopy (FTIR)

FTIR analysis was also carried out in order to confirm the potential chemical functional groups analyzed through ^{1}H-NMR spectroscopy and GC-MS. The FTIR spectra of distillate fractions 100 ^{o}C and 230 ^{o}C are shown in Figures 4 and 5 as representative examples of the data obtained from FTIR. The spectra of lower boiling fractions A and B (Figure 4) showed bands confirming the presence of aliphatic protons (2949-2848 cm^{-1}) and aromatic protons (3076 cm^{-1}). The hydroxyl functional group (3437 cm^{-1}) of alcohols is also observed in the low boiling fractions. The spectra of all fractions show the presence of carbonyl groups (1800-1650 cm^{-1}). However, in the case of the lower boiling fractions (Figure 4), the band at 1715 cm^{-1} indicates the presence of the carbonyl functional group in compounds such as ketones, aldehydes, conjugated esters and/or carboxylic acids. For the higher boiling fractions (Figure 5), similar absorptions can be observed for aliphatic protons (2953-2852 cm^{-1}), aromatic protons (3076 cm^{-1}) and carbonyls (1723 and 1697 cm^{-1}). However, the hydroxyl absorption in Figure 5 (portion in the blue box) is much broader than the one found in Figure 4 (see blue box in Figure 4 for comparison). This combination of a broad hydroxyl absorption (3200-2500 cm^{-1}) and a strong carbonyl band at ~ 1698 cm^{-1} is normally attributed to the carboxylic acid functional group. This broadness of the hydroxyl absorption is due to the strong hydrogen bonding that exists between the molecules of carboxylic acids (Pavia, Lampman, Kriz, & Vyvyan, 2009). The IR data also confirm our GC-MS results.

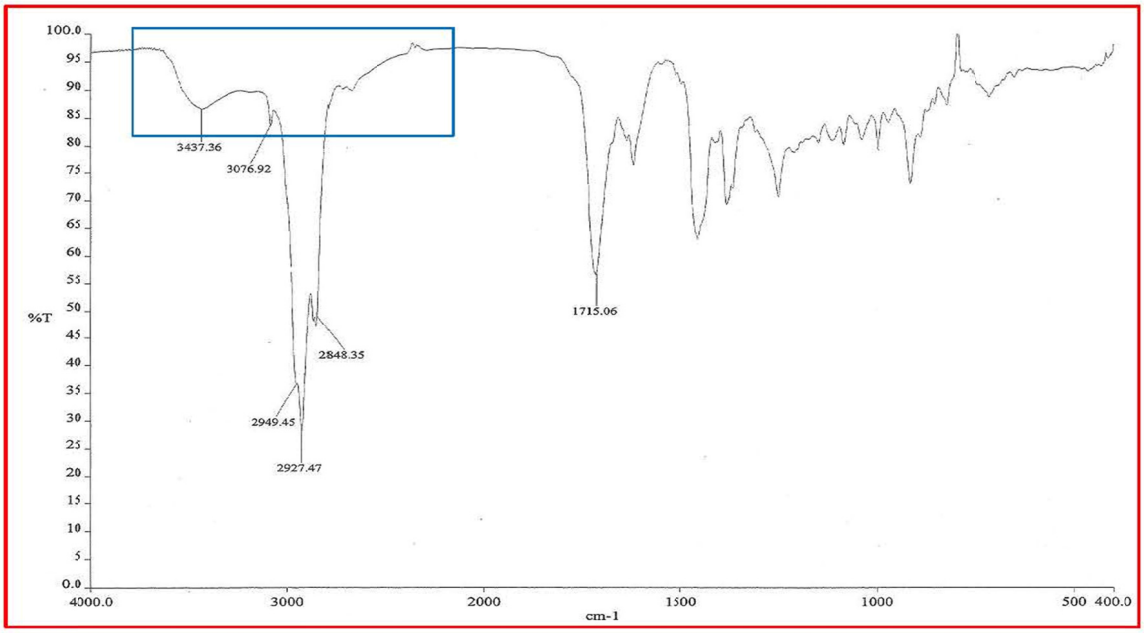

Figure 4. FTIR spectrum of distillate fraction 100 ^{o}C

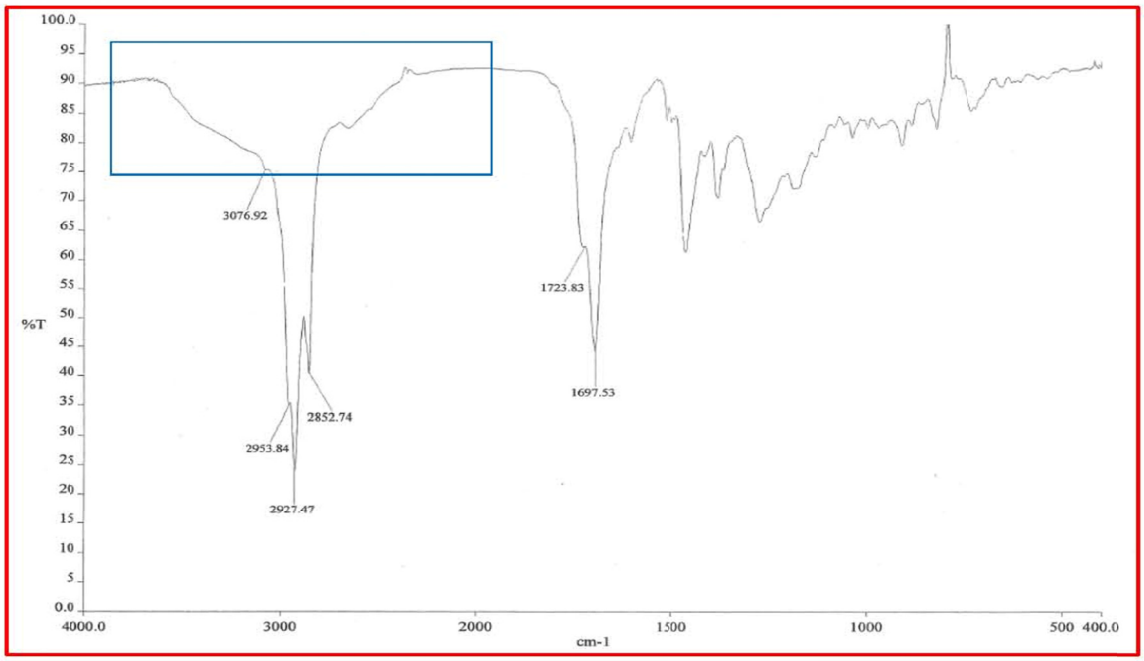

Figure 5. FTIR spectrum of distillate fraction 230 ^{o}C

4. Conclusions

The proper identification and characterization of environmentally hazardous waste is vital to waste management practices. In this investigation we were able to determine the make-up of the tar produced at a wood pellet manufacturing facilities in British Columbia, Canada. A total of 29 compounds were identified by various analytical techniques (GC-MS, TGA, ^{1}H-NMR, FTIR). Ethanol was also identified as a potential solvent to use in the clean up of machinery due to its low cost as well as low toxicity. To our knowledge, this is the first study of this type dealing with tar produced a pellet plants.

Acknowledgements

The authors would like to thank the Natural Sciences and Engineering Research Council of Canada (NSERC) for the financial support. The authors also acknowledge Dr. Quanji Wu and Mr. Charles Bradshaw for helping with various analytical procedures.

References

Blanco, P. H., Wu, C., Onwudili, J. A., & Williams, P. T. (2012). Characterization of tar from the Pyrolysis/ Gasification of Refuse Derived Fuel: Influence of Process Parameters and Catalysis. *Energy & Fuels, 26*, 2107-2115. http://dx.doi.org/10.1021/ef300031j

Blasi, C. D. (2009). Combustion and gasification rates of lignocellulosic chars. *Progess in Energy and Combustion Science, 35*, 121-140. http://dx.doi.org/10.1016/j.pecs.2008.08.001

Chips by Wood-inhabiting Fungi. *Applied* and *Environmental Microbiology, 61*, 222-225.

Crowe, A. S., & Ptacek, C. J. (2008). *Threats to Sources of Drinking Water and Aquatic Ecosystem Health in Canada*. Retrieved December 30, 2012 from (Environment Canada) http://www.ec.gc.ca/inre-nwri/default.asp?lang=En&n=235D11EB-1&offset=13&toc=sh#cur

Devi, L., Ptasinski, K. J., & Janssen, F. J. J. G. (2003). A review of the primary measures for tar elimination in biomass gasification processes. *Biomass & Bioenergy, 24*, 125-140. http://dx.doi.org/10.1016/S0961-9534(02)00102-2

Elder, T., Kush, J. S., & Hermann, S. M. (2011). Thermogravimetric analysis of forest understory grasses. *Thermochimica Acta, 512*, 170-177. http://dx.doi.org/10.1016/j.tca.2010.10.001

Envirochem Services Inc. (2010). *Emissions and Air Pollution Controls for the Biomass Pellet Manufacturing Industry*. Retrieved December 30, 2012 from (Vancouver, Canada) http://www.env.gov.bc.ca/epd/industrial/pulp_paper_lumber/pdf/moe-pellet-industry-051410.pdf

Fieser, L. F., & Campbell, W. P. (1938). Concerning Dehydroabietic Acid and the Structure of Pine Resin Acids. *Journal of the American Chemical Society, 60*, 159-170. http://dx.doi.org/10.1021/ja01268a050

Funk, C., & Croteau, R. (1994). Diterpenoid resin acid biosynthesis in conifers: Characterization of two cytochrome P450-dependent monooxygenases and an aldehyde dehydrogenase involved in abietic acid biosynthesis. *Archives of Biochemistry and Biophysics, 308*, 258-266. http://dx.doi.org/ 10.1006/abbi.1994.1036

Harris, G. C., & Sanderson, T. F. (1948). Resin Acids. I. An Improved Method of Isolation of Resin Acids; The Isolation of a New Abietic-Type Acid, Neoabietic Acid. *Journal of the American Chemical Society, 70*, 334-339. http://dx.doi.org/10.1021/ja01181a104

Haynes, W. M. (Ed.) (2012). *CRC Handbook of Chemistry and Physics* (Vol. 93). Florida: CRC Press: Boca Raton.

Hickman, K. C. D. (1944). High-vacuum Short-path Distillation-A Review. *Chemical Reviews, 34*, 51-106. http://dx.doi.org/10.1021/cr60107a002

Hosoya, T., Kawamoto, H., & Saka, S. (2008). Pyrolysis gasification reactivities of primary tar and char fractions from cellulose and lignin as studied with a closed ampoule reactor. *Journal of Analytical and Applied Pyrolysis, 83*, 71-77. http://dx.doi.org/10.1016/j.jaap.2008.06.002

Hudy, J. A. (1959). Resin Acids. Gas Chromatography of Their Methyl Esters. *Analytical Chemistry, 31*, 1754-1756. http://dx.doi.org/10.1021/ac60155a017

ICIS. (2013). Indicative chemical prices A-Z. Retrieved April 15, 2013 from http://www.icis.com/chemicals/channel-info-chemicals-a-z/

Jiang, J., Wang, Q., Wang, Y., Tong, W., & Xiao, B. (2007). GC/MS Analysis of Coal Tar Composition Produced from Coal Pyrolysis. *Bulletin of the Chemical Society of Ethiopia, 21*, 229-240. http://dx.doi.org/10.4314/bcse.v21i2.21202

Milne, T. A., Evans, R. J., & Abatzoglou, N. (1998). Biomass Gasifier "Tars": Their Nature, Formation and Conversion. Vol. 570. National Renewable Energy Laboratory, Colorado, USA.

Morales, A., Birkholz, D. A., & Hrudey, S. E. (1992). Analysis of Pulp Mill Effluent Contaminants in Water, Sediment, and Fish Bile: Fatty and Resin Acids. *Water Environment Research, 64*, 660-668. http://dx.doi.org/10.2175/WER.64.5.2

Murov, S. (2014). *Properties of Organic Solvents*. Retrieved on August 4, 2014 from http://murov.info/orgsolvents.htm

NAFAA-North American Fire Arts Association. (2001). *Material Safety Data Sheet*. Retrieved on April 17, 2013 from http://www.nafaa.org/ethanol.pdf

Pavia, D. L., Lampman, G. M., Kriz, G. S., & Vyvyan, J. R. (2009). *Introduction to Spectroscopy* (4th ed.). Belmont, CA: Brooks-Cole.

Peng, G., & Roberts, J. C. (2000). Solubility and toxicity of resin acids. *Water Research, 34*, 2779-2785. http://dx.doi.org/ 10.1016/S0043-1354(99)00406-6

Reed, T. B., & Gaur, S. (1998). *Survery of Biomass Gasification-1998*. The National Renewable Energy Laboratory and the Biomass Energy Foundation Inc., Golden, CO, USA.

Scott, W. (2009). *An Overview of the Wood Pellet Industry: A British Columbia Perspective*. Retrieved December 31, 2013 from https://circle.ubc.ca/bitstream/handle/2429/16863/ScottWill_ WOOD_493_Graduating _Essay_2008.pdf?sequence=1

Villeneuve, D. C., Yagminas, A. P., Marino, G. C., & Becking, G. C. (1977). Toxicity studies on dehydroabietic acid. *Bulletin of Environmental Contamination and Toxicology, 18*, 42-47.

Wang, Z., Chen, T., Gao, Y., Breuil, C., & Hiratsuka, Y. (1995). Biological Degradation of Resin Acids in Wood Chips by Wood-inhabiting Fungi. *Applied and Environmental Microbiology, 61*, 222-225.

International Journal of Chemistry; Vol. 6, No. 4; 2014
ISSN 1916-9698 E-ISSN 1916-9701
Published by Canadian Center of Science and Education

An Anomalous Hammett Correlation for a Series of Substituted 3-Benzyl-2-phenyl-1,3-thiazolidin-4-ones

Daniel McGarity[1], John Tierney[1] & Anthony Lagalante[2]

[1] Department of Chemistry, Pennsylvania State University, Brandywine Campus, Media, PA, USA

[2] Villanova University, Villanova, PA, USA

Correspondence: John Tierney, Department of Chemistry, Pennsylvania State University, Brandywine Campus, 25 Yearsley Mill Road, Media, PA 19063, USA. E-mail: jxt4@psu.edu

Received: August 15, 2014 Accepted: October 15, 2014 Online Published: October 20, 2014

doi:10.5539/ijc.v6n4p12 URL: http://dx.doi.org/10.5539/ijc.v6n4p12

Abstract

A series of 3-benzyl-2-phenyl-1,3-thiazolidin-4-one derivatives, with substituents at the N-benzyl site, was synthesized and characterized. Excluding the *p*-MeO and *m*-Br derivatives, distinct correlations between Hammett constant σ and ^{13}C substituent chemical shifts were observed in the C2, C4, and C5 carbons in the thiazolidin-4-one ring. This was unexpected because the transmission of substituent effects appears to be occurring via the sp^3 hybridized N-benzyl carbon. No discernible correlation was seen for the N-benzyl carbon; the carbon through which the effects were occurring. Correlations for substituent chemical shifts to Swain Lupton substituent parameters *r* and *f* constants were also attempted. Similar to the Hammett correlations, C2, C4, and C5 showed a reasonable degree of correlation with minimal to no improvement over Hammett constants; similarly, as with the Hammett correlations, the benzyl carbon exhibited no correlation with Swain Lupton parameters.

Keywords: Thiazolidin-4-ones, ^1H NMR, ^{13}C NMR, substituent effects

1. Introduction

A number of thiazolidinones systems have been investigated for their diverse biological activities, including potential anti-tumor, anti-inflammatory and anti-HIV agents (Hafez & El-Gazzar, 2009; Vigorita et al., 2001; Ravichandran, 2009). A growing series of thiazolidinone systems have been studied (Figure 1), and these studies have been previously been described (Cannon et al., 2013). ^1H NMR data was used to determine how phenyl or benzyl ring substituents for diaryl thiazolidinones (Series 1-4) affected electron density at the C-2 proton (H_x) and diastereotopic protons at C-5 (H_a and H_b).

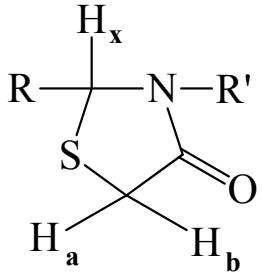

Series 1: R = phenyl, R' = *m*- and *p*-substituted phenyl
Series 2: R = *m*- and *p*-substituted phenyl, R' = phenyl
Series 3: R = R' = *m*- and *p*-substituted phenyl
Series 4: R = *m*- and *p*-substituted phenyl, R' = benzyl
Series 5: R = phenyl, R' = *m*- and *p*-substituted benzyl
Series 6: R = *m*- and *p*-substituted phenyl, R' = 2-pyridyl
Series 7: R = trichloromethyl, R' = *m*- and *p*-substituted phenyl
Series 8: R = *m*- and *p*-substituted phenyl, R' = cyclohexyl

Figure 1. All thiazolidinone studies published to this point. The *meta* and *para* substituents on phenyls designated by R and R' are: *p*-NO_2; *m*-NO_2; *p*-F; *m*-F; *p*-Cl; *m*-Cl; *p*-Br; *m*-Br; H, *p*-Me; *m*-Me; *p*-MeO; *m*-MeO

Thiazolidinone rings can have different conformations when solid and in solution (Figure 2). For 2,3-diaryl thiazolidinones (Series 1, 2 and 6), it was shown that conformer A was the preferred solid state confirmation, while conformer B was predominant in solution according to NMR observations in a number of similar systems

(Yennawar et al., 2014). Similar results have been seen with the unsubstituted N-cyclohexyl compound from Series 8 and recently experiments show that the unsubstituted compound in Series 5 also exhibited A (Figure 2) as the preferred solid state conformation (Fun et al., 2011; Cannon et al., 2013).

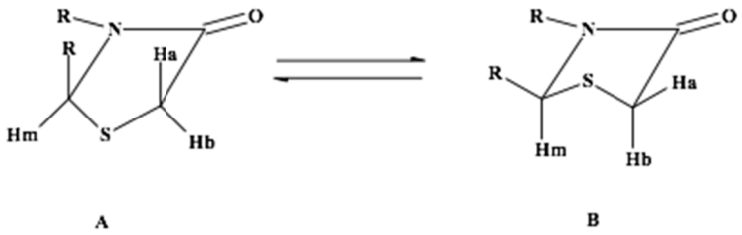

Figure 2. Pseudo-axial and pseudo equatorial ring conformers

The ORTEP model in Figure 3 shows the crystal structure of the unsubstituted 3-benzyl-2-phenyl-1,3-thiazolidin-4-one. The phenyl group has the same orientation relative to the thiazolidinone-4-one ring as the phenyl group in Series 8 (Cannon et al., 2013). The plane of the benzene ring, however, is significantly twisted relative the N-benzyl group in Series 5; the benzyl group having much more freedom to rotate than in the other systems.

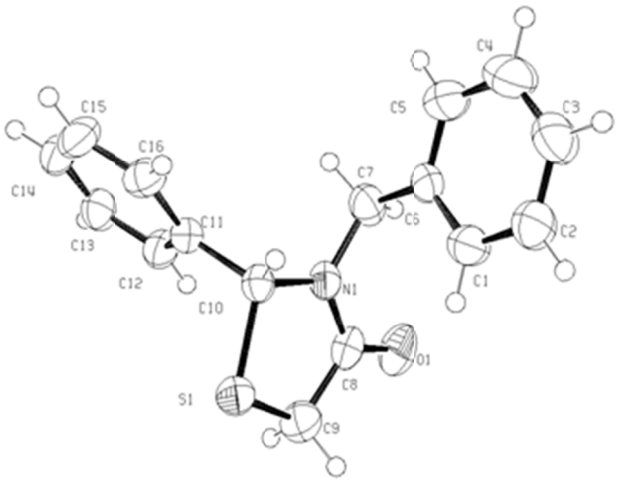

Figure 3. Ortep diagram 3-benzyl-1,3-thiazolidin-4-one. Note that the numeric assignments for atoms are inconsistent with IUPAC nomenclature

Previous work has illustrated that substituent Hammett (σ) and Swain Lupton *r* (resonance) and *f* (inductive) correlations can indicate the degree of electron density at various sites in the thiazolidinone ring subject to substituents in the aryl moieties (Tierney et al., 1996a). These electron density correlations have been studied by measuring ^{13}C chemical shift data at C2, C4 and C5 for Series 1 through 6 (Figure 1), where substituents were attached to either a phenyl or benzyl sites at C2 and N3, respectively. Substituent chemical shifts (SCS) have previously shown a linear relationship with substituent Hammett constants (Silverberg et al., 2013; Tierney et al., 1996b). In this study, SCS was defined by the empirical relation SCS = log (δ_x/δ_h), where δ_x represents the ^{13}C chemical shift for a substituted compound, and δ_h is the chemical shift for the unsubstituted, control compound. SCS values for a series of substituted 3-benzyl-2-phenyl-1.3-thiazolidin-4-ones, (Series 4, Figure 1) were attempted using Hammett constants according to the relationship SCS = ρσ. Previously, a limited investigation of a similar system (Series 5) with three substituents and the unsubstituted compound showed no correlation, and none was expected here. In addition, a substituent chemical shift correlation was also attempted with Swain Lupton dual substituent parameters by the equation SCS = *r* R + *f* F. The results of the study for this more extensively substituted Series 5 than the one previously reported follows (Tierney et al., 1996b).

2. Results and Discussion

For the series under consideration, Series 5, substituent chemical shifts for all of the carbons in the thiazolidinone ring appear to exhibit a linear Hammett correlation as shown in (Figures 4-6), with the exception of the *para*-methoxy and *meta*-bromo groups. This is in agreement with similar work previously carried out for Series 1-3 shown in Figure 1 (Woolston et al., 1992; Tierney et al., 1996a). For Series 8, a Hammett correlation was observed for C2, but not C4 or C5 (Cannon et al., 2013) and the strongest Hammett correlations for all the other series has always been for the transmission of substituent effects to the C2 site in the thiazolidinone ring. As Figure 7 shows, the benzyl carbon did not appear to have any relationship with the benzyl substituent. Hammett correlations were strengthened when the *p*-methoxy and *m*-Br derivatives were excluded (Table 1). Significant deviations with the *para*-methoxy group have been previously noted (Cannon et al., 2013). One proposed reason is that strong donating groups like *para*-methoxy may be responsible for altering the geometry in a way that reduces the degree of conjugation (Johnson, 1978). Although the reason for the deviation due to the *m*-Br group is not yet clear, *meta*-substituted derivatives have been shown to be less reliable at predicting chemical shifts. In this instance the size of the *meta*-bromo group may be altering the geometry of the N-benzyl ring relative to all the other meta substituted compounds. The value of ρ was negative for the C2 and C4 correlations, indicating that those sites favored a positive charge density. The trend for C5 showed a positive ρ value, and therefore, it favors a negative charge density; this agrees with observations from previous work (Cannon et al., 2013).

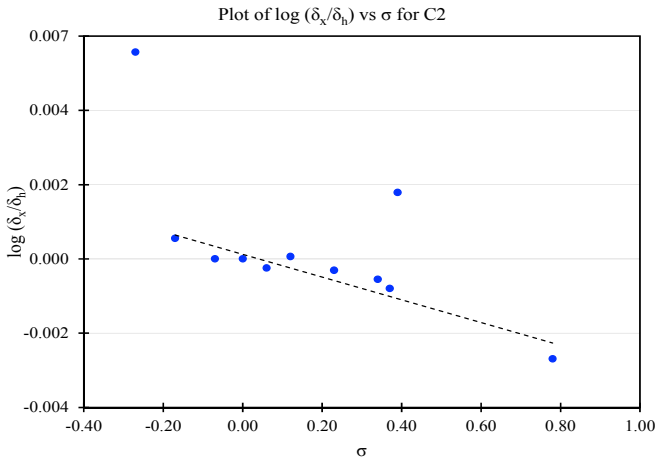

Figure 4. Plot of σ constant *vs* SCS for all ^{13}C shifts for the thiazolidin-4-one C2 carbon

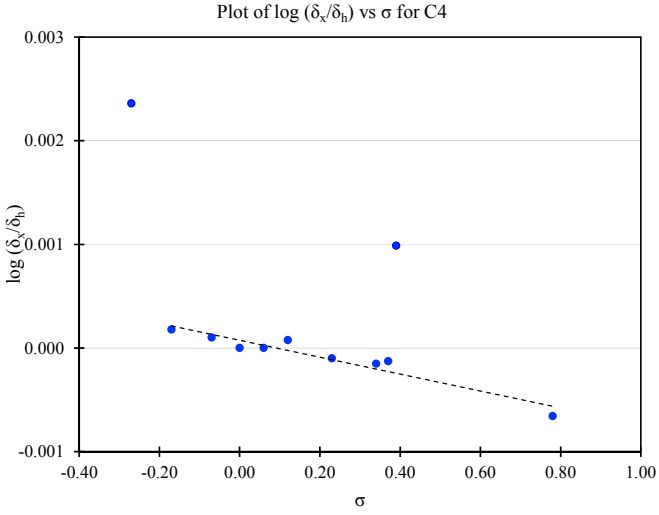

Figure 5. Plot of σ *vs* SCS for all ^{13}C shifts for the thiazolidin-4-one C4 carbon

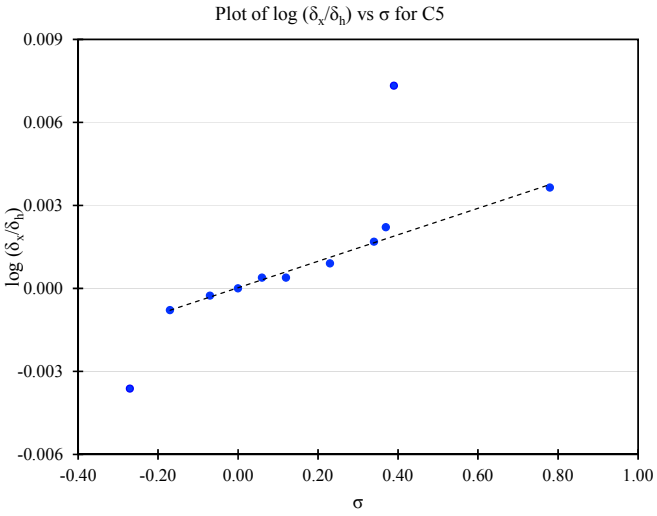

Figure 6. Plot of σ *vs* SCS for all ^{13}C shifts for the thiazolidin-4-one C5 carbon

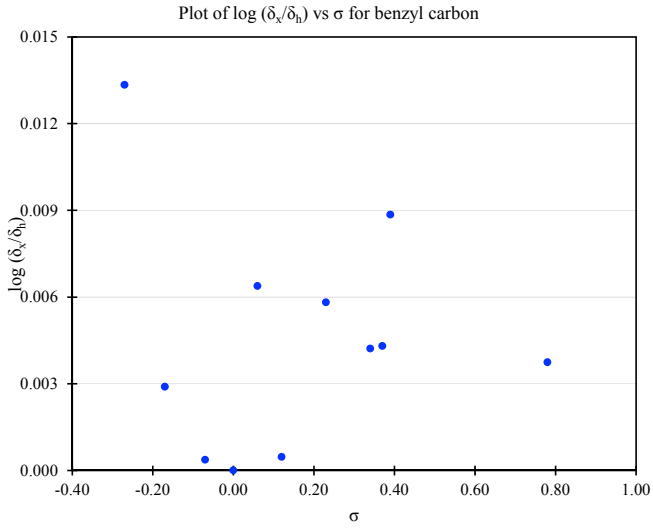

Figure 7. Plot of σ *vs* SCS for all ^{13}C shifts for the N-benzyl carbon

Table 1. Equations for improved correlations between Hammett and Substituent Chemical Shifts when *m*-Br and *p*-methoxy derivatives are removed from consideration

Carbon	Equation	R^2
C2	y = -0.0034x + 1.0E-4	0.8983
C4	y = 0.0008x + 7.42E-5	0.9154
C5	y = 0.0048x + 2.86E-5	0.9814
Benzyl	y = 0.0030x + 2.60E-3	0.1343

The Swain Lupton correlations for C2, C4, and C5 are shown in Table 2 but there is no significant improvement in the correlations. As with the Hammett correlations, there was no noticeable correlation with ^{13}C shifts in the benzyl carbon. Here, it was also noted that correlation improved if the data for the *p*-MeO and *m*-Br derivatives

were not considered in the correlation.

Table 2. Swain Lupton parameters fitted to the equation SCS = *r* R + *f* F when *m*-Br and *p*-MeO were removed from consideration

Carbon	*r*	*f*	R^2
C2	-2.65E-03	-3.44E-03	0.8817
C4	6.41E-04	8.22E-04	0.9202
C5	2.35E-03	5.11E-03	0.8656
Benzyl	8.73E-04	7.01E-03	0.4809

Most interestingly is the observed apparent lack of correlation of substituent effects at the N-benzyl site, particularly when this site emulates, in some respects the C2 site which has previously always shown relatively strong substituent correlations. Further, as previously mentioned, Hammett σ correlations would not be predicted beyond the N-benzyl carbon because it is sp^3 hybridized.

3. Conclusion

This work has quantified the effect of benzyl substituents on the ^{13}C shift for C2, C4, and C5 in the thiazolidinone ring for Series 5 (Figure 1). Excluding the *p*-methoxy and *m*-Br substituents, both Hammett and Swain Lupton constants exhibit a reasonable degree of correlation for the C2, C4 and C5 ^{13}C shifts. The deviations of the *p*-methoxy derivative has been previously observed (Woolston et al., 1992; Tierney et al., 1996a), but this study appears to be the first in which the *m*-Br derivative shows a large deviation which might be attributable to steric effects due to its size in this particular system. There was no discernable substituent correlation for ^{13}C chemical shifts for the N-benzyl carbon yet correlations were observed at sites beyond this carbon. It is unusual that Hammett correlations would be observed at the sites indicated because the transmission of substituent effects requires a high degree of conjugation from substituent to site. This observation calls into question the degree of sp^3 hybridization at the N-benzyl carbon, and the observation has caused us to initiate molecular modelling studies on this system.

4. Experimental

4.1 General

The target compounds were prepared using a previously described procedure (Surrey, 1947). A Mel-Temp capillary melting point apparatus was employed and all Melting points are uncorrected. NMR spectra were recorded on a Bruker 400 at 291 K using parameters that have been reported previously (Cannon, 2013). IR spectra were obtained using NaCl plates supplied by Janos Technology, Inc, the deposition of a thin film, by evaporation. A Nicolet Nexus 670 spectrometer was used and the conditions of operation have been previously reported (Cannon, 2013). An Applied Biosystems API 2000 Triple Quadrupole Mass Spectrometer was used to determine molecular masses implementing an Electrospray ionization technique. A 1% (v:v) formic acid methanol mixture infused at 10 μL/min was used as the electrospray solution. Curtain gas, 20 mL/min; collision gas, 0 mL/min; ionspray potential, 5.5 kV; temperature, 298 K; declustering potential, 60 V; focusing potential, 200 V; entrance potential, 10 V; collision energy, 25 units; cell exit potential, 4 V. Product yields are based on imines (as limiting reactant) produced from reaction of substituted benzyl-amines and benzaldehyde. Maximization of yields was not attempted. All correlations and statistics were obtained using Excel in Microsoft Office. ORTEP models were made with ORTEP version 2013.1 (Farrugia, 2012).

4.2 Synthesis and Characterization of Compounds

3-(*p*-nitrobenzyl)-2-phenyl-1,3-thiazolidin-4-one (5a) (2%); m.p. 150-156 °C; cm^{-1} 1674 (C=O); ^1H NMR ($CDCl_3$) 8.18-7.23 (9H, m, aromatics), 5.42 (1H, d, C2, J = 1.9 Hz), 5.08 (1H, d, J = 15.2 Hz), 3.93 (1H, dd, C5, J = 1.8 Hz, and 15.8 Hz), 3.84 (1H, d, J = 15.1 Hz), 3.82 (1H, d, C5, J = 15.7 Hz); ^{13}C NMR: 171.92 (C4), 147.98, 143.31, 138.76, 130.02, 129.68, 129.50, 127.70, 124.38, (ar), 63.57 (C2), 46.22, 33.18 (C5); (m/z) 315 ($[M+H]^+$) $C_{16}H_{14}N_2O_3S$ (314.36).

3-(*p*-fluorobenzyl)-2-phenyl-1,3-thiazolidin-4-one (5b) (68%); m.p. 152-153 °C; cm^{-1} 1668 (C=O); ^1H NMR ($CDCl_3$) 7.40-6.80 (9H, m, aromatics), 5.39 (1H, d, C2, J = 1.6 Hz), 5.07 (1H, d, J = 14.7 Hz), 3.90 (1H, dd, C5, J = 1.0 Hz, and 15.8 Hz), 3.75 (1H, d, J = 15.6 Hz), 3.55 (1H, d, C5, J = 14.7 Hz); ^{13}C NMR: 171.66 (C4), 139.34, 131.59, 131.55, 130.67, 130.59, 129.73, 129.58, 127.60 (ar), 63.17 (C2), 45.94, 33.43 (C5) ; (m/z) 288 ($[M+H]^+$) $C_{16}H_{14}NOSF$ (287.35).

3-(*m*-fluorobenzyl)-2-phenyl-1,3-thiazolidin-4-one (5c) (17%); m.p. 106-107 °C; cm^{-1} 1674 (C=O); ^1H NMR ($CDCl_3$) 7.39-6.95 (9H, m, aromatics), 5.39 (1H, d, C2, J = 1.8 Hz), 5.09 (1H, d, J = 14.9 Hz), 3.90 (1H, dd, C5, J = 1.3 Hz, and 15.4 Hz), 3.77 (1H, d, J = 15.6 Hz), 3.56 (1H, d, C5, J = 15.0 Hz); ^{13}C NMR: 171.72 (C4), 139.24, 138.29, 138.22, 130.79, 130.71, 129.78, 129.60, 127.61, 124.37, 124.34 (ar), 63.22 (C2), 46.17, 33.33 (C5); (m/z) 288 ($[M+H]^+$) $C_{16}H_{14}NOSF$ (287.35).

3-(*p*-chlorobenzyl)-2-phenyl-1,3-thiazolidin-4-one (5d) (31%); m.p. 156-157 °C; cm^{-1} 1667 (C=O); ^1H NMR ($CDCl_3$) 7.40-7.01 (9H, m, aromatics), 5.36 (1H, d, C2, J = 1.8 Hz), 5.07 (1H, d, J = 14.8 Hz), 3.90 (1H, dd, C5, J = 1.9 Hz, and 14.4 Hz), 3.75 (1H, d, J = 15.6 Hz), 3.55 (1H, d, C5, J = 14.8 Hz); ^{13}C NMR: 171.70 (C4), 139.23, 134.26, 134.24, 130.24, 129.77, 129.60, 129.35, 127.60 (ar), 63.18 (C2), 46.00, 33.39 (C5); (m/z) 303.5 ($[M+H]^+$) $C_{16}H_{14}NOSCl$ (303.81).

3-(*m*-chlorobenzyl)-2-phenyl-1,3-thiazolidin-4-one (5e) (38%); m.p. 82-84 °C; cm^{-1} 1668 (C=O); ^1H NMR ($CDCl_3$) 7.40-6.97 (9H, m, aromatics), 5.39 (1H, d, C2, J = 1.8 Hz), 5.06 (1H, d, J = 14.9 Hz), 3.91 (1H, dd, C5, J = 1.3 Hz, and 15.6 Hz), 3.78 (1H, d, J = 15.7 Hz), 3.56 (1H, d, C5, J = 14.9 Hz); ^{13}C NMR: 171.71 (C4), 139.19, 137.81, 135.02, 130.46, 129.81, 129.60, 128.85, 128.58, 127.63, 126.94 (ar), 63.26 (C2), 46.16, 33.29 (C5); (m/z) 303.5 ($[M+H]^+$) $C_{16}H_{14}NOSCl$ (303.81).

3-(*m*-bromobenzyl)-2-phenyl-1,3-thiazolidin-4-one (5f) (8%); m.p. 82-84 °C; cm^{-1} 1667 (C=O); ^1H NMR ($CDCl_3$) 7.42-7.01 (9H, m, aromatics), 5.39 (1H, d, C2, J = 1.8 Hz), 5.05 (1H, d, J = 14.9 Hz), 3.91 (1H, dd, C5, J = 1.3 Hz, and 16.9 Hz), 3.78 (1H, d, J = 15.6 Hz), 3.56 (1H, d, C5, J = 14.9 Hz); ^{13}C NMR: 171.27 (C4), 138.72, 137.62, 131.34, 131.08, 130.30, 129.39, 129.17, 127.20, 127.00, 122.76 (ar), 62.84 (C2), 45.68, 32.90 (C5); (m/z) 349 ($[M+H]^+$) $C_{16}H_{14}NOSBr$ (348.26).

3-benzyl-2-phenyl-1,3-thiazolidin-4-one (5g) (51%); m.p. 150-151 °C; cm^{-1} 1669 (C=O); ^1H NMR ($CDCl_3$) 7.40-7.09 (10H, m, aromatics), 5.39 (1H, d, C2, J = 1.9 Hz), 5.17 (1H, d, J = 14.7 Hz), 3.91 (1H, dd, C5, J = 1.9 Hz, and 14.4 Hz), 3.77 (1H, d, J = 15.6 Hz), 3.53 (1H, d, C5, J = 14.6 Hz); ^{13}C NMR: 171.66 (C4), 139.56, 135.71, 129.64, 129.56, 129.20, 128.85, 128.36, 127.58 (ar), 63.13 (C2), 46.62, 33.46 (C5); (m/z) 270 ($[M+H]^+$) $C_{16}H_{15}NOS$ (269.36).

3-(*p*-methylbenzyl)-2-phenyl-1,3-thiazolidin-4-one (5h) (50%); m.p. 156-157 °C; cm^{-1} 1665 (C=O); ^1H NMR ($CDCl_3$) 7.39-6.97 (9H, m, aromatics), 5.37 (1H, d, C2, J = 1.8 Hz), 5.14 (1H, d, J = 14.6 Hz), 3.92 (1H, dd, C5, J = 1.8 Hz, and 15.6 Hz), 3.75 (1H, d, J = 15.5 Hz), 3.47 (1H, d, C5, J = 14.6 Hz), 2.34 (3H, s, CH_3); ^{13}C NMR: 171.59 (C4), 139.65, 138.11, 132.61, 129.85, 129.59, 129.54, 128.86, 127.56 (ar), 63.04 (C2), 46.31, 33.52 (C5), 21.66 (CH_3); (m/z) 284 ($[M+H]^+$) $C_{17}H_{17}NOS$ (283.39).

3-(*m*-methylbenzyl)-2-phenyl-1,3-thiazolidin-4-one (5i) (1%); m.p. 80-82 °C; cm^{-1} 1671 (C=O); ^1H NMR ($CDCl_3$) 7.42-6.87 (9H, m, aromatics), 5.39 (1H, d, C2, J = 1.8 Hz), 5.13 (1H, d, J = 14.7 Hz), 3.92 (1H, dd, C5, J = 1.9 Hz, and 15.6 Hz), 3.77 (1H, d, J = 15.6 Hz), 3.48 (1H, d, C5, J = 14.6 Hz), 2.32 (3H, s, CH_3); ^{13}C NMR: 171.62 (C4), 139.66, 138.96, 135.57, 129.60, 129.53, 129.52, 129.10, 129.00, 127.55, 125.90 (ar), 63.13 (C2), 46.58, 33.48 (C5), 21.80 (CH_3); (m/z) 284 ($[M+H]^+$) $C_{17}H_{17}NOS$ (283.39).

3-(*p*-methoxybenzyl)-2-phenyl-1,3-thiazolidin-4-one (5j) (62%); m.p. 147-148 °C; cm^{-1} 1663 (C=O); ^1H NMR ($CDCl_3$) 7.39-6.81 (9H, m, aromatics), 5.37 (1H, d, C2, J = 1.8 Hz), 5.10 (1H, d, J = 14.6 Hz), 3.90 (1H, dd, C5, J = 1.3 Hz, and 15.6 Hz), 3.79 (3H, s, CH_3), 3.73 (1H, d, J = 15.6 Hz), 3.47 (1H, d, C5, J = 14.6 Hz); ^{13}C NMR: 170.73 (C4), 158.87, 128.82, 129.45, 128.77, 128.72, 126.92, 126.76, 113.68 (ar), 62.23 (C2), 54.87 (CH_3), 45.21, 33.74 (C5); (m/z) 301 ($[M+H]^+$) $C_{17}H_{17}NO_2S$ (299.39).

3-(*m*-methoxybenzyl)-2-phenyl-1,3-thiazolidin-4-one (5k) (2%); m.p. 74-75 °C; cm^{-1} 1664 (C=O); ^1H NMR ($CDCl_3$) 7.39-6.63 (9H, m, aromatics), 5.40 (1H, d, C2, J = 1.4 Hz), 5.14 (1H, d, J = 14.7 Hz), 3.91 (1H, dd, C5, J = 1.2 Hz, and 15.8 Hz), 3.77 (3H, s, CH_3), 3.76 (1H, d, J = 15.6 Hz), 3.50 (1H, d, C5, J = 14.8 Hz); ^{13}C NMR: 171.63 (C4), 160.28, 139.58, 137.21, 130.22, 129.63, 129.54, 127.59, 121.07, 114.30, 113.81 (ar), 63.12 (C2), 55.65 (CH_3), 46.57, 33.43 (C5); (m/z) 301 ($[M+H]^+$) $C_{17}H_{17}NO_2S$ (299.39).

Acknowledgements

The work described here was completed by Daniel McGarity in partial fulfilment of his Schreyer Honors Thesis and Bachelor of Science degree at the Pennsylvania State in Spring 2008. We would like to acknowledge the

Pennsylvania State University Schreyer Honors College for funding this work.

References

Barreca, M. L., Chimirri, A., De Luca, L., Monforte, A.,Monforte, P., Rao, A., … Witvrouw, M. (2001). Discovery of 2,3-diaryl-1,3 thiazolidin-4-ones as potent anti-HIV-1 agents. *Bioorganic & Medicinal Chemistry Letters, 11*, 1793-1796. http://dx.doi.org/10.1016/S0960-894X(01)00304-3

Cannon, K., Mascavage, L., Kistler, K., Tierney, J., Yennawar, H., & Lagalante, A. (2013). An Experimental and Theoretical Conformational Study of a Series of Substituted 3-cyclohexyl-2-phenyl-1,3-thiazolidin-4-ones. *International Journal of Chemistry, 5*, 46-56. http://dx.doi.org/10.5539/ijc.v5n3p46

Fun, H.-K., Hemamalini, M., Shanmugavelan, P., Ponnuswamy, A., & Jagatheesan, R. (2011). 3-Benzyl-2-phenyl-1,3-thiazolidin-4-one. *Acta Cryst. E67*, o2706. http://dx.doi.org/10.1107/S1600536811037706

Hafez, N. H., & Gazzar, A. B. A. (2009). ynthesis and antitumor activity of substituted triazolo[4,3-*a*]pyrimidin-6-sulfonamide with an incorporated thiazolidinone moiety. *Bioorganic & Medicinal Chemistry Letters, 19*(15), 4143-4147. http://dx.doi.org/10.1016/j.bmcl.2009.05.126

Ravichandran, V. Prashantha Kumar, B. R., Sankar, S., & Agrawal, R. K. (2009). Predicting anti-HIV activity of 1,3,4-thiazolidinone derivatives: 3D-QSAR approach. *European Journal of Medicinal Chemistry*, *44*(3), 1180-1187. http://dx.doi.org/10.1016/j.ejmech.2008.05.036

Silverberg, L. J., Bear, E. R., Foose, K., Kirkland, K., McElvaney, R., Cannon, K., ... Lagalante, A. (2013) Verifying the Predict ability of ^{13}C Chemical Shifts for a Series of Substituted-2-(4-Chlorophenyl)-3-Phenyl-1,3-thiazolidin-4-ones. *International Journal of Chemistry, 5*(4), 120-127. http://dx.doi.org/10.5539/ijc.v5n4p120

Surrey, A. R. (1947). The Preparation of 4-Thiazolidones by the reaction of thioglycolic acid with Schiff Bases. *Journal of the American Chemical Society, 69*(11), 2911. http://dx.doi.org/10.1021/ja01203a507

Tierney, J., Houghton, G., Sanford, K., Mascavage, L., McCoy, M., Findeisen, A., & Kilburn, J. (1996a). Effects and conformational analysis of some substituted 2,3-diphenyl-1,3-thiazolidin-4-ones. *Magnetic Resonance in Chemistry, 34*, 573-576. http://dx.doi.org/10.1002/(SICI)1097-458X(199608)34:8<573::AID-OMR928>3.0.CO;2-D

Tierney, J., Sheridan, D., Kovalesky, K., Mascavage, L. M., Schneider, K., & Sheely, C. (1996b). Substituent effects for some substituted 3-benzyl-2-phenyl-1,3-thiazolidin-4-ones using ^{1}H and ^{13}C NMR. *Heterocyclic Communications, 6*, 105-111. http://dx.doi.org/10.1515/HC.2000.6.2.105

Vigorita, M. G., Ottana, R., Monforte, F., Maccan, R., Trovatto, A., Monforte, M. T., & Taviano, M. F. (2001). Syn thesis and antiinflammatory, analgesic activity of 3,3'-(1,2-ethanediyl)-bis[2-aryl-4-thiazolidinone] chiral compounds. Part 10. *Bioorganic & Medicinal Chemistry Letters, 11*(21), 2791-2794. http://dx.doi.org/10.1016/S0960-894X(01)00476-0

Woolston, C. R. J., Lee, J. B., Swinbourne, F. J., & Thomas, W. A. (1992). Proton NMR investigation of some substituted 1,3-thiazolidin-4-ones. *Magnetic Resonance in Chemistry, 30*, 1075-1078. http://dx.doi.org/10.1002/mrc.1260301109

Yennawar, H. P., Tierney, J., & Silverberg, L. J. (2014). 2,3-Diphenyl-1,3-thiazolidin-4-one. *Acta Crystallographica, Section E70*, o847. http://dx.doi.org/10.1107/S1600536814015128

Copyrights

International Journal of Chemistry; Vol. 6, No. 4; 2014
ISSN 1916-9698 E-ISSN 1916-9701
Published by Canadian Center of Science and Education

Antibacterial Susceptibility of the Constituents of Ethanol Crude Extract and the Neutral Metabolite of the Root of *Curculigo pilosa* Hypoxidaceae

D. C. Nwokonkwo[1]

[1] Faculty of Physical Sciences, Industrial Chemistry Department Ebonyi State, University Abakaliki, Nigeria

Correspondence: D. C. Nwokonkwo, Faculty of Physical Sciences, Industrial Chemistry Department Ebonyi State, University Abakaliki, Nigeria. E-mail: mirinkwa@gmail.com

Received: August 29, 2014 Accepted: September 30, 2014 Online Published: October 20, 2014

doi:10.5539/ijc.v6n4p19 URL: http://dx.doi.org/10.5539/ijc.v6n4p19

Abstract

Powdered fresh rhizomes of *Curculigo pilosa* Hypoxidaceae (African Crocus) were analyzed for their phytochemicals and antibacterial activities. The crude ethanol extract showed the presence of saponins, flavonoids, steroids, alkaloids, glycosides and phenols. This crude sample was partitioned into acidic, basic and neutral metabolites. The neutral portion indicated the presence of saponin, flavonoid, steroid, glycoside, phenol and alkaloid. The antimicrobial susceptibility tests using the crude sample and the metabolites were carried out on four human pathogens; *Escherichia coli, staphylococcus aureus, pseudomonas aeruginosa and streptococcus faecalis.* At a concentration of 100 mg/mL: the crude sample showed IZD values of 22 mm for *Escherichia coli*, 29 mm for *staphylococcus aureus*, 23 mm for *pseudomonas aeruginosa* and 38 mm for *streptococcus faecalis*. The neutral metabolite at the same concentration gave IZD values of 35 mm for *Escherichia coli*, 36 mm for *staphylococcus aureus*, 35 mm for *pseudomonas aeruginosa* and 43 mm for *streptococcus faecalis*. The acidic and basic metabolites did not show any significant antibacterial activity. The control drug ampiclox at 100 mg/mL showed IZD values of 40 mm for *Escherichia coli*; 32 mm for *staphylococcus aureus*; 26 mm for *pseudomonas aeruginosa and* 22 mm for *streptococcus faecalis* respectively. The minimum inhibitory concentration (MIC) of the ethanol crude extract and the neutral metabolite were at 25 mg/mL, 50 mg/mL and100 mg/mL, the result apparently justified the use of fresh rhizomes of *Curculigo pilosa* in the treatment of infections.

Keywords: antimicrobial, neutral, phytochemicals, root, tests

1. Introduction

Plants have been major sources of medicine and plant secondary metabolites have been attributed to most plant therapeutic activities (Fabeku, 2006; Neumann & Hirsch, 2000). Phytochemicals have shown great promise in the treatment of intractable infectious diseases (Yesileda, 2005). The local uses of plants and plant products in health care are even much higher particularly in those areas with little or no access to modern health services (Saed, Arshad, M. Ahmad, E. Ahmad, & Ishaque, 2004). Traditional medicine is a source of primary health care to 80% of the world's population (Alves & Rosa, 2005; Pei, 2001) the use of herbal medicine has always been part of human culture, and African culture is one of them.

Several herbs from plants most especially have various pharmacologically active compounds that have the potential for the prevention/treatment of several cancers. The antioxidant potency of flavonoids in medicinal plants possess a variety of anticancer effects such as arrest of cell growth, inhibition of kinase activity, induction of apoptosis, reduction in tumour-invasive behavior and suppression of matrix metalloproteinase's secretion (Chau et al., 2000). Many African plants have been hypothesized to have phytochemicals that make them effective anti-inflammatory, antihypertensive, antitussive, antibiotics, anticancer agents and so on.

This article looked at one of these numerous Nigerian's medicinal plants, *Curculigo pilosa*. *Curculigo pilosa* Hypoxidaceae is known as "epakun" in Yoruba language; "orima" in Edo language, "dòòyár kùréégéé" in Hausa language and "pkeve' in Tiv languge. The plant is used in herbal or traditional medicine to treat leukemia, gonorrhea, cough, as astringent agent, aphrodisiac and demulcent in Southwestern Nigeria (Odugbemi & Akinsulire, 2006); there is a hypothesis that the rhizomes could possess anti-cancer or anti-tumour properties.

Soladoye et al. (2012) reported its use as an antidiabetic; the vasoconstictive activity of its benzylbenzoate and non-lignan glucosides were also reported (Palazzino, Galeffi, Federici, Monache, Cometa, & Palmery, 2000).

The research investigated the phytochemicals present in the crude ethanol extract of this plant species and the neutral metabolite derived from it. Also the antibacterial susceptibility of this crude sample and its neutral metabolite were verified. The root of *Curculigo pilosa* Hypoxidaceae from this work had shown itself as a highly promising source of potent antimicrobial drug. It is obviously worthy of large scale investment as the need for antimicrobial, antifungal and antiviral drugs against resistant pathogens persist around the globe.

2. Experimental

2.1 Plant Material

The fresh root of *Curculigo pilosa* (350 g) was purchased from Awolowo Market in Mushin local government of Lagos State in the month of June 2012 and identified by Applied Biology Department, Ebonyi State University Abakaliki. It was washed with distilled water to remove dirt, oven dried at moderate temperature for two days, pulverized and stored in sealed cellophane until needed. Test organisms *candida albicans*, *streptococcus faecali*, *escherichia coli, pseudomonas aeruginosa*, *staphylococcus aureus* and *coliform bacilli* were obtained from the Applied Microbiology Department of Ebonyi State University Abakaliki. All reagents used were of analytical grade.

2.1.1 Extraction

About 300 g of the ground sample was soaked in an aspirator bottle in 500 mL of ethanol and allowed to stay for 72 h. The solvent was filtered and the filtrate distilled off to obtain 50 g greenish gummy substance.

2.1.2 Phytochemical Screening

Ejele and Alinor method (2010) was used in the preparation of the acidic, basic and neutral metabolites. The crude sample and the acidic, basic and neutral metabolites were subjected to phytochemical analysis using the AOAC (2005) method and other methods (Nwokonkwo, 2009) for the presence or absence of saponin, flavonoid, alkaloid, glycoside, tannin, polyphenol and steroid.

2.1.3 Antibacterial Activity

Test organisms used were *candida albicans*, *streptococcus faecali*, *escherichia coli, pseudomonas aeruginosa*, *staphylococcus aureus* and *coliform bacilli*. Agar well diffusion method was used. A cork borer of 1 cm was used to perforate the Mueller-Hinton agar in aseptic condition. The turbidity of the sample was prepared according to Mcfarland standard; a sterile swab stick was used and rotated inside the inoculums. The swab was streaked evenly over the surface of the medium before introduction of the plant extract (Agah et al., 2011). The determination of the minimum inhibitory concentration (MIC) was carried out on the plant extracts at concentrations of 100 mg/mL, 50 mg/mL, 25 mg/mL, 12.5 mg/mL and 6.25 mg/mL according to the method proposed by George and Roger (2002). These were prepared in agar nutrient and distributed into sterile tubes into sterile test tubes. One (1) mL of the extract was separately added to the agar plates for the bacteria and poured into petri dishes. The test organism was spotted on the surface of the solidified extract-agar mixture in increasing order of concentration. The plates were allowed to dry for 30 min and incubated at 37 ^{o}C for 18 h, after which the plates were examined for microbial growth. The lowest concentration of the extract which showed little or no visible growth of the microorganism was taken as the MIC of the extract (Roberts, Shore, Paviour, Holland, & Morris, 2006).

3. Results and Discussion

The phytochemical screening of the crude sample of plant extract is shown on Table 1. The table showed the presence of saponin, flavonoid, steroid, alkaloid and glycoside but absence of tannin (Ejele & Nwokonkwo, 2013). The phytochemical screening of the acidic, basic and neutral metabolite is shown in Table 2. In Table 2, the acidic metabolite showed the presence of saponin, flavonoid, steroid, glycoside and phenol but the absence of alkaloid and tannin. The basic metabolite showed the absence of tannin, flavonoid and steroid but contained saponin, alkaloid, glycoside and phenol. The neutral metabolite showed the presence of all the phytochemicals except tannin. Inhibition zone diameter of the crude sample, acidic, basic and neutral metabolites is shown on Table 3 while Table 4 explains the inhibition zone diameter of the control drug. The crude sample showed IZD values of 22 mm, 29 mm, 23 mm and 38 mm at 100 mg/ mL for *Escherichia coli, Pseudomonas aeruginosa, Streptococcus faecalis and Staphylococcus aureus* respectively. The IZD values obtained showed that the crude sample was potent against the organisms used in the analysis. The IZD values for the neutral metabolite at 100 mg/mL were 35 mm, 36 mm, 35 mm and 43 mm for *Escherichia coli, Pseudomonas aeruginosa, Streptococcus*

faecalis and Staphylococcus aureus, a positive result also indicating the potency of this plant species. The MIC of the crude and neutral metabolite on these microorganisms was at 25 mg/mL, 50 mg/mL and 100 mg/mL. The IZD values of the neutral metabolite were significantly high compared to the control drug except in the case of Escherichia *coli* where the control drug at 100 mg/mL gave IZD value of 40 mm. Alkaloids, phenols, glycosides and saponins have proven to have antibacterial, antifungal, astringent and such like properties and might be the reason why the crude extract gave positive result for the antimicrobial tests. The neutral metabolite which had the same constituents as the crude had higher IZD values and invariably higher inhibitory action against the pathogens. This probably indicated that these active principles were present in high concentration (s) in this medium. The concentration of the alkaloid, saponin and phenol in the basic medium might not have been significant enough to produce the required antibacterial activity. Also, the concentration of the saponin and phenol in the acidic medium might also not have been enough for the lethal dose required for it to be bacteriostatic or bactericidal. The extracts from these two media showed no appreciable MIC at 25 mg/mL, 50 mg/mL and 100 mg/mL.

Table 1. Phytochemical screening of the ethanol crude extract of the plant sample

Test	Observation	Inference
Tannin: **2 mL sample + 5 mL H_2O + 2 drops $FeCl_3$**	formation of bluish precipitate	Tanins not indicated
Saponin: **2 mL sample + 5 mL H_2O and 2 mL olive oil**	formation of frothing	saponin indicated
Flavonoid: **2 mL 10 % NaOH + 2 mL 10 % HCl**	formation of white precipitate	flavonoid ndicated
Steroid: **$CHCl_3$ + 5 mL conc. H_2SO_4**	formation of dark-brown colour	steroid indicated
Alkaloid: **2 mL Wagner's reagent + 2 mL sample**	formation of precipitate	alkaloid indicated
Glycoside: **0.5 mL $CHCl_3$ layer + 2 mL CH_3COOH + 1.0 mL conc. H_2SO_4**	formation of two layers with reddish-brown colour at interface	glycoside indicated
Phenol: **0.5 mL sample + 4 mL H_2O + 0.3 mL 1.0 M $FeCl_3$ solution**	dark-brown precipitate formed	phenol indicated

Table 2. Phytochemical screening of the acidic, basic and neutral metabolites

Phytochemical	Acidic Metabolite	Basic Metabolite	Neutral Metabolite
Tannin:	not indicated	not indicated	not indicated
Saponin:	not indicated	indicated	indicated
Flavonoid:	not indicated	not indicated	indicated
Steroid:	indicated	not indicated	indicated
Alkaloid:	not indicated	indicated	indicated
Glycoside:	indicated	indicated	indicated
Phenol:	indicated	indicated	indicated

Table 3. Inhibition zone diameter of the crude sample, acidic, basic and neutral metabolites

Test Organisms	Diameter of Zone of Inhibition(mm) Concentration (100 mg/mL)			
	Crude	Acidic	Basic	Neutral
Escherichia coli	22	-	-	35
Pseudomonas aeruginosa	29	-	-	36
Streptococcus faecalis	23	-	-	35
Staphylococcus aureus	38	-	-	43

Table 4. Inhibition Zone diameter of Ampliclox the control drug

Test Organisms	Diameter of Zone of Inhibition(mm) Concentration (100 mg/mL)
	Ampiclox
Escherichia coli	40
Pseudomonas aeruginosa	32
Streptococcus faecalis	26
Staphylococcus aureus	22

The partitioning of the crude sample into acidic, basic and neutral metabolites presented a new method of investigation as it helped in concentrating the active constituents/phytochemicals into acidic, basic and neutral media or as in this case, the neutral medium; and would make isolation through column chromatography and final characterization of the isolates easier.

Further research is still continuing; to isolate each phytochemical, test the susceptibility to microorganisms and structure elucidation.

References

Agah, M. V. et al. (2011). Antifungal activity of some selected plant extracts in Nigeria. *Asian Journal of Microbiology, Biotechnology and Enviromental Science, 13*(1), 87-89.

Alves, R. R., & Rosa, I. L. (2005). Why study the user of plants in traditional medicines? *Journal of Ethnomedicine, 1*, 1-5. http://dx.doi.org/10.1076/phbi.39.7.74.5869

AOAC. (2005). *Official Methods of Analysis* (15th ed.). Washington D.C.: Association of Official Analytical Chemist.

Chau, B. N. et al. (2000). A Novel inhibitor of caspase activation binds bcl-x_L and apaf-1. *Molecular Cell Biology, 6*, 31-40.

Ejele, A. E., & Alinor, J. I. (2010). Anti-sickling potentials of aloe vera extract. effects of acidic, basic and neutral metabolites on the gelling and sickling of human hbss erythrocytes. *International Journal of Natural and Applied Sciences, 6*(2), 155-160.

Ejele, A. E., & Nwokonkwo, D. C. (2013). Effect of microbial spoilage on an antimicrobial potential and phytochemical composition of *ipecae* root extract. *International Research Journal of Microbiology, 4*(4), 106-112.

Fabeku, P. O. (2006). Traditional medicine: The art, ways and practice. In T. Odugbemi (Ed.), *outlines and pictures of medicinal plants from Nigeria* (pp. 13-24). University of Lagos Press.

George, D. P., & Roger, M. D. (2002). *Encyclopaedia of Medicinal Plant* (5th ed.). Spainish 1.

Neumann, R. R., & Hirsch, E. (2000). Commercialization of non-timber forest products: Review and analysis for research. Indonesia, 176.

Nwokonkwo, D. C. (2009). Phytochemical constitution and antimicrobial activity of the stem bark of *ficus*

asperifolia (sand paper) tree. *Journal of Chemical Society of Nigeria, 34*(2), 119-122.

Odugbemi, T., & Akinsulire, O. (2006). Medicinal Plants by Species Names. In *Outlines and Pictures of Medicinal Plants from Nigeria*. Nigeria: University of Lagos Press.

Palazzino, G., Galeffi, C., Federici, E., Monache, F. D., Cometa, M. F., & Palmery, M. (2000). Benzylbenzoate and norlignan glucosides from *curculigo pilosa*: structural analysis and invitro vascular activity. *Phytochemistry, 55*, 411-417. http://dx.doi.org/10.1016/S0031-9422(00)00256-9

Pei, S. J. (2001). Ethnobotanical approaches to traditional medicine: some experiences from Asia. *Pharmaceutical Biology, 39*, 74-79.

Roberts, S. A., Shore, K. P., Paviour, S. D., Holland, D., & Morris, A. J. (2006). Antimicrobial susceptibility of anaerobic bacteria in New Zealand. *Journal of Antimicrobial Chemotherapy, 57*, 92-98. http://dx.doi.org/10.1093/jac/dkl052

Saed, M., Arshad, M., Ahmad, M., Ahmad, E., & Ishaque, M. (2004). Ethnophytotherapies for the treatment of various by the local people of selected areas of NWFP (Pakistan). *Journal of Biological Science, 7*, 1104-1108. http://dx.doi.org/10.3923/pjbs.2004.1104.1108

Soladoye, M. O. et al. (2012). An avalanche of plant species for the traditional cure of diabetes mellitus in south western Nigeria. *Journal of Natural Product Plant Resources, 2*, 60-72.

Yesileda, E. (2005). Past and future contributions of traditional medicine in the healthcare system of the middle east. *Journal of Ethnopharmacolology, 100*, 135-137. http://dx.doi.org/10.1016/j.jep.2005.06.003

International Journal of Chemistry; Vol. 6, No. 4; 2014
ISSN 1916-9698 E-ISSN 1916-9701
Published by Canadian Center of Science and Education

Determination of Adulterants in Diesel by Multivariate Calibration Associated With LED Spectrofluorimetry

Marilena Meira[1], Cristina M. Quintella[2], Erika M. de O. Ribeiro[2], Alexandre K. Guimarães[2] & Weidson Leal Silva[2]

[1] Instituto Federal de Educação, Ciência e Tecnologia da Bahia, Campus Simões Filho, BA, Brazil

[2] Instituto de Química, Universidade Federal da Bahia, Campus de Ondina, Salvador, BA, Brazil

Correspondence: Marilena Meira, Instituto Federal de Educação, Ciência e Tecnologia da Bahia, Campus Simões Filho, CEP: 43.700-000, BA, Brazil. E-mail: marilenameira@gmail.com

Received: June 17, 2014 Accepted: September 11, 2014 Online Published: October 20, 2014

doi:10.5539/ijc.v6n4p24 URL: http://dx.doi.org/10.5539/ijc.v6n4p24

Abstract

In this paper, multivariate calibration models have been developed for determination of common adulterants (kerosene, turpentine and residual oil from fried foods) added to diesel. The samples were analyzed by LED spectrofluorimetry and the multivariate calibration models were developed by Partial Least Squares (PLS). The proposal is suggested as an analytical methodology of low-cost, fast and non-destructive able to quantify the presence of contaminants in the diesel. The results showed that adulterants concentrations were adequately reproduced by the fluorescence spectral data.

Keywords: adulteration, diesel, PLS, spectrofluorimetry

1. Introduction

The intentional addition of adulterants to diesel has a negative effect on fuel properties and on the engine performance, such as fuel consumption, engine start-up control and engine heating. In addition, adulteration of fuel increases the emission of exhaust gases, hydrocarbons and particulate material (Corgozinho, Pasa, & Barbeira, 2008).

Several analytical methodologies have been developed for identification or quantification of adulterants in diesel and biodiesel-diesel blends in recent years. Patra and Mishra developed a method for detected contamination in diesel by excitation-emission matrix spectral subtraction fluorescence (Patra & Mishra, 2002). Corgozinho et al. related a method for quantifying of residual vegetable oil in diesel oil using synchronous spectrofluorimetry and PLS (Corgozinho, Pasa, & Barbeira, 2008). Oliveira et al. reported a method to determine adulteration of diesel/biodiesel blends by vegetable oil using Fourier transform (FT) near infrared spectrometry and FT-Raman spectroscopy (Oliveira, Brandão, Ramalho, Costa, Suarez, & Rubim, 2007). Vasconcelos et al. using near-infrared overtone regions determined biodiesel content and adulteration of diesel/biodiesel blends with vegetable oils (Vasconcelos, Souza Jr., Pimentel, Pontes, & Pereira, 2012). Pontes et al. detected adulteration in diesel/biodiesel blends using a method based near infrared spectrometry and multivariate classification (Pontes, Pereira, Pimentel, Vasconcelos, & Silva, 2011). Gaydou et al. detected vegetable oil as an adulterant in diesel/biodiesel blends associating NIR/MIR PLS (Gaydou, Kister, & Dupuy, 2011). Roy developed a fiber-optic sensor for determining kerosene as an adulterant in petrol and diesel (Roy, 1999). Souza et al. determined adulteration of Brazilian S-10 diesel by lubricant oil using MIR spectroscopy and PLS (Souza, Mitsutake, Gontijo, & Borges Neto, 2014). Brandão et al. used high performance liquid chromatography and multivariate methods to determine adulteration of diesel by vegetable oils and fats (Brandão, Braga, & Suarez, 2012).

In a previous work, our team developed a method and a sensor for monitoring quality in processes for obtaining fuels using spectrofluorimetry and Principal Component Analysis (PCA) (Quintella, Guimarães, & Musse, 2009). Also we reported a method for identification of the adulteration to diesel by the addition of residual cooking oil using spectrofluorimetry total 3D and PCA (Meira et al., 2011) and a spectrofluorimeter was patented (Quintella et al., 2011). This present study focuses on the quantification of adulterants added to diesel (kerosene, turpentine and residual oil from fried foods) by high-power light-emitting diode (LED) spectroluorimetry and partial least squares (PLS) regression. LEDs have the following advantages as alternatives sources of excitation in

spectrofluorimetry: They are near monochromatic, have low cost, produce very little heat, have no coherence problems, have extended life, are small and can easily be modulated (Young, Garini, Dietrich, van Oel, & Liqui Lung, 2004).

2. Materials and Methods

Standard of diesel was supplied by Petrobras-Brazil and the mixtures of diesel with adulterants (kerosene, turpentine and residual oil from fried foods) were prepared at concentrations of 0 to 100%. Diesel neat and mixtures were analyzed in a LED Fluorescence Spectrometer of Quimis Q-798FIL. These standards were analyzed in duplicate without any prior treatment being used the natural fluorescence of fluids, with quartz cuvettes of 1 cm. The standards were excited with violet LED and emission was detected from 335-1000 nm at intervals of 0.38 nm in LED spectrofluorimeter.

To assess the applicability of the fluorescence method for quantifying the adulterants content multivariate calibration models were developed by Partial Least Squares (PLS) using the software Unscrambler X 10.0.1. Through the PLS models fluorescence spectra are correlated with the corresponding values of the concentration of each adulterant. Each PLS was developed using mean centered fluorescence spectra as independent variables and the concentration values as dependent variables. In calibration step of each PLS, the relationship between spectra and concentration values was estimated from a set of reference samples, and in the validation step the results of the calibration were used to estimate the concentrations from samples that were not used in the calibration step. In this case, mixtures of diesel with adulterant (kerosene, turpentine or residual oil from fried foods).

3. Results and Discussion

3.1 Calibration of the PLS models

Table 1 shows the mixtures of each adulterant added to diesel (kerosene, turpentine and residual oil from fried foods) analyzed by LED spectroluorimetry and used in the construction of the multivariate calibration models that were developed by partial least squares (PLS) regression using the entire spectral and the entire calibration set described in Table 1. The PLS models were built using the whole fluorescent spectra as independent variables and the values of the concentrations of each adulterant in diesel as dependent variables (Table 1).

Table 1. Concentration of adulterant added to diesel used in the construction of the PLS models

Kerosene (%)	Turpentine (%)	Residual oil from fried foods (%)
0	0	0
2	2	2
4	4	4
6	6	6
8	8	8
10	10	10
20	20	20
30	30	30
40	40	40
50	50	50
60	60	60
70	70	70
80	80	80
90	90	90
100	100	100

Figures 1 and 2 present respectively fluorescence spectra and PLS for the mixtures of kerosene in diesel. The

coefficient of correlation of the curve presented near to 1 (0.9969) and R^2 of 0.99818 indicate the strength of the association between the two variables and the efficiency of the PLS to carry out the predictions. Figure 3 presents that two latent variables predicted 100% of the total variance (almost 100% for the first latent variable). Therefore, the model was proved useful to predict changes in concentration of turpentine added to diesel based on the fluorescence spectral variance.

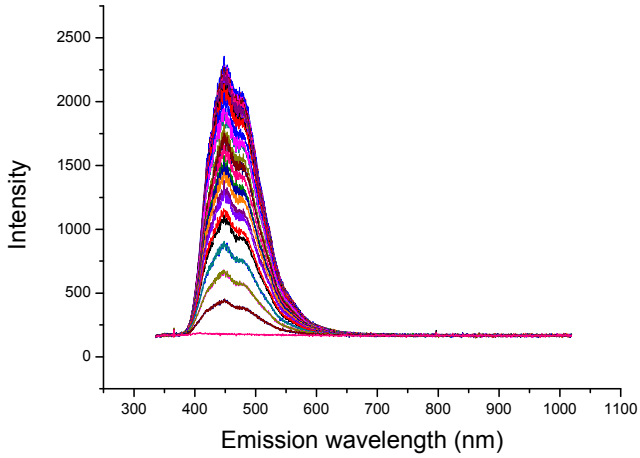

Figure 1. Fluorescence espectra of mixtures of kerosene in diesel (0-100%)

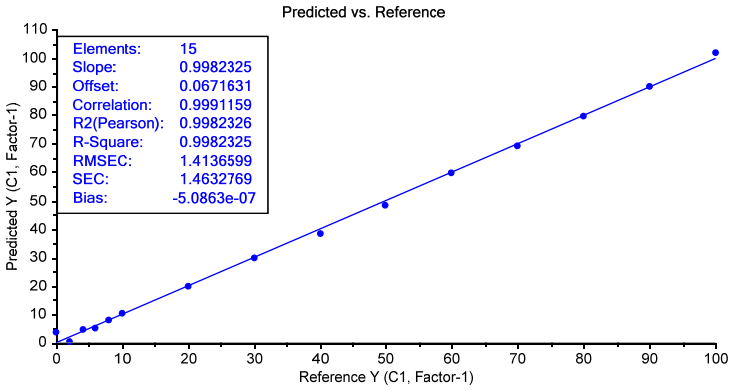

Figure 2. PLS model de mixtures of kerosene added to diesel

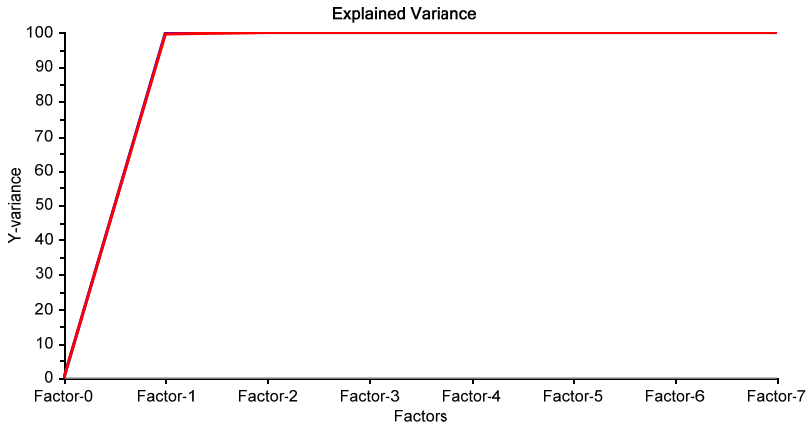

Figure 3. Explained variance of the PLS model de mixtures of kerosene added to diesel

Figures 4 and 5 present respectively fluorescence spectra and PLS for the mixtures of turpentine in diesel. The coefficient of correlation of the curve presented near to 1 (0.9991) and R^2 of 0.9982 indicate the strength of the association of the two variables and the efficiency of the PLS to carry out the predictions. Only two latent variables predicted almost 100% of the total variance (Figure 6).

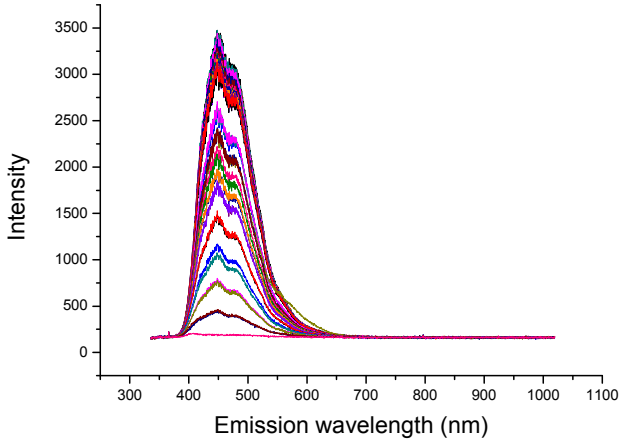

Figure 4. Fluorescence spectra for mixture of turpentine in diesel (0-100%)

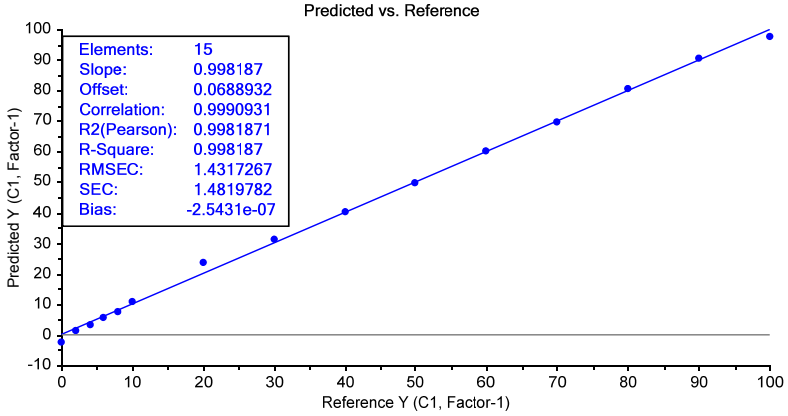

Figure 5. PLS model de mixtures of turpentine added to diesel

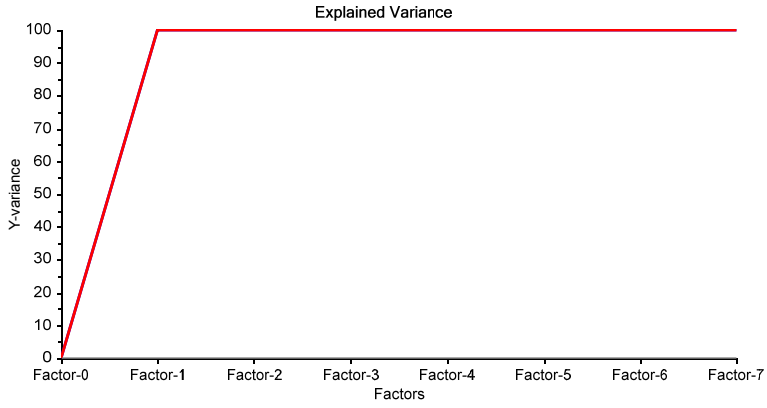

Figure 6. Explained variance of the PLS model de mixtures of turpentine added to diesel

Figures 7 and 8 present respectively fluorescence spectra and PLS for the mixtures of residual oil from fried foods in diesel. The coefficient of correlation of the curve presented near to 1 (0.9991) and R^2 of 0.9938 indicated the strength of the association of the two variables and the efficiency of the PLS to carry out the predictions. For mixtures of residual oil from fried foods added to diesel only two latent variables were shown to predict almost 100% of the total variance, 86% for the first and 13% for the second latent variable) (Figure 9). Therefore, the model was proved useful to predict changes in concentration of residual oil from fried foods added to diesel based on the fluorescence spectral variance.

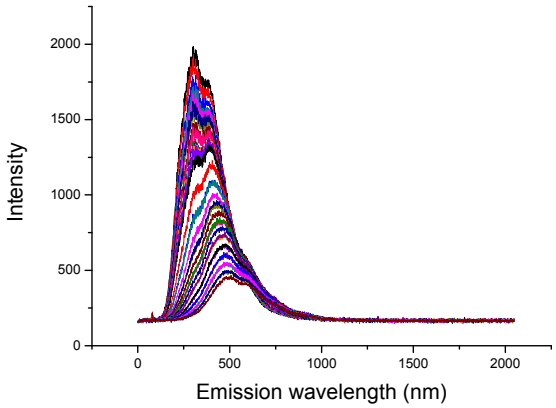

Figure 7. Fluorescence spectra for mixture of residual oil from fried foods in diesel (0-100%)

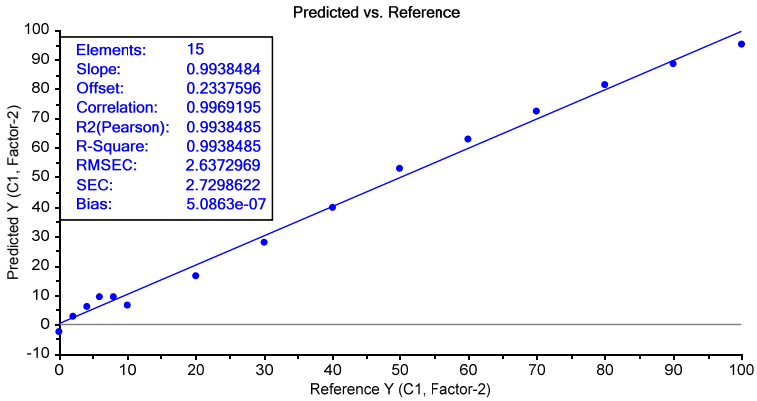

Figure 8. PLS model de mixtures of residual oil from fried foods added to diesel

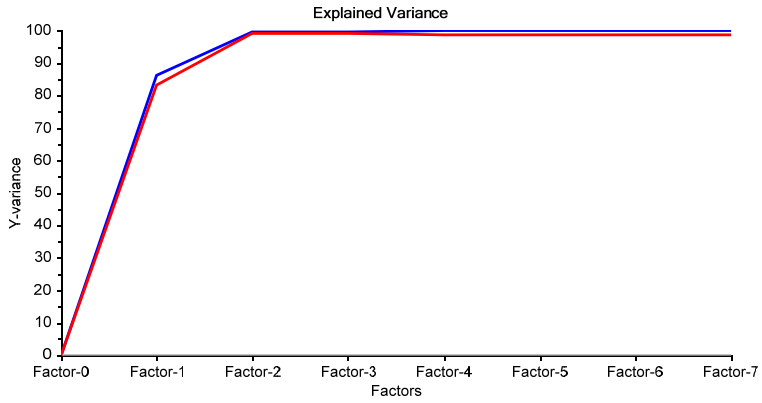

Figure 9. Explained variance of the PLS model de mixtures of residual oil from fried foods added to diesel

3.2 Validation of the PLS Models

The results of the calibration were used to estimate the concentrations from samples that were not used in the PLS models. The concentration values of the mixtures of diesel with adulterant (kerosene, turpentine or residual oil from fried foods) used in this validation procedure are show in the Table 2. The mixtures of each adulterant added to diesel were analyzed by LED values. Table 2 also shows the values of the concentrations predicted by the PLS models. For mixtures of turpentine in diesel and residual oil in diesel some anomalous samples determined by the software Unscrambler were excluded of the data set of validation.

Table 2. Concentration values of the mixtures of diesel with adulterant (kerosene, turpentine or residual oil from fried foods) used in validation procedure

Kerosene		**Turpetine**		**Residual oil from fried foods**	
Reference concentration (%)	**Predicted concentration (%)**	**Reference concentration (%)**	**Predicted concentration (%)**	**Reference concentration (%)**	**Predicted concentration (%)**
4	4.447487	4	2.275425	4	4.882298
6	7.13217	6	6.629976	8	7.487326
7	6.610565	7	6.524025	9	8.7575
8	6.716967	8	8.505703	20	16.39527
9	10.24765	9	10.05119	25	22.19561
10	11.11698	10	8.880089	35	32.90361
15	15.35029	20	23.57909	40	38.77464
20	19.18914	30	31.68184	45	45.54182
25	26.73995	35	37.47498	50	52.12151
30	29.39688	45	44.97174	60	62.11739
35	33.88729	50	49.81948	70	72.27793
40	40.12534	60	59.53387	80	80.72224
45	43.4324	70	72.39371	90	88.56984
50	50.78994	80	81.3277		
60	56.99543	90	90.1039		
70	69.38918				
80	79.42979				
90	90.06597				

4. Conclusion

The association of spectrofluorimetry and PLS was suitable for predict the concentration of adulterants (kerosene, turpentine or residual oil from fried foods) added to diesel

The advantages of the fluorescence spectroscopy inducted by LED, such as simplicity, quickness, low-cost suggest this method as a analytical procedure for the evaluation of the concentration of adulterants previously identified qualitatively in diesel.

The R^2 near to 1 for mixtures of diesel with kerosene, turpentine and residual oil from fried foods indicated the accuracy of the models to predict concentrations values of this adulterants added to diesel.

Acknowledgements

We acknowledge the CNPq, FAPESB and CAPES for technological scholarships and financial support.

References

Brandão, L. F. P., Braga, J. W. B., & Suarez, P. A. Z. (2012). Determination of vegetable oils and fats adulterants

in diesel oil by high performance liquid chromatography and multivariate methods. *Journal of Chromatography A, 1225*, 150-157. http://dx.doi.org/10.1016/j.chroma.2011.12.076

Corgozinho, C. N. C., Pasa, V. M. D., & Barbeira, P. J. S. (2008). Determination of residual oil in diesel oil by spectrofluorimetric and chemometric analysis. *Talanta, 76*, 479-484. http://dx.doi.org/10.1016/j.talanta.2008.03.003

Gaydou, V., Kister, J., & Dupuy. N. (2011). Evaluation of multiblock NIR/MIR PLS predictive models to detect adulteration of diesel/biodiesel blends by vegetal oil. *Chemom Intell Lab Syst, 106*, 190-197. http://dx.doi.org/ 10.1016/j.chemolab.2010.05.002

Meira, M., Quintella, C. M., Ferrer, T. M., Silva, H. R. G., Guimarães, A. K., Santos, M. A., … Pepe, I. M. (2011). Identification of adulteration of biofuel by addition of residual oil instead of biodiesel to the diesel by total spectrofluorimetry and principal component analysis. *Quim Nova, 34*, 621-624. http://dx.doi.org/10.1590/S0100-40422011000400013

Oliveira, F. C. C., Brandão, C. R. R., Ramalho, H. F., Costa, L. A. F., Suarez, P. A. Z., & Rubim, J. C. (2007). Adulteration of diesel/biodiesel blends by vegetable oil as determined by Fourier transform (FT) near infrared spectrometry and FT-Raman spectroscopy. *Anal. Chim. Acta., 587*, 194-199. http://dx.doi.org/10.1016/j.aca.2007.01.045

Patra, D., & Mishra, A. K. (2002). Study of diesel fuel contamination by excitation emission matrix spectral subtraction fluorescence. *Anal. Chim. Acta, 454*, 209-215. http://dx.doi.org/10.1016/S0003-2670(01)01568-9

Pontes, M. J. C., Pereira, C. F., Pimentel, M. F., Vasconcelos, F. V. C., & Silva, A. G. B. (2011). Screening analysis to detect adulteration in diesel/biodiesel blends using near infrared spectrometry and multivariate classification. *Talanta, 85*, 2159-2165. http://dx.doi.org/10.1016/j.talanta.2011.07.064

Quintella, C. M, Guimarães, A. K., Musse, A. P., & Patent, B. R. (2009). PI000022080730742-1.

Quintella, C. M., Meira, M., Silva, H. R. G., Guimarães, A. K., Ferrer, T. M., Santos, M. A., ... Pepe, I. M. (2011). Patent BR PI 011110000662.

Roy, S. (1999). Fiber optic sensor for determining adulteration of petrol and diesel by kerosene. *Sensors Actuat B: Chem. Actuat. B*: *Chemical, 55*, 212-216. http://dx.doi.org/10.1016/S0925-4005(99)00171-9

Souza, L. M., Mitsutake, H., Gontijo, L. C., & Borges, N. W. (2014). Quantification of residual automotive lubricant oil as an adulterant in Brazilian S-10 diesel using MIR spectroscopy and PLS. *Fuel, 15*, 257-262. http://dx.doi.org/10.1016/j.fuel.2014.03.051

Vasconcelos, F. V. C., Souza, Jr., P. F. B., Pimentel, M. F., Pontes, M. J. C., & Pereira, C. F. (2012). Using near-infrared overtone regions to determine biodiesel content and adulteration of diesel/biodiesel blends with vegetable oils. *Anal. Chim. Acta, 716*, 101-107. http://dx.doi.org/10.1016/j.aca.2011.12.027

Young, I. T., Garini, Y., Dietrich, H. R. C., van Oel, W., & Liqui Lung, G. (2004). LEDs for fluorescence microscopy. *Proc. of SPIE, 5324*, 208-215. http://dx.doi.org/10.1117/12.525932

International Journal of Chemistry; Vol. 6, No. 4; 2014
ISSN 1916-9698 E-ISSN 1916-9701
Published by Canadian Center of Science and Education

Identification of Adulteration of Olive Oil with Other Edible Oils by LED-induced Fluorescence and Multivariate Calibration

Marilena Meira[1], Cristina M. Quintella[2], Erika M. de O. Ribeiro[2], Mariana A. Santos[3], Saionara Luna[2], & Alexandre Lopes Del Cid[2]

[1]Instituto Federal de Educação, Ciência e Tecnologia da Bahia – IFBA, Campus de Simões Filho, BA, Brazil. CEP: 43.700-000.

[2]Instituto de Química, Universidade Federal da Bahia, Campus de Ondina, Salvador, BA, Brazil. CEP: 40.170-290.

[3]Instituto Federal de Educação, Ciência e Tecnologia da Bahia– IFBA, Campus Salvador, BA, Brazil, CEP: 40110-150.

Correspondence: Marilena Meira, Instituto Federal de Educação, Ciência e Tecnologia da Bahia – IFBA, Campus de Simões Filho, BA, Brazil, CEP: 43.700-000. E-mail: marilenameira@gmail.com

Received: July 28, 2014 Accepted: August 18, 2014 Online Published: October 24, 2014

doi:10.5539/ijc.v6n4p31 URL: http://dx.doi.org/10.5539/ijc.v6n4p31

Abstract

The most common adulterants found in extra-virgin olive oil are refined olive oil and other vegetable oils, such as sunflower, soybean, corn, and canola. In addition to constituting economic fraud, adulteration can cause serious damage to the health of the consumer. This study focuses on the detection and quantification of the adulteration of extra-virgin olive oil with edible oils, using spectrofluorimetry and chemometrics. The data were analyzed by Principal Components Analysis (PCA) and Partial Least Squares (PLS) analysis. Through PCA, it was possible to separate the samples into two distinct areas, olive oil and other edible oils, based on their chemical composition. The PLS model, built with the spectra of mixtures of soybean oil in extra-virgin olive oil, exhibited an R^2 of 0.99412 and low RMSEP (Root Mean Square Error of Prediction) (3.59), RMSEC (Root Mean Square Error of Calibration) (2.32) and bias (4.77. 10^{-7}) values. Thus, the PLS model was considered exact for calibration and prediction.

Keywords: virgin and extra-virgin olive oil, adulterations, fluorescence, PCA, PLS.

1. Introduction

Olive oil is a type of oil produced from the fruit of the olive tree. The name “olive oil” can only be applied to pure oil obtained from olives, not to mixtures composed of this oil and other oils such as soybean or corn, which are generically known as oil compounds. The use of olive oil dates back millennia, but its exact origin is unknown. Olive cultivation has occurred for more than 5000 years. The Phoenicians, Syrians, and Armenians were the first people to consume olive oil, and it was introduced to Europe and the West by the Greeks and Romans. For a long time, the consumption of olive oil was restricted to the Mediterranean, but in the sixteenth century, the Spaniards reported its use in the regions of South America, Central America, and the United States. There are records detailing the use of olive oil 5000 years ago by Mesopotamian peoples, who anointed their bodies with oil to protect themselves from extreme cold. In the Roman Empire, olive oil was used to soften skin and dry hair. In Greece, athletes used the oil to improve their performance. In the sixteenth century, olive oil was the basis for many drugs (Oliva, 2011).

The importance of olive oil has grown over the years due to its multiple uses in food, medicine, hygiene, and cosmetics. Many of the benefits of olive oil vaunted by popular wisdom have been proven by several scientific studies. The major differentiation of olive oil from other edible oils is associated with the higher content of monounsaturated fatty acids such as oleic acid, and reduced content of saturated fatty acids, which assist in the control of cholesterol in the blood, helping to reduce “bad” cholesterol (LDL) while maintaining an appropriate level of “good” cholesterol (HDL) (Huang & Sumpio, 2008; Van Tol *et al*., 1999). Olive oil also distinguishes

itself by its high level of the triterpene squalene, which promotes the excretion of toxins and has anticarcinogenic effects. The presence of steroids such as ß-sitosterol helps to lower cholesterol and to aid in the prevention and treatment of prostate cancer, colon cancer and breast cancer (Menendez *et al*., 2006). Olive oil also has phenolic compounds, vitamin E and β-carotene, which are powerful antioxidants that react with free radicals, thus inhibiting platelet aggregation and preventing LDL oxidation (Aguilera *et al*., 2004). Due to its composition, olive oil provides a major contribution to the prevention and treatment of many diseases such as atherosclerosis (Acń *et al*., 2005), thrombosis (De La Cruz *et al*., 2000), diabetes mellitus (De La Cruz *et al*., 2010), biliary disease, cataracts and eye diseases (Aparicio-Ruiz, Mńguez-Mosquera & Gandul-Rojas, 2011), depression (Logan, 2005), bone mineralization (Coxam, Puel & Davicco, 2010), hypertension (Perona *et al*., 2004), and cancer (breast, prostate, digestive tract) (Fabiani & Morozzi, 2010; Fernández-Arroyo *et al*., 2012; Flynn & Mega, 2010; Menendez *et al*., 2006). In addition, regular consumption of olive oil has a protective effect against free radicals in the skin, and increases life expectancy because it strengthens the immune system and protects against memory loss due to age (Viola & Viola, 2009; Baccouri *et al*., 2008).

According to the Brazilian Association of Producers, Importers and Traders of Olive Oil (Oliva, 2011), olive oil is graded based on organoleptic characteristics (taste and aroma), chemistry (acidity and other chemical data) and the following three types of extraction:

- Extra-virgin olive oil is produced by a mechanical pressing extraction process. It has flawless flavor and taste and less than 1% acidity.
- Olive oil is also produced by a mechanical pressing extraction process. It has outstanding flavor and aroma with acidity below 2%.
- Pure olive oil is formed by blending refined olive oil and virgin olive oil and has less than 1.5% acidity.

Olive pomace is one of the main sub-products of the processing of olives after pressing to extract the oil. The olive residue has a low oil content and low oxidative stability due to a moisture content that accelerates the hydrolysis of triacylglycerol. Generally, olive oil from the pomace is extracted with solvent and subjected to the refining process, including neutralization, bleaching and deodorizing.

Due to its low price, sometimes refined oil is used to adulterate olive oil of better quality, such as pure, virgin and extra-virgin olive oil. Similarly, due to lower market prices, edible oils such as soybean, corn, canola, cotton, sunflower, peanut and almond are likely to be used as illicit adulterants of olive oil. Therefore, a rapid method to detect adulteration is important for purposes of quality control and labeling olive oils of better quality (Guimet, Ferré & Boqué, 2005).

Several analytical methodologies have been developed in recent years to ensure the authenticity of olive oil. These methods include chromatographic techniques (Bosque-Sendra *et al*., 2012; Baccouri *et al*., 2008) and spectroscopic techniques, such as mass spectrometry (Calvano *et al*., 2012), Nuclear Magnetic Resonance (NMR) (Fragaki *et al*., 2005), near-infrared spectroscopy (Mignani *et al*., 2011), Raman spectroscopy (Dong *et al*., 2012), chemiluminescence (Papadopoulos *et al*., 2002), fluorescence spectroscopy (Sikorska, Khmelinskii & Sikorski, 2012), and synchronous fluorescence (Poulli, Mousdis & Georgiou, 2007).

This study focuses on the detection and quantification of adulteration of extra-virgin olive oil with edible oils, using a combination of LED-induced spectrofluorimetry and chemometrics.

2. Materials and Methods

2.1 Samples

Oils were purchased from a supplier located in Salvador in Bahia, Brazil.We used 56 samples of oils, 10 being of extra-virgin olive oil, 10 of soybean, 13 of corn, 10 of canola and 13 of sunflower.

Mixtures of extra-virgin olive oil with adulterants

Mixtures of extra-virgin olive oil with soybean oil as an adulterant were analyzed at 0%, 5%, 10%, 15%, 30%, 35%, 45%, 50%, 55%, 60%, 65%, 70%, 75%, 85%, 90% and 100%.

2.2 Principal Component Analysis

A Perkin Elmer-LS55 spectrofluorometer (U.S.A.) and 1 cm quartz cuvettes were used. The fluorescent emission spectra of the samples were obtained at 230-800 nm in intervals of 0.5 nm, while the sample was excited at wavelengths from 200-775 nm with increments of 25 nm. A total of 24 excitation wavelengths and 1142 emission wavelengths were obtained for each sample. The measurements were made with a slit of 2.5 nm and a scan speed of 1200 nm/min. The spectrofluorimetric maps were generated with Origin8.0®.

For PCA of pure samples, the spectra were initially organized in a cube with the following dimensions: 5 samples x 1142 emission wavelengths x 24 excitation wavelengths. The cube was transformed by the command unfoldm in MatLab6.1® to generate a general matrix with dimensions of 5 x 27408. This matrix was mean centered and then subjected to multivariate analysis with MatLab6.1®.

2.3 PLS Analysis

For the PLS analysis, mixtures of extra-virgin olive oil with soybean oil were assessed using a Quimis LED spectrofluorometer model Q-798FIL (Brazil) equipped with a violet LED centered at 400 nm, and the emission was captured in the range of 400-1018 nm. The amount of soybean oil added to the extra-virgin olive oil is described in Table 1.

Table 1. Mixtures of extra-virgin olive oil and soybean oil in the range of 0-100%.

Sample number	% Soybean oil	% Extra-virgin olive oil
1	0	100
2	5	95
3	10	90
4	15	85
5	30	70
6	35	65
7	45	55
8	50	50
9	55	45
10	60	40
11	65	35
12	70	30
13	75	25
14	85	15
15	90	10
16	100	0

3. Results and Discussion

3.1 Fluorescence Maps

Comparing the fluorescence maps of extra-virgin olive oil (Figure 1) with other oils (Figure 2) shows that the extra-virgin olive oil has an emission-excitation band concentrated in three distinct regions, with peaks at 375 nm excitation and 520 nm emission, 325 nm excitation and 400 nm emission, and 375 nm excitation and 430 nm emission. The other oils have concentrated bands at approximately 350 nm excitation and 450 nm emission.

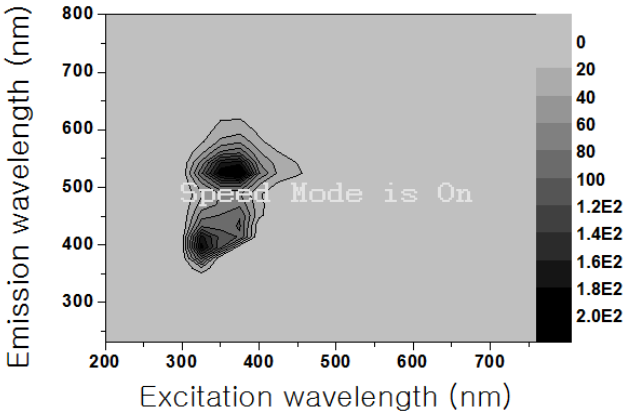

Figure 1. Contour map of the fluorescence spectra of extra-virgin olive oil.

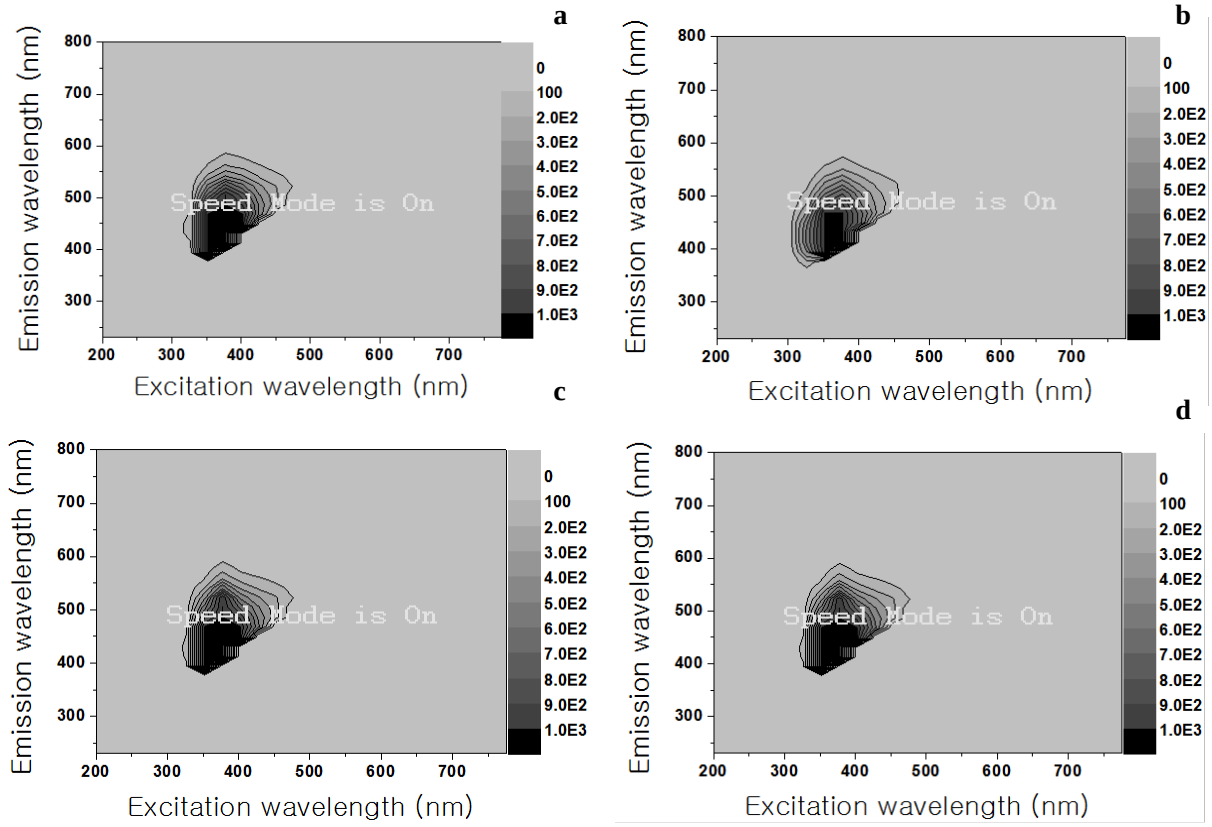

Figure 2. Contour maps of the fluorescence spectra of canola (a), sunflower (b), corn (c) and soybean (d).

3.2 PCA of Pure Samples

Through PCA, we found that only two principal components (PC) explained 89.87 % of the variance of the data, 79.33 % by PC1 and 10.54% by PC2. PC1 separated the samples by their chemical composition into two distinct areas, olive oil and other edible oils (Figure 3). The sample of extra-virgin olive oil has negative scores, and the samples of vegetable oils have positive scores.

The different fatty acid compositions of olive oil and other oils (ANVISA, 1999; Lee *et al*., 1998; Kim *et al*., 2010) may explain the differences found among the excitation-emission matrices shown by PCA. Extra-virgin olive oil is rich in oleic acid (55-83%), which is monounsaturated, while corn, soybean and sunflower oils predominantly contain polyunsaturated fatty acids. Sunflower oil has the highest content of linoleic acid (55-75%), which has two double bonds. Canola oil has an oleic acid composition similar to that of olive oil. However, canola oil has 5-13% linolenic acid (three double bonds), while olive oil has less than 0.9%. In addition, because extra-virgin olive oil is pressed, it retains higher levels of other fluorophores such as tocopherols, β-carotene and phenolic compounds that are refined out of other oils.

The spectra that most influenced the separation of extra-virgin olive oil (PC1 negative) from other vegetable oils (PC1 positive) were the peaks at 325 nm excitation and 382, 523 nm emission on the negative axis, and at 350, 375, 400 nm excitation and 440, 452, 459 nm emission, respectively, on the positive axis.

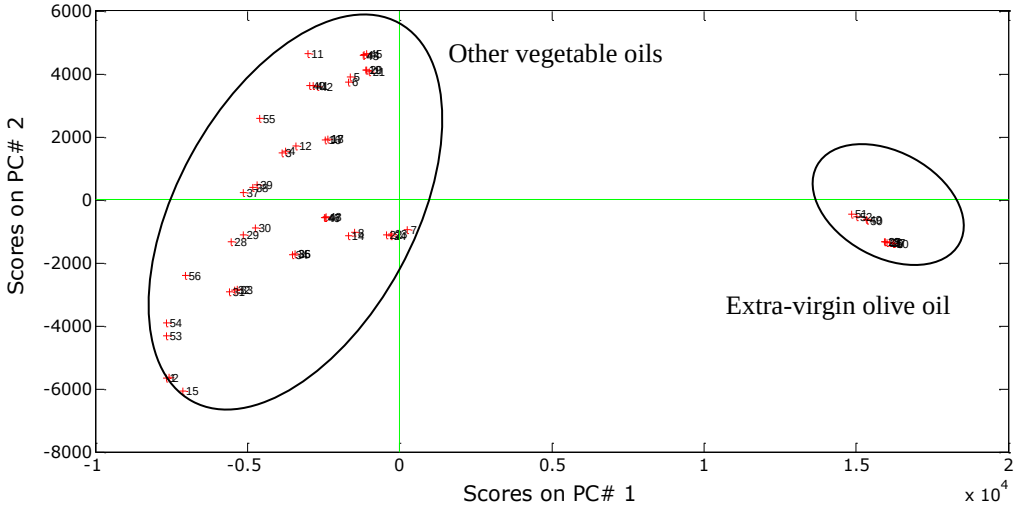

Figure 3. PC1 x PC2 scores for samples of extra virgin olive oil and other vegetable oils (corn, soybean, canola and sunflower)

3.3 PLS of spectra of mixtures of soybean oil in extra-virgin olive oil

Through the Partial Least Squares (PLS) multivariate calibration technique, it was possible to build a model correlating the concentration of extra-virgin olive oil with the fluorescence spectra. The PLS model had an R^2 of 0.99412 and low RMSEP (3.59), RMSEC (2.32) and bias (4.77. 10-7) values. Thus, one can consider the model exact for both calibration and prediction (Figure 4).

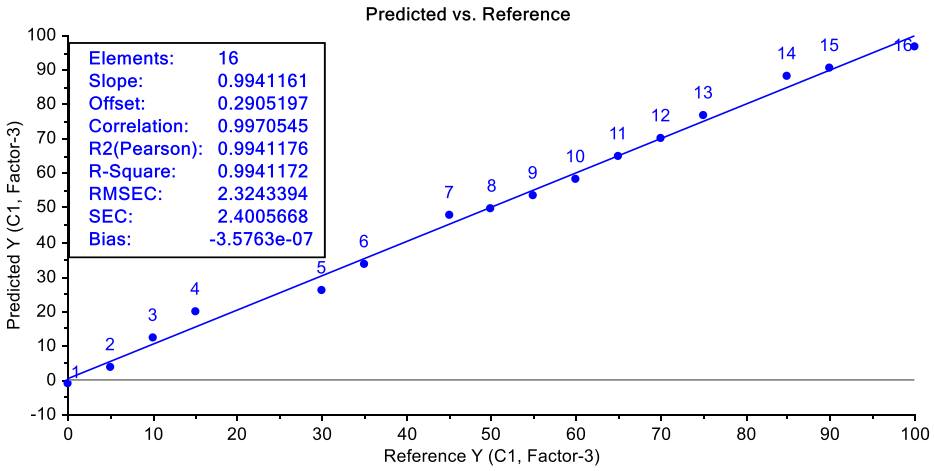

Figure 4. PLS mixtures of olive oil, extra-virgin olive oil and soybean oil in the range of 0-100%

4. Conclusions

Due to lower market prices, edible oils such as soybean, corn, canola, and sunflower are likely to be used as adulterants of extra-virgin olive oil for illicit enrichment. The method proposed in this paper, which combined spectrofluorimetry with PCA and PLS, was characterized as fast and accurate in detecting tampering and has the potential to be used for quality control and labeling of the best-quality olive oils.

Acknowledgments

The authors thank Fapesb and CNPq for financial aid and scholarships.

References

Ac ń, S., Navarro, M.A., Carnicer, R., Arbon és-Mainar, J.M., Guzm án, M.A., Arnal, C., Beltr án, G., Uceda, M., Maeda, N., & Osada, J. (2005). Dietary cholesterol suppresses the ability of olive oil to delay the

development of atherosclerotic lesions in apolipoprotein E knockout mice. *Atherosclerosis. 182*(1), 17-28. http://dx.doi.org/10.1016/j.atherosclerosis.2005.01.050

Aguilera, C.M., Mesa, M.D., Ramirez-Tortosa, M.C., Nestares, M.T., Ros, E. Gil, A. (2004). Sunflower oil does not protect against LDL oxidation as virgin olive oil does in patients with peripheral vascular disease. *Clinical Nutrition*. *23*(4), 673-681. http://dx.doi.org/10.1016/j.clnu.2003.11.005

ANVISA. Resolução nº 482. (1999). Regulamento técnico para fixação de identidade e qualidade de óleos e gorduras vegetais. *Diário Oficial da República Federativa do Brasil*.

Aparicio-Ruiz, R., Mínguez-Mosquera, M.I., & Gandul-Rojas, B. (2011). Thermal degradation kinetics of lutein, β-carotene and β-cryptoxanthin in virgin olive oils. *Journal of Food Composition*, *24*(6), 811-820. http://dx.doi.org/10.1016/j.jfca.2011.04.009

Baccouri, O., Guerfel, M., Baccouri, B., Cerretani, L., Bendini, A., Lercker, G., Zarrouk, M., & Miled, D.D.B. (2008). Chemical composition and oxidative stability of Tunisian monovarietal virgin olive oils with regard to fruit ripening. *Food Chemistry*. *109* (4), 743-754. http://dx.doi.org/10.1016/j.foodchem.2008.01.034

Bosque-Sendra, J.M., Cuadros-Rodríguez, L., Ruiz-Samblás, C., & De La Mata, A.P. (2012). Combining chromatography and chemometrics for the characterization and authentication of fats and oils from triacylglycerol compositional data: A review. *Analytica Chimica Acta*, *724*, 1-11. http://dx.doi.org/10.1016/j.aca.2012.02.041

Calvano, C.D., De Ceglie, C., D'Accolti, L., & Zambonin, C.G. (2012). MALDI-TOF mass spectrometry detection of extra-virgin olive oil adulteration with hazelnut oil by analysis of phospholipids using an ionic liquid as matrix and extraction solvent. *Food Chemistry*, *134*(2), 1192-1198. http://dx.doi.org/10.1016/j.foodchem.2012.02.154

Coxam, V., & Puel, C. Davicco, M.J. (2010). Olives and olive oil in the prevention of osteoporosis. In Victor R. Preedy and Ronald Watson (Eds.), *Olives and olive oil in health and disease prevention*, 1195-1203. Elsevier.

De La Cruz, J.P., Villalobos, M.A., Carmona, J.A., Martín-Romero, M., Smith-Agreda, J.M., & De La Cuesta, F.S. (2000). Antithrombotic potential of olive oil administration in rabbits with elevated cholesterol. *Thrombosis Research*, *100*(4), 305-315. http://dx.doi.org/10.1016/S0049-3848(00)00321-2

De La Cruz, J.P., Del Río, S., Arrebola, M.M., López-Villodres, J.A., Jebrouni, N., & González-Correa, J.A. (2010). Effect of virgin olive oil plus acetylsalicylic acid on brain slices damage after hypoxia-reoxygenation in rats with type 1-like diabetes mellitus. *Neuroscience Letters*. *471*(2,3), 89-93. http://dx.doi.org/10.1016/j.neulet.2010.01.017

Dong, W., Zhang, Y., Zhang, B., & Wang, X. (2012). Quantitative analysis of adulteration of extra virgin olive oil using Raman spectroscopy improved by Bayesian framework least squares support vector machines. *Analytical Methods*, *4*, 2772-2777. http://dx.doi.org/10.1039/C2AY25431J

Fabiani, R., & Morozzi, G. (2010). Anticarcinogenic properties of olive oil phenols: Effects on proliferation, apoptosis and differentiation. In Victor R. Preedy and Ronald Watson (Eds.), *Olives and olive oil in health and disease*, pp. 981-988. Elsevier.

Fernández-Arroyo, S., Gómez-Martínez, A., Rocamora-Reverte, L., Quirantes-Piné, R., Segura-Carretero, A., Fernández-Gutiérrez, A., & Ferragut, J.A. (2012). Application of nanoLC-ESI-TOF-MS for the metabolomic analysis of phenolic compounds from extra-virgin olive oil in treated colon-cancer cells. *Journal of Pharmaceutical and Biomedical Analysis*, *63*, 128-134. http://dx.doi.org/10.1016/j.jpba.2012.01.033

Flynn, M.M., & Mega, A. (2010). Treating Recurrent prostate cancer with a plant-based, olive oil diet. *Journal of the American Dietetic Association*, *110*(9), Supplement, A12. http://dx.doi.org/10.1016/j.jada.2010.06.037

Fragaki, G., Spyros, A., Siragakis, G., Salivaras, E., Dais, P. (2005). Detection of extra virgin olive oil adulteration with lampante olive oil and refined olive oil using nuclear magnetic resonance spectroscopy and multivariate statistical analysis. *Journal of Agricultural and Food Chemistry*, *53*(8), 2810-2816. http://dx.doi.org/10.1021/jf040279t

Guimet, F., Ferré, J., Boqué, R. (2005). Rapid detection of olive–pomace oil adulteration in extra virgin olive oils from the protected denomination of origin "Siurana" using excitation–emission fluorescence spectroscopy and three-way methods of analysis. *Analytica Chimica Acta*, *544*(1, 2), 143-152.

http://dx.doi.org/10.1016/j.aca.2005.02.013

Huang, C.L., Sumpio, B.E. (2008). Olive oil, the Mediterranean diet, and cardiovascular health. *Journal of the American College, 207*(3), 407-416. http://dx.doi.org/10.1016/j.jamcollsurg.2008.02.018

Kim, J., Kim, D.N., Lee, S.H., Yoo, S.H., Lee, S. (2010). Correlation of fatty acid composition of vegetable oils with rheological behaviour and oil uptake. *Food Chemistry, 118*(2), 398-402. http://dx.doi.org/10.1016/j.foodchem.2009.05.011

Lee, D.S., Noh, B.S., Bae, S.Y., Kim, K. (1998). Characterization of fatty acids composition in vegetable oils by gas chromatography and chemometrics. *Analytica Chimica Acta, 358*(2), 163-175. http://dx.doi.org/10.1016/S0003-2670(97)00574-6

Logan, A.C. (2005). Omega-3 and depression research: Hold the olive oil. *Prostaglandins, Leukotrienes and Essential Fatty Acids, 72*(6), 441. http://dx.doi.org/10.1016/j.plefa.2005.02.006

Menendez, J.A., Papadimitropoulou, A., Vellon, L., Lupu, R. (2006). A genomic explanation connecting "Mediterranean diet", olive oil and cancer: Oleic acid, the main monounsaturated fatty acid of olive oil, induces formation of inhibitory "PEA3 transcription factor-PEA3 DNA binding site" complexes at the Her-2/neu (erbB-2) oncogene promoter in breast, ovarian and stomach cancer cells. *European Journal of Cancer, 42*(15), 2425-2432. http://dx.doi.org/10.1016/j.ejca.2005.10.016

Mignani, A.G., Ciaccheri, L., Ottevaere, H., Thienpont, H., Conte, L., Marega, M. *et al.* (2011). Visible and near-infrared absorption spectroscopy by an integrating sphere and optical fibers for quantifying and discriminating the adulteration of extra virgin olive oil from Tuscany. *Analytical and Bioanaytical Chemistry, 399*(3), 1315–1324. http://dx.doi.org/10.1007/s00216-010-4408-y

OLIVA: Conhecendo melhor o azeite de oliva, 2011. URL: http://www.oliva.org.br/conhecendo-o-azeite.php. Accessed 19 07.13.

Papadopoulos, K., Triantis, T., Tzikis, C.H., Nikokavoura, A., & Dimotikali, D. (2002). Investigations of extra virgin olive oils with seed oils using weak chemiluminescence. *Analytica Chimica Acta, 464*(1), 135-140. http://dx.doi.org/10.1016/S0003-2670(02)00436-1

Perona, J.S., Cañizares, J., Montero, E., Sánchez-Domínguez, J.M., Catalá, A., & Ruiz-Gutiérrez, V. (2004). Virgin olive oil reduces blood pressure in hypertensive elderly subjects. *Clinical Nutrition, 23*(5), 1113-1121. http://dx.doi.org/10.1016/j.clnu.2004.02.004

Poulli, K.I., Mousdis, G.A., & Georgiou, C.A. (2007). Rapid synchronous fluorescence method for virgin olive oil adulteration assessment, *105*, 369-375. http://dx.doi.org/10.1016/j.foodchem.2006.12.021

Sikorska, E., Khmelinskii, I., & Sikorski, M. (2012). Analysis of olive oils by fluorescence spectroscopy: Methods and applications. In Boskou Dimitrios (Ed.), Agricultural and Biological Sciences – Olive Oil – Constituents, Quality, Health Properties and Bioconversions**,** pp.63-88. http://dx.doi.org/10.5772/30676

Van Tol, A., Terpstra, A.H.M., Van den Berg, P., & Beynen, A.C. (1999). Dietary corn oil versus olive oil enhances HDL protein turnover and lowers HDL cholesterol levels in hamsters. *Atherosclerosis, 147*(1), 87-94. http://dx.doi.org/10.1016/S0021-9150(99)00167-7

Viola, P., & Viola, M. (2009). Virgin olive oil as a fundamental nutritional component and skin protector. *Clinics in Dermatology, 27*(2), 159-165. http://dx.doi.org/10.1016/j.clindermatol.2008.01.008

International Journal of Chemistry; Vol. 6, No. 4; 2014
ISSN 1916-9698 E-ISSN 1916-9701
Published by Canadian Center of Science and Education

Numerical Simulation of Black Oil-three Compound Combination Flooding

Yirang Yuan[1], Aijie Cheng[1], Danping Yang[1] & Changfeng Li[1,2]

[1] School of Mathematics, Shandong University, Jinan, China

[2] School of Economics, Shandong University, Jinan, China

Correspondence: Yirang Yuan, School of Mathematics, Shandong University, Jinan, Shandananlu 27, China. Tel: 86-531-8836-4732. E-mail: yryuan@sdu.edu.cn

Received: July 28, 2014 Accepted: September 9, 2014 Online Published: October 25, 2014

doi:10.5539/ijc.v6n4p38 URL: http://dx.doi.org/10.5539/ijc.v6n4p38

The research is financed by the National Tackling Key Project (Grant Nos: 2011ZX05011-004, 2011ZX05052, 20050200069), National Natural Science Foundation of China (Grant Nos: 11101244, 11271231, 10771124, 10372052), National Doctoral Foundation (Grant No: 20030422047) and Natural Science Foundation of Shandong Province (Grant No: ZR2011AM015)

Abstract

Numerical methods of permeation fluid mechanics for black oil (water, oil and gas)--three compound combination flooding (polymer, surface active agent and alkali) in porous media is discussed in this paper. In view of petroleum geology, geochemistry, computational mechanics of flow and computer technology, a mechanics model of three-phase flow (water, oil and gas)--three compound combination flooding (the polymer, surface active agent and alkali) is presented firstly, then the characters and the application are stated in this paper. A numerical algorithm consisting of a full implicit program, an implicit computation for the pressure and an implicit/explicit program respective for the pressure and the concentration is given by structuring an upstream sequence and an iterative algorithm of implicit fined upwind fractional step finite difference to solve the pressure equation, the saturation equation and the concentration of chemical substance components and the petroleum acid concentration equation. This program runs quickly and is of high accuracy. The design of this software is given and can be applied in major industries, which is made up on ten-meters steps, hundreds of thousands nodes and tens of years and has been carried out successfully in analysis and simulation of national major oil-fields extraction such as Daqing Oilfield, Shengli Oilfield and Dagang Oilfield and others, which gives rise to outstanding economic and social benefits. A precise analysis is given for a simplified model and the numerical simulation system depends on mathematics and mechanics. An idea is presented to solve this international famous problem.

Keywords: three compound combination flooding (the polymer, surface active agent, alkali), permeation fluid mechanics of black oil (water, oil and gas), model and numerical simulation, actual application of oil fields, theoretical analysis

1. Introduction

A popular numerical simulation way, water flooding, is applied in the world to keep the reservoir pressure, and the recovery efficiency is more outstanding than any other natural exploring forms. This gives more benefits and helps Chinese oil fields keep high quantity production. It continues to be more important how a strategic project works to develop the exploiting efficiency of crude oil in the way of water-flooding driving.

There remains plenty of residual crude oil in the reservoir after water-flooding exploiting because the constraint of capillary force weakens the motion and the volume of influenced regions is small due to the disadvantageous fluidity ratio between displacement phase and driven phase. Then it is more important to develop the displacement efficiency. A popular method is considered that the mixture is injected into the underground fluid including chemical addition agents such as polymer, surface active agent and alkali. The polymer can optimize the fluidity of displacement phase, modify the ratio with respect to driven phases, balance the leading edges well, weaken the inner porous layer flow, improve the efficiency of displacement phase and increase the pressure

gradient. Surface active agent and alkali can decrease interfacial tensions of different phases, then make the bounded oil move and gather.

Some hypotheses are given as follows to find the mathematical models. The mixture fluid flows along isothermal curves, different phases keep equilibrium state, different components have no chemical reaction and expanded Darcy Theory holds and so on. In view of the pressure $p(x,t)$ and the saturation $c_i(x,t)$, the flow equation and convection-diffusion equations are derived with corresponding boundary value conditions and initial conditions.

The mass balance relation of multi-phase, multi-components and slight compressible mixture is formulated by a nonlinear coupled partial differential equations. It is hard to solve this system because many modern numerical methods such as mixed element, finite element, finite difference and numerical algebra, will be involved in the simulation. In general speaking, based on physical meanings the pressure function is solved by an implicit scheme and the concentration values are obtained by an explicit solver or an implicit solver. The scholars try to find good ways analyzing the data and numerical results and accomplishing some research work in simulation, and the results can describe the whole process of chemistry displacements very well and help the engineers control the rules and process of displacement and forecast the recovery efficiency of natural oil and compute the oil percentage of output liquid and the percent of polymer and surface active agent. By numerical research the curves describing different components motion are shown, and some plans are made about the beginning and end of injected liquid and some related parameters of natural oil efficiency are derived. These conclusions, important techniques in chemistry displacements, can used in forecasting the characters of fields, choosing different optimization plans, establishing the models of chemical displacements of reservoir, completing computational software and carrying out the numerical simulation. Petroleum engineers and mathematicians pay more attention to modern new techniques of exploiting natural oil.

Yuan visited United States and accomplished some work cooperate with Prof. R. E. Ewing during 1985 to 1988, and kept a series of research in theoretical analysis and applications of numerical simulation. Yuan and his research group (1993,1993,1994) undertake some important projects from 1991 to 1995 such as "Eighth-Five" national key science and technology program (the Program for Tackling Key Programs) (85-203- 01-087) entitled "research and application of the polymer displacement software"[1]. The software has been applied in designing plan and research work of polymer displacements in industrial production region of Daqing Oilfield. Many conclusions from actual numerical results are illustrated by Yuan, Yang and Qi (1998,2000) such as effects of fragments, fragments setting of rinsing protection, quantity of polymer, and used in actual simulations which give rise to outstanding economic and social benefits[2]. Later the authors undertook a key tackling program of Daqing Petroleum Administration Bureau (DQYJ-1201002-2006-JS-9565)----solving development of mathematical models and completing explain of reservoir[3]. This software system is also applied in numerical simulation of the polymer displacement of Zaobei fault block of Dagang Oilfield, optimization of designing plan of expanded experimental area of three compound combination flooding of Gudong Little Well experimental region of Shengli Oilfield, polymer flooding of Gudong Middle One experimental region, Gudong West region and feasibility of active water flooding of Gudong eighth region, and many interesting results are obtained[4]. In recent years the research group finishes the successive key tackling project of Daqing Petroleum Administration Bureau (DQYJ-1201002-2009-JS-1077)--research on alkali flooding principle model of chemical displacement simulator and horizontal wells model structuring and solving methods[5] and presents many important results.

[1] Institute of Mathematics, Shandong University, Exploration Institute of Daqing Petroleum Administration. Research and application of the polymer flooding software (summary of "Eighth-Five" national key science and technology program, Grant No. 85-203-01-08), 1995.10.

[2] China National Petroleum Corporation. Evaluation report of executive condition of "Eighth-Five" national key science and technology program (Grant no. 85-203-01-08). 1995.10.

[3] Institute of Mathematics, Shandong University, Exploration and development of Daqing Petroleum Corporation. Modification of solving mathematical models of the polymer and improvement of reservoir description. 2006.

[4] Institute of Mathematics, Shandong University, Shengli Oilfield Branch, China Petroleum & Chemical. Research on key technology of high temperature and high salinity chemical agent displacement, Chapter 4, § 4.1 Numerical method, 83-106. 2011.3.

[5] Institute of Shandong University, Exploration and development of Daqing Petroleum Corporation. Research on alkali flooding principle model of chemical displacement simulator and horizontal wells model structuring

This paper concludes the former research and discusses proceeding analysis, mainly consisting of permeation fluid mechanical mathematical models of numerical simulation of black oil--three compound combination flooding in porous media, numerical methods, applicable software structuring, theoretical analysis and applications of actual oilfields.

2. Permeation Fluid Mechanical Model of Black Oil--three Compound Combination Displacement

The numerical simulation program of black oil model is shown based on the following factors: three phases (oil, gas and water) in the reservoir, oil-component and solution gas-component of the oil phase, water-component of the water phase, gas-component of the gas phase and the exchange of gas-component between the oil phase and the gas phase because of the changing pressure. An improved black-oil model is given to simulate the displacement process of three compound combinations (polymer, surface active agent and alkali) and a new simulation system is made for three compound combinations by considering the black oil module and the chemical reaction balance equation, and revising and adding three compound combinations module.

The oil, water and gas three phases are considered in the system, where the oil phase consists of oil component and solution gas component, the water phase includes water component, the chemical agent component includes polymer, surface active agent, petroleum acid and so on, and the gas phase only has gas component. Petroleum acid is contained in the water phase and oil phase and the other chemical components are only in the water phase. The exchange of gas components occurs between the oil phase and the gas phase when the pressure of neighbor environments changes. The solving system consists of three basic modules: the program for solving the three-phase flow, the program for solving the component equations and the program for solving the chemical balance equation.

The solving module of three phases inherits a partial algorithm of the black oil model. The water viscosity is a variable in three compound combinations displacement because of the chemical agent component but a constant in the black oil model. Additional design structure and algorithm should be compatible with the black oil model for solving the components equation and chemical reaction balance equation, and some computational programs are modified for solving the system to satisfy engineering applications of wedge-out area, fault and edge-bottom water.

Then two different algorithms are presented in this paper.

(I) Full implicit algorithm (FIA). It is one of the most dependable finite differences to compute the values of variables implicitly such as the pressure, the water saturation, the gas saturation and the ratio of solution gas and oil. More computational time is spent for a full implicit scheme to complete each extrapolation iterative. The full implicit scheme proceeds more stable than an implicit/explicit algorithm for the pressure and saturation (IEAFPS) which is invalid sometimes because of strong stability conditions, so a large time step is introduced to decrease the total simulation cost.

(II) Implicit/explicit algorithm for the pressure and saturation (IEAFPS). This algorithm means a coupled numerical system consisting of an implicit scheme for solving the pressure and an explicit scheme for solving the saturation dependent on an assumption: no distinct flow of the fluid occurs though the saturation varies during one time step. Under this hypothesis the unknown saturation variable of discretized convection equation can canceled and the pressure is computed coupled implicitly only at different iterations. The values of saturation is updated point by point explicitly once the pressure change rules are determined during one iteration process. While the IEAFPS is unstable as the saturation changes more large with respect to time step. This implicit/explicit algorithm is really efficient as the time step is taken sufficiently small to decrease the rangeability (the relative rangeability usually is 5%).

Let "*w*" and "*o*" denote the water phase and the oil phase of water-oil two phases problem, whose mathematical model of permeation fluid mechanics is stated as follows (see Ewing, Yuan, & Li, 1989; Yuan, 2013; Yuan, Yang, & Qi, 1998; Yuan, 2000):

$$\frac{\partial}{\partial x}\left[\lambda_l\left(\frac{\partial p_l}{\partial x}-\gamma_l\frac{\partial z}{\partial x}\right)\right]=\frac{\partial}{\partial t}\left(\phi\frac{\partial S_l}{\partial B_l}\right)-q_l, l=w,o; \tag{1a}$$

$$p_c=p_o-p_w, S_o+S_w=1.0. \tag{1b}$$

Let "*w*", "*o*" and "*g*" respectively denote the water phase, the oil phase and the gas phase, and the mathematical model of three phases permeation fluid mechanics is followed[12345],

$$\begin{cases} \dfrac{\partial}{\partial x}\left[\lambda_w\left(\dfrac{\partial p_w}{\partial x}-\gamma_w\dfrac{\partial z}{\partial x}\right)\right]=\dfrac{\partial}{\partial t}\left(\phi\dfrac{\partial S_w}{\partial B_w}\right)-q_w, \\ \dfrac{\partial}{\partial x}\left[\lambda_o\left(\dfrac{\partial p_o}{\partial x}-\gamma_o\dfrac{\partial z}{\partial x}\right)\right]=\dfrac{\partial}{\partial t}\left(\phi\dfrac{\partial S_o}{\partial B_o}\right)-q_o, \\ \dfrac{\partial}{\partial x}\left[R_s\lambda_o\left(\dfrac{\partial p_o}{\partial x}-\gamma_o\dfrac{\partial z}{\partial x}\right)\right]+\dfrac{\partial}{\partial x}\left[\lambda_g\left(\dfrac{\partial p_g}{\partial x}-\gamma_g\dfrac{\partial z}{\partial x}\right)\right]=\dfrac{\partial}{\partial t}\left(\phi R_s\dfrac{1-S_w-S_g}{\partial B_o}+\phi\dfrac{\partial S_g}{B_o}\right)-R_s q_o-q_g; \end{cases} \tag{2a}$$

$$p_o-p_w=p_{cow}, p_g-p_o=p_{cog}, \tag{2b}$$

$$\lambda_l=\frac{KK_{rl}}{\mu_l B_l}, l=w,o,g, \gamma_l=\rho_l g, \tag{2c}$$

$$\mathrm{u}_l=\lambda_l\left(\nabla p_l-\gamma_l\nabla z\right), l=w,o,g. \tag{2d}$$

where ϕ means the porosity, p_l is the pressure of l-phase, S_l is the concentration of l-phase, K is the absolute permeability, B_l is the volume factor of l-phase, K_{rl} is the relative permeability of l-phase, μ_l is the viscosity of l-phase, ρ_l is the density of l-phase, R_s is the ratio of solution gas and oil, and q_l is the source sink term of l-phase (floor condition).

The viscosity of water phase μ_w is a constant of black oil model, while the viscosity is a function with respect to the density of polymer of black oil-polymer displacement, $\mu_w=\mu_w(C_{pw})$, where C_{pw} denotes the concentration of polymer relative to water. The compound combination flooding components move in water, the concentration affects in turn the viscosity field of the water phase, then influences the flow of the three phase fluid accompanying the motion of components. The coupled algorithm runs consistent with the nonlinear coupled system consisting of a convection-diffusion equation of the polymer and the mathematical model of black oil. At a time step the motion values of three phases are computed first, the flow field is obtained, then the solution of three compound combination flooding by solving a convection diffusion equation are gotten, then the viscosity field of water phase is updated. Then the computation proceeds at the next time step.

$$\frac{\partial}{\partial t}\left(\phi S_w C\right)+\mathrm{div}\left(C\,\mathrm{u}_w-\phi S_w K\nabla C\right)=Q, \tag{2e}$$

$$\mu_w=\mu_w\left(C\right). \tag{2f}$$

Surface active agents can change interfacial tension, thus increase capillary number, then decrease the residual oil saturability. The curve of relative permeability is updated by an interpolation of the relative permeability curves of lower capillary number and upper capillary number.

The primary principle of alkaline flooding is stated as follows. The alkali is injected into the fluid and surface active agents arise because of a chemical reaction of the alkali and petroleum acid. These agents can decrease interfacial tension of the fluid and reduce bottom oil. Petroleum acid components exist both water phase and oil phase, so mass transfer takes place between different phases. An assumption is given that the petroleum acids in water and oil can level off instantaneously, and the equation of total concentration of petroleum acid (a type of convection) is stated.

$$\frac{\partial\left(C_{tot_{HA}}\right)}{\partial t}+\nabla\cdot\left(\mathrm{u}_w C_{HA_w}-\phi S_w\bar{K}_{HA_w}\nabla C_{HA_w}\right)+\nabla\cdot\left(\mathrm{u}_o C_{HA_o}-\phi S_o\bar{K}_{HA_o}\nabla C_{HA_o}\right)=q_w C_{HA_w}+q_o C_{HA_o}, \tag{2g}$$

where $\bar{K}_{HA_w}$ and $\bar{K}_{HA_o}$ denote petroleum acid dispersion tensors (including molecular diffusion and dispersion) of water phase and oil phase, respectively. The total concentration $C_{tot_{HA}}$ is defined as follows

$$C_{tot_{HA}}=\frac{S_w C_{HA_w}}{B_w}+\frac{S_o C_{HA_o}}{B_o}. \tag{2h}$$

Eqs. (1a), (1b), (2e), (2f), (2g) and (2h) give a full description of the mathematical model of water and oil two-phase polymer displacement, and eqs. (2a), (2b), (2c), (2d), (2e), (2f), (2g) and (2h) represent the full

explanation of the mathematical model of water-oil-gas three phases polymer displacement.

The computation of the black oil-polymer displacement model runs in the following steps:

Step 1. At the time level t^1, solve the pressure and saturation, then solve the concentrations of different chemical components.

Step 2. Correct the viscosity of water phase dependent on the concentration.

Step 3. At the time level t^2, solve the pressure and saturation, then solve the concentrations of different chemical components.

Step 4. Correct the viscosity of water phase dependent on the concentration.

……

In a similar way the pressure and saturation of the (n+1)th time step t^{n+1} are obtained, the concentration of different chemical components at t^{n+1} is computed, then the viscosity of water phase is corrected according to the concentration.

……

The program ends.

3. Numerical Methods

Two different numerical methods are presented as follows.

3.1 Full Implicit Numerical Method of the Three Phase Flow

It aims to cancel some spare unknown variables and compute only three unknown variables, generally meaning the pressure of oil phase, the concentrations of water and gas phases. All the values of the left side of the equation such as the pressure, the saturation, the quantity, the relative permeability, the capillary force and other parameters are replaced by the latest numerical values during implicit computations. The resulting implicit difference is a nonlinear algebraic equations solved by iteration and its computation scale is more rich seven times the implicit/explicit method of one iteration (outer iteration). Because the full implicit method is unconditionally stable, it is applied to compute some difficult and complicated problems such as black oil simulation. In this paper let $\bar{\delta}$ denote the difference of a function between the n-th time level and the (n+1)-th level and let δ be the difference during a time step by one iteration such as from the k-th iteration to the (k+1)-th iteration.

$$\bar{\delta} f = f^{n+1} - f^n, \quad \delta f = f^{k+1} - f^k, \quad \bar{\delta} f \approx f^{k+1} - f^n = f^k + \delta f - f^n.$$

Applying Euler backwards finite difference method for eq. (2),

$$\begin{aligned} &\left\{\left(\Delta T_l \Delta(p_l - \gamma_l z)\right)^{n+1} + \omega\left[\Delta\left(T_o R_s \Delta(p_o - \gamma_o z)\right)^{n+1} + \left(q_o R_s\right)^{n+1}\right]\right\}_i \\ &= \frac{V_b}{\Delta t}\left\{\left(\phi \frac{S_l}{B_l}\right) + \omega\left(\frac{1}{B_o} R_s S_o\right)\right\}_i^{n+1} - q_{li}^{n+1}, l = w, o, g, \end{aligned} \tag{3}$$

where $\omega = 1$ as l=g and $\omega = 0$ as l=w,o, and $V_b = \Delta x \Delta y \Delta z$.

Then a full implicit finite difference algorithm for the black oil model is derived as follows

$$\Delta T_l^{n+1} \Delta \Phi_l^{n+1} + q_l^{n+1} + \omega\left[\Delta\left(T_o R_s \Delta \Phi_o\right)^{n+1} + \left(q_o R_s\right)^{n+1}\right] = \frac{V_b}{\Delta t} \bar{\delta}\left[\phi b_l S_l + \omega(b_o R_s S_o)\right], l = w, o, g, \tag{4}$$

where $b_l = 1/B_l$ and $\Phi_l = p_l - \gamma_l D$. Rewrite the above expression as follows by using an operator δ ,

$$\Delta(T_l^k + \delta T_l)\Delta(\Phi_l^k + \delta\Phi_l) + q_l^k + \delta q_l + \omega\left\{\left[\Delta\left(T_o R_s\right)^k + \delta\left(T_o R_s\right)\right]\left[\Delta\left(\Phi_o^k + \delta\Phi_o\right) + \left(q_o R_s\right)^k + \delta\left(q_o R_s\right)\right]\right\}$$

$$= \frac{V_b}{\Delta t}\left\{\left[\phi b_l S_l + \omega(b_o R_s S_o)\right]^k + \delta\left[\phi b_l S_l + \omega(\phi b_o R_s S_o)\right] - \left[\phi b_l S_l + \omega(\phi b_o R_s S_o)\right]^n\right\}, l = w, o, g.$$

Give an expansion of the above equation and omit quadratic terms, and the remainder after the k-th iteration is

$$\begin{aligned} R_l^k \equiv\ & \Delta T_l^k \Delta \Phi_l^k + q_l^k + \omega\left[\Delta\left(T_o R_s\right)^k \Delta \Phi_o^k + \left(q_o R_s\right)^k\right] \\ & - \frac{V_b}{\Delta t}\left\{\left[\phi b_l S_l + \omega(b_o R_s S_o)\right]^k - \left[\phi b_l S_l + \omega(\phi b_o R_s S_o)\right]^n\right\}, l = w, o, g. \end{aligned}$$

Continue to express the above equation with a remainder term as,

$$\Delta(\delta T_l)\Delta\Phi_l^k + \Delta T_l^k\Delta(\delta\Phi_l) + \delta q_l + \omega\Big[\Delta\delta\left(T_oR_s\right)\Delta\Phi_o^k + \Delta\left(T_oR_s\right)^k\Delta(\delta\Phi_o) + \delta\left(q_oR_s\right)\Big] = \frac{V_b}{\Delta t}\delta\left[\phi b_l S_l + \omega(\phi b_o R_s S_o)\right] - R_l^k. \tag{5}$$

The iterations are convergent as $R_l^k \to 0$ for l=w,o,g and k=1,2,…. A resulting formulation is

$$RHS_l = C_{l1}\delta p_o + C_{l2}\delta S_w + C_{l3}\delta S_g - R_l^k, l = w, o, g. \tag{6}$$

First, the equation is turned into a linearized expansion. Solving variables are denoted by δp_o, δS_w and δS_g, and the right side term is considered later.

Notice that $\delta(ab) = a^{k+1}\delta b + b^k\delta a$ and consider the right side term of the water phase equation,

$$RHS_w = \frac{V_b}{\Delta t}\delta(\phi b_w S_w) - R_w^k = C_{w1}\delta p_o + C_{w2}\delta S_w + C_{w3}\delta S_g - R_w^k,$$

where

$$C_{w1} = \frac{V_b}{\Delta t}S_w^k(\phi^{k+1}b_w' + b_w^k\phi'), C_{w2} = \frac{V_b}{\Delta t}\phi^{k+1}(b_w^{k+1} - S^k b_w' p_{cwo}'), C_{w3} = 0,$$
$$R_w^k = \Delta T_w^k\Delta\Phi_w^k + q_w^k - \frac{V_b}{\Delta t}\Big[(\phi b_w S_w)^k - (\phi b_w S_w)^n\Big]. \tag{7}$$

Consider the right side term of oil phase equation,

$$RHS_o = \frac{V_b}{\Delta t}\delta(\phi b_o S_o) - R_o^k = C_{o1}\delta p_o + C_{o2}\delta S_w + C_{o3}\delta S_g - R_o^k,$$

where

$$C_{o1} = \frac{V_b}{\Delta t}S_o^k(\phi^{k+1}b_o' + b_o^k\phi'), C_{o2} = \frac{V_b}{\Delta t}\phi^{k+1}(\phi b_o)^{k+1}, C_{w3} = -\frac{V_b}{\Delta t}\phi^{k+1}(\phi b_o)^{k+1},$$
$$R_o^k = \Delta T_o^k\Delta\Phi_o^k + q_o^k - \frac{V_b}{\Delta t}\Big[(\phi b_o S_o)^k - (\phi b_o S_o)^n\Big]. \tag{8}$$

For the right side term of the gas phase equation,

$$RHS_g = \frac{V_b}{\Delta t}\delta\Big[(\phi b_g S_g) + (\phi b_o R_s S_o)\Big] - R_g^k = C_{g1}\delta p_o + C_{g2}\delta S_w + C_{g3}\delta S_g - R_g^k,$$

where

$$C_{g1} = \frac{V_b}{\Delta t}\Big\{(b_g S_g + b_o R_s S_o)^k\phi_r C_r + \phi^{k+1}\Big[S_g^k b_g' + S_o^n(R_s^{k+1}b_o' + b_o^k R_s')\Big]\Big\},$$
$$C_{g2} = -\frac{V_b}{\Delta t}(\phi b_o R_s)^{k+1}, C_{g3} = -\frac{V_b}{\Delta t}\phi^{k+1}(b_g^{k+1} + S_g^k b_g' p_{cgo}') + C_{g2}, \tag{9}$$
$$R_g^k = \Delta T_g^k\Delta\Phi_g^k + q_g^k + \Big[\Delta(T_oR_s)^k\Delta\Phi_o^k + (q_oR_s)^k\Big] - \frac{V_b}{\Delta t}\Big\{\Big[\phi(b_gS_g + b_oR_sS_o)\Big]^k - \Big[\phi(b_gS_g + b_oR_sS_o)\Big]^n\Big\}.$$

In the above expressions b_l' and ϕ' present the derivatives of volume factor and porosity with respect to the pressure, p_{cow}' denotes the derivative of p_c with respect to S_w and p_{cgo}' is the derivative of p_c with respect to S_g.

Two operators are introduced to discuss the left side term,

$$M_l = \Delta T_l^k\Delta(\delta\Phi_l)^k + \omega\Big[\Delta(T_oR_s)^k\Delta(\delta\Phi_o)\Big], N_l = \Delta(\delta T_l)\Delta\Phi_l^k + \omega\Big[\Delta\delta(T_oR_s)\Delta\Phi_o^k\Big].$$

Then,

$$M_l + N_l + \delta q_l + \omega\delta(q_oR_s) = RHS_l, l = w, o, g. \tag{10}$$

Here an expansion of M_l is only considered. For water phase,

$$M_w = \Delta T_w^k\Delta(\delta\Phi_w) \approx \Delta T_w^k\Delta(\delta p) - \Delta T_w^k\Delta(p_{cwo}'\delta S_w),$$

for oil phase,

$$M_o = \Delta T_o^k\Delta(\delta\Phi_o) \approx \Delta T_o^k\Delta[\delta(p - \gamma_o D)] \approx \Delta T_o^k\Delta(\delta p),$$

and for gas phase,

$$M_g = \Delta T_g^k\Delta(\delta\Phi_g) + \Delta(\mathrm{T_oR_s})^k\Delta(\delta\Phi_o) \approx \Delta(T_g + \mathrm{T_oR_s})^k\Delta(\delta p) + \Delta T_g^k\Delta(p_{cgo}'\delta S_g).$$

The values of conductivity coefficient appearing in two-order difference operator are given according to upstream rule, and let i_+ and i_- denote the upstream nodes between the i-th node and the (i+1)-th node and between the i-th node and the (i-1)-th node, respectively,

$$\Delta T_l \Delta(\delta f)_i = T_{li_+}(\delta f_{i+1} - \delta f_i) - T_{li_-}(\delta f_i - \delta f_{i-1}), l = w, o, g.$$

Substitute the left side and the right side terms into the initial difference equation, and get the algebraic system.

3.2 Implicit/explicit Algorithm for the Pressure and the Saturation

The implicit/explicit method is based on an equation only involved of the pressure by combining the flow equations, and the values of the saturation are obtained explicitly as the pressure at some time level is known.

Discrete difference scheme of eq. (2) is written related with p_o and the saturation,

$$\Delta\left[T_w(\Delta p_o - \Delta p_{cow} - \gamma_w \Delta z)\right] = C_{1p}\Delta_t p_w + \sum_t C_{1l}\Delta_t S_l + q_w, \quad \Delta\left[T_o(\Delta p_o - \gamma_o \Delta z)\right] = C_{2p}\Delta_t p_o + \sum_t C_{2l}\Delta_t S_l + q_o,$$

$$\Delta\left[T_g(\Delta p_o - \Delta p_{cog} - \gamma_g \Delta z)\right] + \Delta\left[R_s T_o(\Delta p_o - \gamma_o \Delta z)\right] = C_{3p}\Delta_t p_g + \sum_t C_{3l}\Delta_t S_l + R_s q_o + q_g.$$

A basic hypothesis is assumed for deriving the implicit/explicit scheme that the capillary pressure of the flow term of the left side is a constant number during a time step computation. The values of some terms related of Δp_{cow} and Δp_{cog} at the previous time level can be computed explicitly, and $\Delta_t p_w = \Delta_t p_o = \Delta_t p_g$. The notation p_o is simplified to be replaced by p.

$$\begin{aligned}
&\Delta\left[T_w(\Delta p^{n+1} - \Delta p_{cow}^n - \gamma_w \Delta z)\right] = C_{1p}\Delta_t p + C_{1w}\Delta_t S_w + q_w, \Delta\left[T_o(\Delta p^{n+1} - \gamma_o \Delta z)\right] = C_{2p}\Delta_t p + C_{1o}\Delta_t S_o + q_o, \\
&\Delta\left[T_g(\Delta p^{n+1} - \Delta p_{cog}^n - \gamma_g \Delta z)\right] + \Delta\left[R_s T_o(\Delta p^{n+1} - \gamma_o \Delta z)\right] = C_{3p}\Delta_t p + C_{3o}\Delta_t S_o + C_{3g}\Delta_t S_g + R_s q_o + q_g.
\end{aligned} \tag{11}$$

The coefficient C is defined by

$$\begin{aligned}
C_{1p} &= \frac{V_b}{\Delta t}\left[(S_w\phi)^n b_w^{'} + S_w^n b_w^{n+1}\phi^{'}\right], \quad C_{1w} = \frac{V_b}{\Delta t}(\phi b_w)^{n+1}, \\
C_{2p} &= \frac{V_b}{\Delta t}\left[(S_o\phi)^n b_o^{'} + S_o^n b_o^{n+1}\phi^{'}\right], \quad C_{2o} = \frac{V_b}{\Delta t}(\phi b_o)^{n+1}, \\
C_{3p} &= \frac{V_b}{\Delta t}\left[R_s^n(S_o^n\phi^n b_o^{'} + S_o^n b_o^{n+1}\phi^{'}) + S_g^n\phi^n b_g^{'} + S_g^n b_g^{n+1}\phi^{'} + (\phi S_o b_o)^{n+1} R_s^{'}\right], \\
C_{3o} &= \frac{V_b}{\Delta t}\left[R_s^n(\phi b_o)^{n+1}\right], \quad C_{3g} = \frac{V_b}{\Delta t}(\phi b_g)^{n+1}.
\end{aligned} \tag{12}$$

Consider the three equations of (11) together and cancel all the $\Delta_t S_l$ terms by multiplying the water phase equation by A, testing the gas equation by B, and adding three equations. The right term is

$$(AC_{1p} + C_{2p} + BC_{3p})\Delta_t p + (-AC_{1w} + C_{2o} + BC_{3o})\Delta_t S_o + (-AC_{1w} + BC_{3p})\Delta_t S_g.$$

The numbers A and B are defined by the following relations.

$$-AC_{1w} + C_{2o} + BC_{3o} = 0, \quad -AC_{1w} + BC_{3g} = 0.$$

By simple algebraic calculations,

$$B = C_{2o}/(C_{3g} - C_{3o}), \quad A = B\,C_{3g}/C_{1w}. \tag{13}$$

Then the pressure equation turns into

$$\begin{aligned}
&\Delta\left[T_o(\Delta p^{n+1} - \gamma_o \Delta z)\right] + A\Delta\left[T_w(\Delta p^{n+1} - \gamma_w \Delta z)\right] + B\Delta\left[T_o R_s(\Delta p^{n+1} - \gamma_o \Delta z) + T_g(\Delta p^{n+1} - \gamma_g \Delta z)\right] \\
&= \left(C_{2p} + AC_{1p} + BC_{3p}\right)\Delta_t p + A\Delta(T_w \Delta p_{cow}^n) - B\Delta(T_w \Delta p_{cog}^n) + q_o + Aq_w + B(R_s q_o + q_g).
\end{aligned} \tag{14}$$

It is a typical finite difference equation from a parabolic type, whose matrix form is

$$Tp^{n+1} = D(p^{n+1} - p^n) + G + Q,$$

where T denotes a tridiagonal matrix and D is a diagonal matrix. The vector G is dependent of gravity and capillary pressure.

Given the pressure, taken in the former two equations of (11), the saturation S_l^{n+1} is obtained explicitly. Then the capillary pressure p_{cow}^{n+1} and p_{cog}^{n+1} are considered, which are used explicitly in next time level.

3.3 Numerical Method for Component Concentration Equations

The components meaning sorts of chemical agents in water phase such as surface active agents, polymer, alkali

and kinds of ions and so on are considered in this paper. The physical nature, conversation of mass, is described by a convection-diffusion equation but convection-dominated. It is more efficient and high order of accuracy to decompose the equation into a hyperbolic equation only related of diffusion and a parabolic equation only related of dispersion. The former is discretized by an implicit upwind scheme and an upstream rule inheriting some advantages of explicit algorithms such as solving the values point by point. The latter is solved by an alternating direction finite difference method, which can accelerate the computation speed and improve the efficiency. For simplicity, the concentration equation of components is rewritten by a typical convection diffusion type.

$$\frac{\partial}{\partial t}\left(\phi S_w C\right) + \operatorname{div}\left(C\,\mathrm{u}_w - \phi S_w K \nabla C\right) = Q, \tag{15}$$

where dispersion tensor is a matrix of diagonal type. When the saturation S_w and the flow velocity field $\boldsymbol{u}_w$ of water phase at t^{n+1} are given, it is to compute the concentration C^{n+1} at the first direction, the second and then the third direction alternatively. C denotes the concentration of any component ignoring the subscript k. A convection equation is discussed by an implicit upwind scheme,

$$\begin{aligned}&\frac{\phi_{ijk}^{n+1}S_w^{n+1}C_{ijk}^{n+1,0} - \phi_{ijk}^{n}S_w^{n}C_{ijk}^{n}}{\Delta t} + \frac{C_{i_+jk}^{n+1,0}u_{w,ijk}^{n+1} - C_{i\_jk}^{n+1,0}u_{w,i-1,jk}^{n+1}}{\Delta x} + \frac{C_{ij_+k}^{n+1,0}u_{w,ijk}^{n+1} - C_{ij\_k}^{n+1,0}u_{w,i,j-1,k}^{n+1}}{\Delta y}\\ &+ \frac{C_{ijk_+}^{n+1,0}u_{w,ijk}^{n+1} - C_{ijk\_}^{n+1,0}u_{w,ij,k-1}^{n+1}}{\Delta z} = Q_{ijk}^{n+1},\end{aligned} \tag{16}$$

where $\boldsymbol{u}_w=(u_{wx},u_{wy},u_{wz})^T$ is a velocity vector. By which $C^{n+1,0}$ is obtained. Then the dispersion equation is discussed alternatively in three directions. First consider x-direction,

$$\begin{aligned}&\frac{\phi_{ijk}^{n+1}S_w^{n+1}C_{ijk}^{n+1,1} - \phi_{ijk}^{n}S_w^{n}C_{ijk}^{n+1,0}}{\Delta t}\\ &-\frac{1}{(\Delta x)^2}\left\{\phi_{i+1/2,jk}S_{w,i_+jk}^{n+1}K_{xx,i+1/2,jk}(C_{i+1,jk}^{n+1,1} - C_{ijk}^{n+1,1}) - \phi_{i-1/2,jk}S_{w,i\_jk}^{n+1}K_{xx,i-1/2,jk}(C_{ijk}^{n+1,1} - C_{i-1,jk}^{n+1,1})\right\} = 0.\end{aligned} \tag{17a}$$

Secondly consider y-direction,

$$\begin{aligned}&\frac{\phi_{ijk}^{n+1}S_w^{n+1}C_{ijk}^{n+1,2} - \phi_{ijk}^{n}S_w^{n}C_{ijk}^{n+1,1}}{\Delta t}\\ &-\frac{1}{(\Delta y)^2}\left\{\phi_{i,j+1/2,k}S_{w,ij_+k}^{n+1}K_{xx,i,j+1/2,k}(C_{i,j+1,k}^{n+1,2} - C_{ijk}^{n+1,2}) - \phi_{i,j-1/2,k}S_{w,ij\_k}^{n+1}K_{xx,i,j-1/2,k}(C_{ijk}^{n+1,2} - C_{i,j-1,k}^{n+1,2})\right\} = 0.\end{aligned} \tag{17b}$$

Thirdly consider z-direction, then C^{n+1} is computed by

$$\begin{aligned}&\frac{\phi_{ijk}^{n+1}S_w^{n+1}C_{ijk}^{n+1} - \phi_{ijk}^{n}S_w^{n}C_{ijk}^{n+1,2}}{\Delta t}\\ &-\frac{1}{(\Delta z)^2}\left\{\phi_{ij,k+1/2}S_{w,ijk_+}^{n+1}K_{xx,ij,k+1/2}(C_{ij,k+1}^{n+1,1} - C_{ijk}^{n+1,1}) - \phi_{ij,k-1/2}S_{w,ijk\_}^{n+1}K_{xx,ij,k-1/2}(C_{ijk}^{n+1} - C_{ij,k-1}^{n+1})\right\} = 0.\end{aligned} \tag{17c}$$

The values of p_o^{n+1}, S_w^{n+1}, S_g^{n+1} and C^{n+1} are obtained, and the computation ends at present time level then continues at next time level. A technique is introduced in actual applications to overcome some difficulties and effects of grids orientation (such as the symmetrical computation kept consistently with symmetric physical problems). The values are obtained in two continuous processes, x-direction first then y-direction, then y-direction first then x-direction, then the algorithm continues in z-direction by using an average result of the above computational values. This efficient method is applied in present software.

3.4 Newton-Raphson Iterations of Chemical Reaction Balance Equations

The chemical balance equations, a nonlinear system consisting of liquid chemical agent, solid chemical agent and ions adsorbed in rocks, are solved by Newton-Raphson iterations. Considering the nonlinear equations $\boldsymbol{F}(\boldsymbol{X})=\boldsymbol{0}$,

$$
\begin{aligned}
&F_1(x_1, x_2, \cdots, x_{N-1}, x_N) = 0,\\
&F_2(x_1, x_2, \cdots, x_{N-1}, x_N) = 0,\\
&\vdots\\
&F_{N-1}(x_1, x_2, \cdots, x_{N-1}, x_N) = 0,\\
&F_N(x_1, x_2, \cdots, x_{N-1}, x_N) = 0,
\end{aligned}
$$

where $\boldsymbol{F}=(F_1,F_2,\ldots,F_N)^T$, $\boldsymbol{X}=(x_1,x_2,\ldots,x_N)^T$, $\boldsymbol{0}=(0,0,\ldots,0)^T$. Its Newton-Raphson iterations are

$$X^{k+1} = X^k - \frac{F(\mathrm{X}^k)}{DF(\mathrm{X}^k)}, \quad k = 0,1,\cdots, \tag{18}$$

where k denotes the number of iterations, $F(X) = (F_1^k, F_2^k, \cdots, F_{N-1}^k, F_N^k)^T$, $F_i^k = F_i(x_1^k, x_2^k, \cdots, x_{N-1}^k, x_N^k)$, and the convergent condition is defined by $\| F(X^k) \| < \varepsilon$ or by $\| \mathrm{X}^{k+1} - X^k \| < \varepsilon$. The choice of the initial values X^0 affects the convergence of Newton-Raphson iteration sequences. $DF(X^k)$, a Jacobian matrix, is defined by

$$DF(X^k) = \begin{pmatrix} \frac{\partial F_1^k}{\partial x_1} & \frac{\partial F_1^k}{\partial x_2} & \cdots & \frac{\partial F_1^k}{\partial x_N} \\ \frac{\partial F_2^k}{\partial x_1} & \frac{\partial F_2^k}{\partial x_2} & \cdots & \frac{\partial F_2^k}{\partial x_N} \\ \vdots & \vdots & \ddots & \vdots \\ \frac{\partial F_N^k}{\partial x_1} & \frac{\partial F_N^k}{\partial x_2} & \cdots & \frac{\partial F_N^k}{\partial x_N} \end{pmatrix}, \tag{19}$$

where $\frac{\partial F_i^k}{\partial x_j} = \frac{\partial F_i}{\partial x_j}(x_1^k, x_2^k, \cdots, x_{N-1}^k, x_N^k)$ denotes the partial derivative value of $F_i(x_1, x_2, \cdots, x_{N-1}, x_N)$ with respect to x_j at $(x_1^k, x_2^k, \cdots, x_{N-1}^k, x_N^k)$.

4. Computation Program Illustration

This section illustrates three computation programs[1,2,3,5]: the program of black oil-three compound combination flooding, the data program of upstream sequence algorithm of fault-joints, the implicit computational program of the water phase concentration equation, the explicit computation program of the total concentration equation of petroleum acid components, the computation program of relative permeability and the computation program of chemical reaction balance equation (see Fig.1, Fig.2, Fig.3, Fig.4, Fig.5 and Fig.6).

5. Experimental Tests in Oil Fields of Black Oil-three Compound Combination Alkali Flooding

5.1 Test I

The model grids scale of experimental tests is defined by 46×83×7, and oil displacement efficiency is tested under different petroleum acid numbers and different concentrations of injected alkali. Three SLUGs are installed and the simulation period, 1970.1.1-1994.1.1, is divided into three time segments: water flooding segment 1970.1.1-1982.1.1, injected polymer and three compound combination flooding segment 1982.1.1 -1988.1.1 and water flooding segment 1988.1.1-1994.1.1. There are five strategies considered in the simulation and let X45ASP be the polymer flooding. X45ASP2 denotes the compound flooding combination the polymer with alkali, the acid number is 0.0006, and the concentration values of injected Na ions and CO_3 ions are 0.3351 and 0.3929 in the second way. X45ASP3 is the compound flooding combination the polymer with alkali, the acid number is 0.006 and the concentration values of Na ions and CO_3 ions are 0.3351 and 0.3929 in the third way. X45ASP4 is the compound flooding combination the polymer with alkali, the acid number is 0.0006 and the concentration values of Na ions and CO_3 ions are 0.3351 and 0.3929 in the fourth way. X45ASP5 is the compound flooding combination the polymer with alkali, the acid number is 0.006 and the concentration values of Na ions and CO_3 ions are 0.3351 and 0.3929 in the fifth way. The moisture content, instantaneous oil production and accumulative oil production in five different strategies are compared in the following curves (Fig. 7a, Fig. 7b and Fig. 7c).

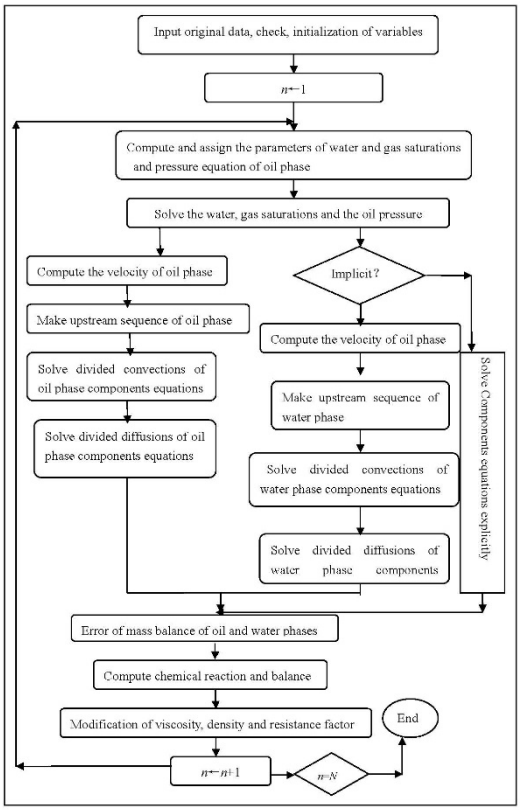

Fig. 1. Computation program illustration of black oil—three compound combinations flooding

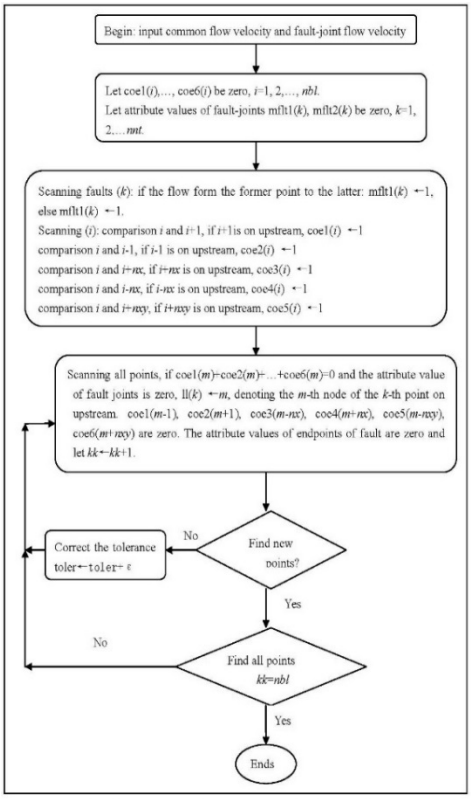

Fig. 2 Data program of upstream sequence of fault-joint points

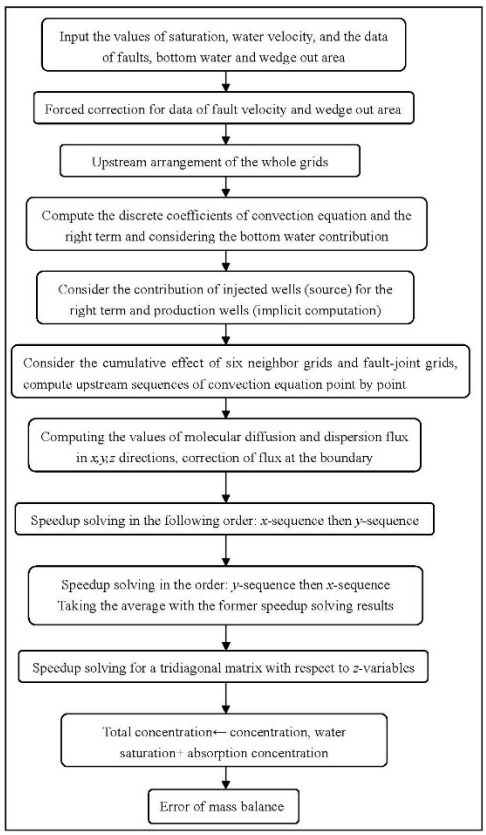

Fig. 3 Computation program of implicit scheme of component concentration equation

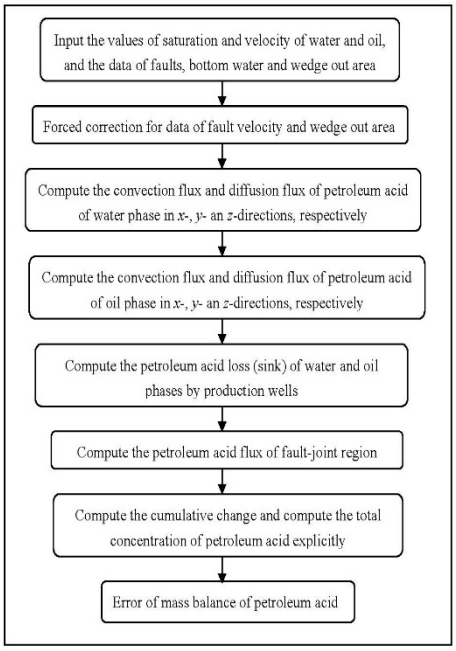

Fig. 4 Computation program of implicit scheme of component concentration (total) equation of petroleum acid

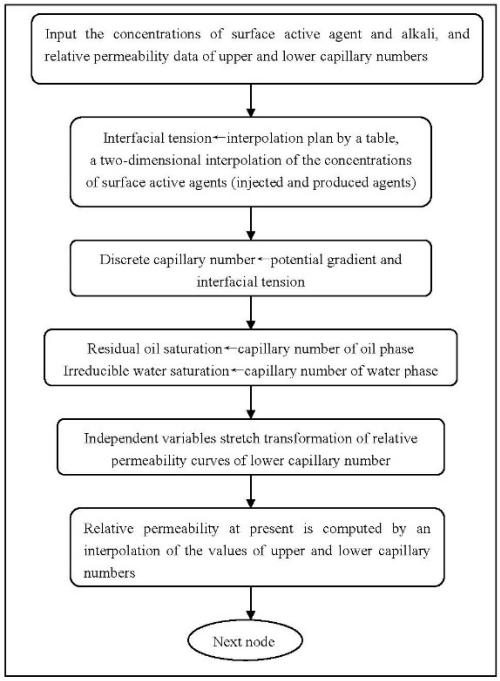

Fig. 5 Computation program of relative permeability

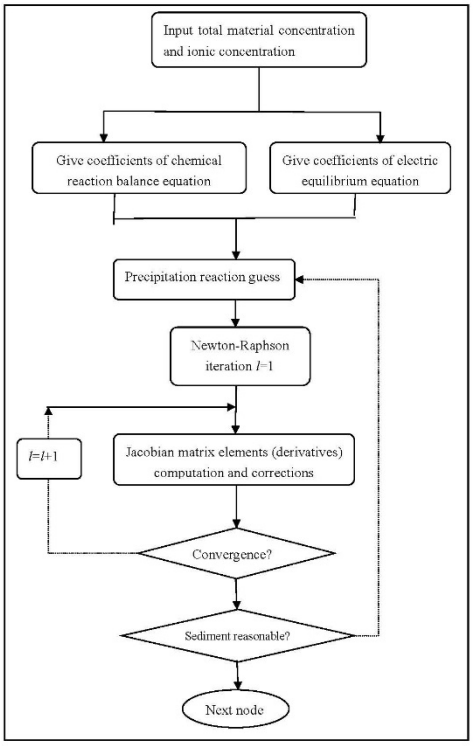

Fig. 6 Computation program of chemical reaction balance equation

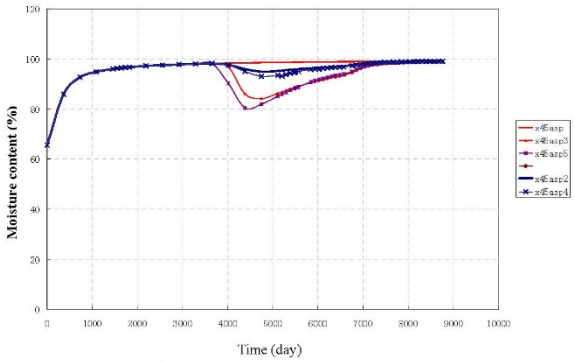

Fig. 7a. Curve of moisture content, alkaline flooding test I of oil fields

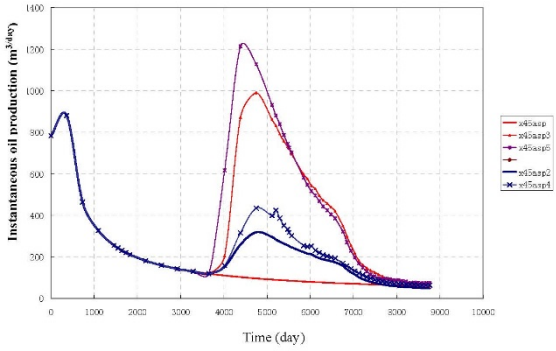

Fig. 7b. Curve of instantaneous oil production, alkaline flooding test I of oil fields

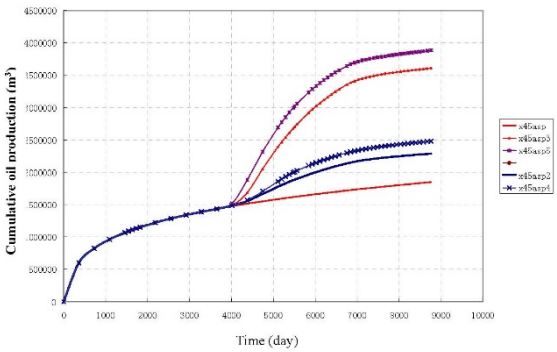

Fig. 7c. Curve of cumulative oil production, alkaline flooding test I of oil fields

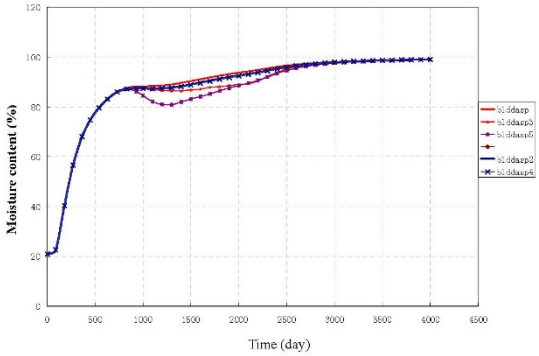

Fig. 8a. Curve of moisture content, alkaline flooding test II of oil fields

5.2 Test II

The model grids scale in this test is defined by 119×79×9 (84609 nodes), and oil displacement efficiency is tested under different petroleum acid numbers and different concentrations of injected alkali. Three SLUGs are installed and the simulation period is 4000 days divided into three time segments: water flooding segment during

the former 730 days, injected polymer and three compound combination flooding segment during the middle thirteen hundreds and seventy days and water flooding segment during the last nineteen hundreds days. There are five strategies considered in the simulation and let B1DDASP be the polymer flooding. B1DDASP2 denotes the compound flooding combination the polymer with alkali, the acid number is 0.0006, and the concentration values of injected Na ions and CO_3 ions are 0.3351 and 0.3929 in the second way. B1DDASP3 is the compound flooding combination the polymer with alkali, the acid number is 0.006 and the concentration values of Na ions and CO_3 ions are 0.3351 and 0.3929 in the third way. B1DDASP4 is the compound flooding combination the polymer with alkali, the acid number is 0.0006 and the concentration values of Na ions and CO_3 ions are 0.3351 and 0.3929 in the fourth way. B1DDASP5 is the compound flooding combination the polymer with alkali, the acid number is 0.006 and the concentration values of Na ions and CO_3 ions are 0.3351 and 0.3929 in the fifth way. The moisture content, instantaneous oil production and accumulative oil production in five different strategies are compared in the following curves (Fig. 8a, Fig. 8b and Fig. 8c).

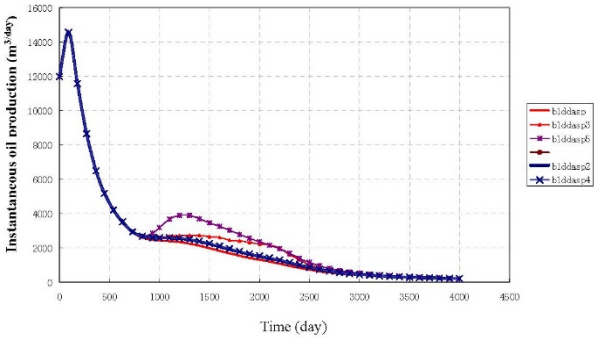

Fig. 8b. Curve of instantaneous oil production, alkaline flooding test II of oil fields

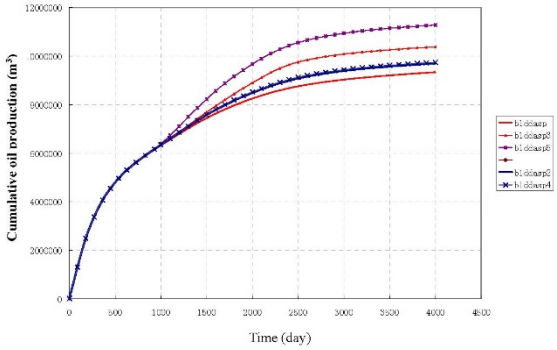

Fig. 8c. Curve of cumulative oil production, alkaline flooding test II of oil fields

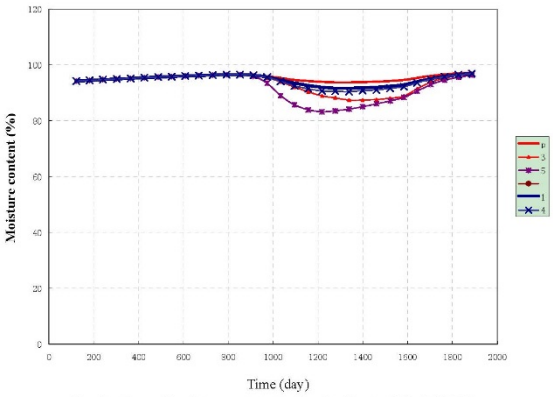

Fig. 9a. Curve of moisture content, alkaline flooding test III of oil fields

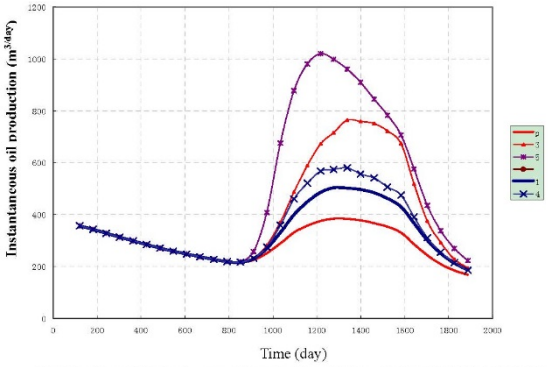

Fig. 9b. Curve of instantaneous oil production, alkaline flooding test III of oil fields

5.3 Test III

The model grids scale of this test is defined by 149×149×7 (155407 nodes), and oil displacement efficiency is tested under different petroleum acid numbers and different concentrations of injected alkali. Three SLUGs are installed and the simulation period, 2010.9.1-2015.11.1, is divided into three time segments: water flooding segment 2010.9.1-2012.11.1, injected polymer and three compound combination flooding segment 2012.11.1-2014.11.1 and water flooding segment 2014.11.1-2015.11.1. There are five strategies considered in the simulation and let P be the polymer flooding. The number 1 denotes the compound flooding combination the polymer with alkali, the acid number is 0.0006, and the concentration values of injected Na ions and CO_3 ions are 0.3351 and 0.3929 in the second way. The number 3 is the compound flooding combination the polymer with alkali, the acid number is 0.006 and the concentration values of Na ions and CO_3 ions are 0.3351 and 0.3929 in the third way. The number 4 is the compound flooding combination the polymer with alkali, the

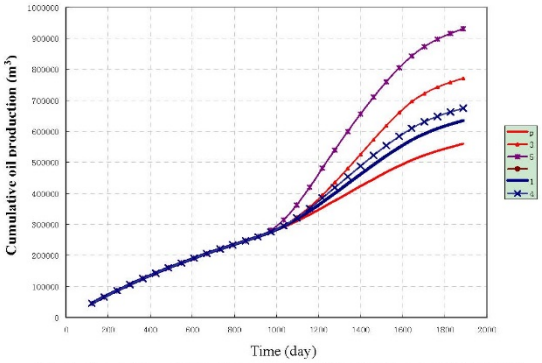

Fig. 9c. Curve of cumulative oil production, alkaline flooding test III of oil fields

acid number is 0.0006 and the concentration values of Na ions and CO_3 ions are 0.3351 and 0.3929 in the fourth way. The number 5 is the compound flooding combination the polymer with alkali, the acid number is 0.006 and the concentration values of Na ions and CO_3 ions are 0.3351 and 0.3929 in the fifth way. The moisture content, instantaneous oil production and accumulative oil production in five different strategies are compared in the following curves (Fig. 9a, Fig. 9b and Fig. 9c).

The conclusion is derived from above figures that the more efficient the oil flooding is, the larger the acid number of petroleum acid and the concentration value of injected alkali. Error data of mass balance are shown in the following table (Table 1).

Table 1. Error results of mass balance

	Water	Oil	Polymer	Mg^{2+}	CO_3^{2-}	Na^+	H	HA
P	5*E*-5	4*E*-5	3*E*-13	3*E*-10	9*E*-11	4*E*-11	3*E*-11	3*E*-10
1	8*E*-5	3*E*-4	5*E*-13	2*E*-10	5*E*-11	1*E*-11	3*E*-11	1*E*-9
3	9*E*-6	3*E*-5	5*E*-13	2*E*-10	5*E*-11	2*E*-11	3*E*-11	7*E*-10
4	1*E*-5	4*E*-5	5*E*-13	6*E*-11	2*E*-11	2*E*-13	3*E*-11	2*E*-9
5	2*E*-4	1*E*-3	4*E*-13	6*E*-11	2*E*-11	9*E*-13	3*E*-11	9*E*-10

6. Theoretical Analysis of the Model

Theoretical analysis of numerical simulation is given for three dimensional three phases (oil, water and gas) –three compound combination flooding in porous media. A simplified model is discussed in theoretical analysis without loss of generality, that is to say a compressible oil water two phase displacement of three dimensional multi-components problem in porous media is discussed in a nonlinear partial differential equations with initial and boundary values (see Ewing, Yuan, & Li, 1989; Yuan, 2013; Ewing, 1983; Yuan, 2002, 1999, 2003, 2001).

$$d(c)\frac{\partial p}{\partial t}+\nabla\cdot\mathbf{u}=q(x,t),x=(x_1,x_2,x_3)^T\in\Omega,t\in J=(0,T], \tag{20a}$$

$$\mathbf{u}=-a(c)\nabla p,x\in\Omega,t\in J, \tag{20b}$$

$$\Phi(x)\frac{\partial c_\alpha}{\partial t}+b_\alpha(c)\frac{\partial p}{\partial t}+\mathbf{u}\cdot\nabla c_\alpha-\nabla\cdot(D\nabla c_\alpha)=g(x,t,c_\alpha),x\in\Omega,t\in J,\alpha=1,2,\cdots,n_c-1, \tag{20c}$$

where $p(x,t)$ is the pressure of the mixture, $c_\alpha(x,t)$ is the saturation of the α -th component, $\alpha=1,2,\cdots,n_c$ and n_c is the number of components. There are n_c-1 independent components because of $\sum_{\alpha=1}^{n_c}c_\alpha(x,t)=1$. Let $c(x,t)=(c_1(x,t),c_2(x,t),\ldots,c_{nc\text{-}1}(x,t))^T$ be the vector function of component saturations, $d(c)=\Phi(x)\sum_{\alpha=1}^{n_c}z_\alpha c_\alpha$, $\Phi(x)$ be the porosity of rock, z_α be the compressible invariant of α, $\boldsymbol{u}$ be Darcy velocity of the mixture, $a(c)=\kappa(x)\mu(c)^{-1}$, $\kappa(x)$ be the permeability, $\mu(c)$ be the viscosity, $b_\alpha(c)=\Phi c_\alpha\{z_\alpha-\sum_{j=1}^{n_c}z_j c_j\}$, and let $D=D(x)$ be the diffusion parameter. The pressure $p(x,t)$ and the saturation vector $c(x,t)$ are basic unknown functions to compute.

Boundary condition without permeation:

$$\mathbf{u}\cdot\gamma=0,x\in\partial\Omega,(D\nabla c_\alpha-\mathrm{c}_\alpha\,\mathbf{u})\cdot\gamma=0,x\in\partial\Omega,t\in J,\alpha=1,2,\cdots,n_c-1, \tag{21}$$

where γ is the outer normal vector of boundary surface $\partial\Omega$ of Ω.

Initial conditions:

$$p(x,0)=p_0(x),x\in\Omega,c_\alpha(x,0)=c_{\alpha,0}(x),x\in\Omega,\alpha=1,2,\cdots,n_c-1. \tag{22}$$

Douglas (1983) presents a fundamental paper to analyze a type of two dimensional incompressible two-phase displacement problems. Because the computation of modern reservoir exploration and development is of huge scale, its simulation region is large, its simulation time is really long and there are tens of thousands or hundreds

of thousands nodes, it is impossible to solve so complicated problems of this type by using common methods. Alternating direction finite difference methods are put forward by Peaceman (1980) and Douglas (1963) and are successfully applied in two dimensional problems but there is substantial difficulty to give theoretical analysis. Using Fourier method Peaceman and Douglas discuss the stability and convergence for the problems with constant coefficients, while this method is not able to generalize in variable coefficient problems. Yanenke (1967), and Marchuk (1990) give many important results on fractional steps methods. Yuan (1999) presents a characteristic finite difference fractional steps method for compressible two-phase displacement problem and discusses convergence analysis. An implicit upwind finite difference fractional steps method is considered for black oil and polymer flooding problem and some substantial improvements are given in this paper. The three dimensional problem is turned into three one-dimensional problems and this can greatly reduce the computation and can solve actual problems. Error estimates in L^2 norm are presented by using variation, energy analysis, decomposition of high order difference operators and theory and technique of product commutativity.

For simplicity, assume computational domain $\Omega=\{[0,1]\}^3$ and the problem is Ω-periodic. The nonpermeation boundary condition can be dropped. Let $h=1/N$, $X_{ijk}=(ih,jh,kh)^T$, $t^n=n\Delta t$ and $W(X_{ijk},t^n)=W_{ijk}^n$, and let

$$A_{i+1/2,jk}^n=\frac{1}{2}\left[a(X_{ijk},C_{ijk}^n)+a(X_{i+1,jk},C_{i+1,jk}^n)\right], \tag{23a}$$

$$\delta_{\bar{x}_1}\left(A^n\delta_{x_1}P^{n+1}\right)_{ijk}=h^{-2}\left[A_{i+1/2,jk}^n(\mathrm{P}_{i+1,jk}^{n+1}-\mathrm{P}_{ijk}^{n+1})-A_{i-1/2,jk}^n(\mathrm{P}_{ijk}^{n+1}-\mathrm{P}_{i-1,jk}^{n+1})\right]. \tag{23b}$$

Difference operators $A_{i,j+1/2,k}^n$, $A_{ij,k+1/2}^n$, $\delta_{\bar{x}_2}\left(A^n\delta_{x_2}P^{n+1}\right)_{ijk}$ and $\delta_{\bar{x}_3}\left(A^n\delta_{x_3}P^{n+1}\right)_{ijk}$ can be defined similarly.

The implicit finite difference fractional steps algorithm for the flow equation (20a) is shown as follows,

$$d(C_{ijk}^n)\frac{P_{ijk}^{n+1/3}-P_{ijk}^n}{\Delta t}=\delta_{\bar{x}_1}\left(A^n\delta_{x_1}P^{n+1/3}\right)_{ijk}+\delta_{\bar{x}_2}\left(A^n\delta_{x_2}P^n\right)_{ijk}+\delta_{\bar{x}_3}\left(A^n\delta_{x_3}P^n\right)_{ijk}+q(X_{ijk},t^{n+1}),1\le i\le N, \tag{24a}$$

$$d(C_{ijk}^n)\frac{P_{ijk}^{n+2/3}-P_{ijk}^{n+1/3}}{\Delta t}=\delta_{\bar{x}_2}\left(A^n\delta_{x_2}(P^{n+2/3}-P^n)\right)_{ijk},1\le j\le N, \tag{24b}$$

$$d(C_{ijk}^n)\frac{P_{ijk}^{n+1}-P_{ijk}^{n+2/3}}{\Delta t}=\delta_{\bar{x}_3}\left(A^n\delta_{x_3}(P^{n+1}-P^n)\right)_{ijk},1\le k\le N. \tag{24c}$$

Darcy velocity $\boldsymbol{U}=(U_1,U_2,U_3)^T$ is computed by the following expression

$$U_{1,ijk}^{n+1}=-\frac{1}{2}\left[A_{i+1/2,jk}^n\frac{P_{i+1,jk}^{n+1}-P_{ijk}^{n+1}}{h}+A_{i-1/2,jk}^n\frac{P_{ijk}^{n+1}-P_{i-1,jk}^{n+1}}{h}\right], \tag{25}$$

and analogous forms $U_{2,ijk}^{n+1}$, $U_{3,ijk}^{n+1}$ can be derived.

The implicit upwind finite difference fractional steps algorithm for the saturation equations is

$$\begin{aligned}\Phi_{ijk}\frac{C_{\alpha,ijk}^{n+1/3}-C_{\alpha,ijk}^n}{\Delta t}&=\delta_{\bar{x}_1}\left(D\delta_{x_1}C_\alpha^{n+1/3}\right)_{ijk}+\delta_{\bar{x}_2}\left(D\delta_{x_2}C_\alpha^n\right)_{ijk}+\delta_{\bar{x}_3}\left(D\delta_{x_3}C_\alpha^n\right)_{ijk}\\&\quad-b_\alpha(C_{\alpha,ijk}^n)\frac{P_{ijk}^{n+1}-P_{ijk}^n}{\Delta t}+g(X_{ijk},t^n,C_{\alpha,ijk}^n),1\le i\le N,\alpha=1,2,\cdots,N_c-1,\end{aligned} \tag{26a}$$

$$\Phi_{ijk}\frac{C_{\alpha,ijk}^{n+2/3}-C_{\alpha,ijk}^{n+1/3}}{\Delta t}=\delta_{\bar{x}_2}\left(D\delta_{x_2}(C_\alpha^{n+2/3}-C_\alpha^n)\right)_{ijk},1\le j\le N,\alpha=1,2,\cdots,N_c-1, \tag{26b}$$

$$\Phi_{ijk}\frac{C_{\alpha,ijk}^{n+1}-C_{\alpha,ijk}^{n+2/3}}{\Delta t}=\delta_{\bar{x}_3}\left(D\delta_{x_3}(C_\alpha^{n+1}-C_\alpha^n)\right)_{ijk}-\sum_{\beta=1}^{3}\delta_{U_\beta^{n+1},x_\beta}C_{\alpha,ijk}^{n+1},1\le k\le N,\alpha=1,2,\cdots,N_c-1, \tag{26c}$$

where

$$\delta_{U_\beta^{n+1},x_\beta}C_{\alpha,ijk}^{n+1}=U_{\beta,ijk}^{n+1}\{H(U_{\beta,ijk}^{n+1})\delta_{\bar{x}_\beta}+(1-H(U_{\beta,ijk}^{n+1}))\delta_{x_\beta}\}C_{\alpha,ijk}^{n+1},\beta=1,2,3,\alpha=1,2,\cdots,n_c-1,\quad H(z)=\begin{cases}1,z\ge 0,\\0,z<0.\end{cases}$$

Initial approximation:

$$P_{ijk}^0=p_0(X_{ijk}),C_{\alpha,ijk}^0=c_{\alpha,0}(X_{ijk}),1\le i,j,k\le N,\alpha=1,2,\cdots,n_c-1. \tag{27}$$

The implicit upwind fractional steps algorithm runs as follows. Given $\{P_{ijk}^n, C_{\alpha,ijk}^n, \alpha = 1,2,\cdots,n_c-1\}$, the values of transition layer by (24a) and speedup method in x_1 direction firstly. Then $\{P_{ijk}^{n+2/3}\}$ and $\{P_{ijk}^{n+1}\}$ are computed by (24b) and by (24c), respectively. Using (25) we can have the numerical values of velocity $\{U_{ijk}^{n+1}\}$. Secondly, $\{C_{\alpha,ijk}^{n+1/3}\}$ is computed by (26a) and speedup method in x_1 direction. $\{C_{\alpha,ijk}^{n+2/3}\}$ and $\{C_{\alpha,ijk}^{n+1}\}$ are obtained similarly by (26b) and (26c). Notice the problem is positive definite, so the solution of (24)-(26) exists and is unique.

Let $\pi = p - P$ and $\xi_\alpha = c_\alpha - C_\alpha$ where p, c_α are exact solutions and P, C_α are numerical solutions. The pressure equation is considered firstly, and its equivalent difference expression is

$$\begin{aligned} & d(C_{ijk}^n)\frac{P_{ijk}^{n+1}-P_{ijk}^n}{\Delta t} - \nabla_h\left(A^n\nabla_h P^{n+1}\right)_{ijk} = q(X_{ijk},t^{n+1}) - (\Delta t)^2\left\{\delta_{\bar{x}_1}\left(A^n\delta_{x_1}(d^{-1}(C^n)\delta_{\bar{x}_2}(A^n\delta_{x_2}))\right)\right. \\ & \left.+\delta_{\bar{x}_1}\left(A^n\delta_{x_1}(d^{-1}(C^n)\delta_{\bar{x}_3}(A^n\delta_{\bar{x}_3}))\right)+\delta_{\bar{x}_2}\left(A^n\delta_{x_2}(d^{-1}(C^n)\delta_{\bar{x}_3}(A^n\delta_{x_3}))\right)\right\}d_tP_{ijk}^n \\ & +(\Delta t)^3\delta_{\bar{x}_1}\left(A^n\delta_{x_1}(d^{-1}(C^n)\delta_{\bar{x}_2}(A^n\delta_{x_2}(d^{-1}(C^n)\delta_{\bar{x}_3}(A^n\delta_{\bar{x}_3}d_tP^n)\cdots)\right)_{ijk}, 1\le i,j,k\le N. \end{aligned} \tag{28}$$

Then the error equation of the pressure is

$$\begin{aligned} & d(C_{ijk}^n)\frac{\pi_{ijk}^{n+1}-\pi_{ijk}^n}{\Delta t} - \nabla_h\left(A^n\nabla_h\pi^{n+1}\right)_{ijk} = -(\Delta t)^2\left\{\delta_{\bar{x}_1}\left(A^n\delta_{x_1}(d^{-1}(C^n)\delta_{\bar{x}_2}(A^n\delta_{x_2}))\right)+\delta_{\bar{x}_1}\left(A^n\delta_{x_1}(d^{-1}(C^n)\delta_{\bar{x}_3}(A^n\delta_{\bar{x}_3}))\right)\right. \\ & \left.+\delta_{\bar{x}_2}\left(A^n\delta_{x_2}(d^{-1}(C^n)\delta_{\bar{x}_3}(A^n\delta_{x_3}))\right)\right\}d_t\pi_{ijk}^n+(\Delta t)^3\delta_{\bar{x}_1}\left(A^n\delta_{x_1}(d^{-1}(C^n)\delta_{\bar{x}_2}(A^n\delta_{x_2}(d^{-1}(C^n)\delta_{\bar{x}_3}(A^n\delta_{\bar{x}_3}d_tP^n)\cdots)\right)_{ijk} \\ & +(\Delta t)^2\left\{\delta_{\bar{x}_1}\left(A^n\delta_{x_1}(d^{-1}(C^n)\delta_{\bar{x}_2}(A^n\delta_{x_2}))\right)+\cdots\right\}d_tp_{ijk}^n \\ & -(\Delta t)^3\delta_{\bar{x}_1}\left(A^n\delta_{x_1}(d^{-1}(C^n)\delta_{\bar{x}_2}(A^n\delta_{x_2}(d^{-1}(C^n)\delta_{\bar{x}_3}(A^n\delta_{\bar{x}_3}d_tp^n)\cdots)\right)_{ijk}+\sigma_{ijk}^{n+1}, 1\le i,j,k\le N, \end{aligned} \tag{29}$$

where $d_t\pi^n = (\pi^{n+1}-\pi^n)/\Delta t, |\sigma_{ijk}^{n+1}| \le M\{h^2+\Delta t\}$.

Multiplying both sides of error equation (29) by $\delta_t\pi^n = \pi^{n+1}-\pi^n = d_t\pi^n\Delta t$, summing by parts, and obtaining an inner product form

$$\begin{aligned} & \left\langle d(C^n)d_t\pi^n, d_t\pi^n\right\rangle\Delta t+\frac{1}{2}\left\{\left\langle A^n\nabla_h\pi^{n+1},\nabla_h\pi^{n+1}\right\rangle-\left\langle A^n\nabla_h\pi^n,\nabla_h\pi^n\right\rangle\right\} \\ & \le M\left\{h^4+(\Delta t)^2\right\}\Delta t+\varepsilon\left|d_t\pi^n\right|_0^2\Delta t-(\Delta t)^2\left\{\left\langle\delta_{\bar{x}_1}\left(A^n\delta_{x_1}(d^{-1}(C^n)\delta_{\bar{x}_2}(A^n\delta_{x_2}d_t\pi^n))\right),d_t\pi^n\right\rangle\right. \\ & \left.+\left\langle\delta_{\bar{x}_1}\left(A^n\delta_{x_1}(d^{-1}(C^n)\delta_{\bar{x}_3}(A^n\delta_{\bar{x}_3}d_t\pi^n))\right),d_t\pi^n\right\rangle+\left\langle\delta_{\bar{x}_2}\left(A^n\delta_{x_2}(d^{-1}(C^n)\delta_{\bar{x}_3}(A^n\delta_{x_3}d_t\pi^n))\right),d_t\pi^n\right\rangle\right\}\Delta t \\ & +(\Delta t)^3\left\langle\delta_{\bar{x}_1}\left(A^n\delta_{x_1}(d^{-1}(C^n)\delta_{\bar{x}_2}(A^n\delta_{x_2}(d^{-1}(C^n)\delta_{\bar{x}_3}(A^n\delta_{\bar{x}_3}d_t\pi^n)\cdots),d_t\pi^n\right\rangle\Delta t. \end{aligned} \tag{30}$$

Then it follows from (30) by complicated estimates,

$$\left|d_t\pi^n\right|_0^2\Delta t+\frac{1}{2}\left\{\left\langle A^n\nabla_h\pi^{n+1},\nabla_h\pi^{n+1}\right\rangle-\left\langle A^n\nabla_h\pi^n,\nabla_h\pi^n\right\rangle\right\}\le M\left\{\left|\pi^{n+1}\right|_1^2+\left|\pi^n\right|_1^2+h^4+(\Delta t)^2\right\}\Delta t. \tag{31}$$

Secondly an error analysis proceeds for the saturation equations. Eq. (26) is rewritten in the following equivalent form

$$\begin{aligned} & \Phi_{ijk}\frac{C_{\alpha,ijk}^{n+1}-C_{\alpha,ijk}^n}{\Delta t}-\nabla_h\left(D\nabla_hC_\alpha^{n+1}\right)_{ijk} = -\sum_{\beta=1}^3\delta_{U_\beta^{n+1},x_\beta}C_{\alpha,ijk}^{n+1}+b_\alpha(C_{ijk})\frac{P_{ijk}^{n+1}-P_{ijk}^n}{\Delta t}+g(X_{ijk},t^{n+1},C_{\alpha,ijk}^{n+1}) \\ & -(\Delta t)^2\left\{\delta_{\bar{x}_1}\left(D\delta_{x_1}(\Phi^{-1}\delta_{\bar{x}_2}(D\delta_{x_2}))\right)+\delta_{\bar{x}_1}\left(D\delta_{x_1}(\Phi^{-1}\delta_{\bar{x}_3}(D\delta_{x_3}))\right)+\delta_{\bar{x}_2}\left(D\delta_{x_2}(\Phi^{-1}\delta_{\bar{x}_3}(D\delta_{x_3}))\right)\right\}d_tC_{\alpha,ijk}^n \\ & +(\Delta t)^3\delta_{\bar{x}_1}\left(D\delta_{x_1}(\Phi^{-1}\delta_{\bar{x}_2}(D\delta_{x_2}(\Phi^{-1}\delta_{\bar{x}_3}(D\delta_{x_3}d_tC_\alpha^n)\cdots)\right)_{ijk}, 1\le i,j,k\le N, \alpha=1,2,\cdots,n_c-1. \end{aligned} \tag{32}$$

From (20c) and (32),

$$\begin{aligned} & \Phi_{ijk}\frac{\xi_{\alpha,ijk}^{n+1}-\xi_{\alpha,ijk}^n}{\Delta t}-\nabla_h\left(D\nabla_h\xi_\alpha\right)_{ijk}^{n+1} = -\sum_{\beta=1}^3\left[\delta_{U_\beta^{n+1},x_\beta}C_{\alpha,ijk}^{n+1}-\delta_{u_\beta^{n+1},x_\beta}c_{\alpha,ijk}^{n+1}\right]+g(X_{ijk},t^{n+1},C_{\alpha,ijk}^{n+1})-g(X_{ijk},t^n,C_{\alpha,ijk}^n) \\ & +b_\alpha(C_{ijk}^n)\frac{\pi_{ijk}^{n+1}-\pi_{ijk}^n}{\Delta t}-\left[b_\alpha(C_{ijk}^{n+1})-b_\alpha(c_{ijk}^n)\right]\frac{p_{ijk}^{n+1}-p_{ijk}^n}{\Delta t}+(\Delta t)^2\left\{\delta_{\bar{x}_1}\left(D\delta_{x_1}(\Phi^{-1}\delta_{\bar{x}_2}(D\delta_{x_2}))\right)\right. \end{aligned}$$

$$+\delta_{\bar{x}_1}\left(D\delta_{x_1}(\Phi^{-1}\delta_{\bar{x}_3}(D\delta_{x_3}))\right)+\delta_{\bar{x}_2}\left(D\delta_{x_2}(\Phi^{-1}\delta_{\bar{x}_3}(D\delta_{x_3}))\right)\Big\}d_t\xi^n_{\alpha,ijk}$$
$$+(\Delta t)^3\delta_{\bar{x}_1}\left(D\delta_{x_1}(\Phi^{-1}\delta_{\bar{x}_2}(D\delta_{x_2}(\Phi^{-1}\delta_{\bar{x}_3}(D\delta_{x_3}d_t\xi^n_\alpha)\cdots)\right)_{ijk}+\varepsilon^{n+1}_{\alpha,ijk},1\le i,j,k\le N,\alpha=1,2,\cdots,n_c-1, \tag{33}$$

where $|\varepsilon^{n+1}_{\alpha,ijk}|\le M\{h+\Delta t\}$.

Testing both sides of the above equation by $\delta_t\xi^n_{\alpha,ijk}=\xi^{n+1}_{\alpha,ijk}-\xi^n_{\alpha,ijk}=d_t\xi^n_{\alpha,ijk}\Delta t$, summing by parts, and obtaining an inner product form

$$\begin{aligned}&\left\langle\Phi d_t\xi^n_\alpha,d_t\xi^n_\alpha\right\rangle+\frac{1}{2}\left\{\left\langle D\nabla_h\xi^{n+1}_\alpha,\nabla_h\xi^{n+1}_\alpha\right\rangle-\left\langle D\nabla_h\xi^n_\alpha,\nabla_h\xi^n_\alpha\right\rangle\right\}\\&\le M\left\{\left|\xi^n\right|^2_0+\left|\xi^{n+1}\right|^2_0+\left|\pi^{n+1}\right|^2_1+h^2+(\Delta t)^2\right\}\Delta t+\varepsilon\left|d_t\xi^n_\alpha\right|^2_0\Delta t+\left\langle b_\alpha(C^n)d_t\pi^n,d_t\pi^n\right\rangle\Delta t\\&-(\Delta t)^2\left\{\left\langle\delta_{\bar{x}_1}\left(D\delta_{x_1}(\Phi^{-1}\delta_{\bar{x}_2}(D\delta_{x_2}d_t\xi^n_\alpha))\right),d_t\xi^n_\alpha\right\rangle\right.\\&\left.+\left\langle\delta_{\bar{x}_1}\left(D\delta_{x_1}(\Phi^{-1}\delta_{\bar{x}_3}(D\delta_{\bar{x}_3}d_t\xi^n_\alpha))\right),d_t\xi^n_\alpha\right\rangle+\left\langle\delta_{\bar{x}_2}\left(D\delta_{x_2}(\Phi^{-1}\delta_{\bar{x}_3}(D\delta_{x_3}d_t\xi^n_\alpha))\right),d_t\xi^n_\alpha\right\rangle\right\}\Delta t\\&+(\Delta t)^3\left\langle\delta_{\bar{x}_1}\left(D\delta_{x_1}(\Phi^{-1}\delta_{\bar{x}_2}(D\delta_{x_2}(\Phi^{-1}\delta_{\bar{x}_3}(D\delta_{\bar{x}_3}d_t\xi^n_\alpha)\cdots)\right),d_t\xi^n_\alpha\right\rangle\Delta t,\alpha=1,2,\cdots,n_c-1,\end{aligned} \tag{34}$$

where $|\xi^n|^2_0=\sum_{\alpha=1}^{n_c-1}|\xi^n_\alpha|^2_0$.

Using complicated calculations of (34),

$$\left|d_t\xi^n_\alpha\right|^2_0\Delta t+\left\langle D\nabla_h\xi^{n+1}_\alpha,\nabla_h\xi^{n+1}_\alpha\right\rangle-\left\langle D\nabla_h\xi^n_\alpha,\nabla_h\xi^n_\alpha\right\rangle\le M\left\{\left|\xi^n\right|^2_1+\left|\xi^{n+1}\right|^2_1+\left|\pi^{n+1}\right|^2_1+h^2+(\Delta t)^2\right\}\Delta t. \tag{35}$$

Note $\pi^0=0,\xi^0_\alpha=0(\alpha=1,2,\cdots,n_c-1)$, and

$$\left|\pi^{L+1}\right|^2_0\le\varepsilon\sum_{n=0}^{L}|d_t\pi^n|^2_0\Delta t+M\sum_{n=0}^{L}|\pi^n|^2_0\Delta t,\quad \left|\xi^{L+1}_\alpha\right|^2_0\le\varepsilon\sum_{n=0}^{L}|d_t\xi^n_\alpha|^2_0\Delta t+M\sum_{n=0}^{L}|\xi^n_\alpha|^2_0\Delta t.$$

Summing on $0\le n\le L$ for (31) and (35) with respect to *t*, and summing $1\le\alpha\le n_c-1$ for (35) with respect to α,

$$\sum_{n=0}^{L}|d_t\pi^n|^2_0\Delta t+\left|\pi^{L+1}\right|_1\le\varepsilon\sum_{n=0}^{L}|d_t\xi^n|^2_0\Delta t+M\left\{h^2+(\Delta t)^2+\sum_{n=1}^{L}|\pi^{n+1}|^2_1\Delta t\right\}, \tag{36a}$$

$$\sum_{n=0}^{L}|d_t\xi^n|^2_0\Delta t+\left|\xi^{L+1}\right|_1\le M\left\{h^2+(\Delta t)^2+\sum_{n=1}^{L}\left[|\xi^{n+1}|^2_1+|\pi^n|^2_1\right]\Delta t\right\}, \tag{36b}$$

where $|d_t\xi^n|^2_0=\sum_{\alpha=1}^{n_c-1}|d_t\xi^n_\alpha|^2_0,\cdots$.

Collecting (36a) and (36b),

$$\sum_{n=0}^{L}\left\{|d_t\xi^n|^2_0+|d_t\pi^n|^2_0\right\}\Delta t+\left|\xi^{L+1}\right|^2_1+\left|\pi^{L+1}\right|^2_1\le M\left\{h^2+(\Delta t)^2\right\}. \tag{37}$$

Theorem Suppose that the exact solutions of (20)-(22) are suitably smooth. Applying implicit upwind difference fractional steps method (24)-(26) to compute layer by layer, we can conclude the following error estimates,

$$\|p-P\|_{\bar{L}^\infty(J;h^1)}+\sum_{\alpha=1}^{n_c-1}\|c_\alpha-C_\alpha\|_{\bar{L}^\infty(J;h^1)}+\|d_t(p-P)\|_{\bar{L}^2(J;l^2)}+\sum_{\alpha=1}^{n_c-1}\|d_t(c_\alpha-C_\alpha)\|_{\bar{L}^2(J;l^2)}\le M^*\{h+\Delta t\}, \tag{38}$$

where $M*$ depends on $p(x,t)$, $c_\alpha(x,t)(\alpha=1,2,\cdots,n_c-1)$ and their derivatives.

7. Discussion

Theory, method and application of numerical simulation of three-dimensional three-phase (water, oil and gas) percolation mechanics of three compound combination flooding (the polymer, surface active agents and alkali) in porous media are discussed in this paper consisting of six sections. Summary is first stated about our project and the full process of this project. Mathematical model of permeation fluid mechanics, basic physical assumption and the characters of the model are presented in the second section. A full implicit numerical scheme and implicit/explicit algorithm for the pressure and the saturation are given, and an upwind difference fractional

steps algorithm based on upstream sequence is structured in the third section. This program runs quickly, is of high accuracy and applied in general cases. A type of software applicable in major industries has been accomplished, mostly carried out with the spacial step of ten-meters, tens of thousands nodes and tens of years simulation period in the fourth section. Some experimental tests occurring successfully in national major oil fields such as Daqing Oilfield, Shengli Oilfield and Dagang Oilfield, are illustrated in the fifth section. This gives outstanding social benefits and economic benefits, and accelerates the development of energy sciences. Numerical analysis proceeds for the model problem and precise theoretical results are stated on mathematical and mechanical consideration in the sixth section. This research brings important theoretical values for the design and development of enhanced oil recovery simulation, the principle, method and the software.

Acknowledgments

The authors express their deep appreciation to prof. J. Douglas Jr, prof. R. E. Ewing and prof. Jiang Lishang for their many helpful suggestions in the serial of research of chemical production.

References

Douglas, Jr. J. (1983). Finite difference methods for two-phase incompressible flow in porous media. *SIAM. J. Numer. Anal*., *20*(4), 681-696. http://dx.doi.org/10.1137/0720046

Douglas, Jr. J., & Gun, J. E. (1963). Two order correct difference analogues for the equation of multidimensional heat flow. *Math. Comp.*, *81*, 71-80. http://dx.doi.org/10.1090/S0025-5718-1963-0149676-2

Ewing, R. E. (1983). *The Mathematics of Reservoir Simulation*. SIAM, Philadelphia.

Ewing, R. E., Yuan, Y. R., & Li, G. (1989). *Finite element for chemical-flooding simulation*. Proceeding of the 7th International conference finite element method in flow problems, 1264-1271. The University of Alabama in Huntsville, Huntsville, Alabama: UAHDRESS. http://dx.doi.org/10.1137/1.9781611971071

Marchuk, G. I. (1990). *Splitting and Alternating Direction Methods*. In: Ciarlet P G, Lions J L, eds, Handbook of Numerical Analysis. Paris: Elservier Science Publishers BV., 197-400.

Peaceman, D. W. (1980). *Fundamental of Numerical Reservoir Simulation*. Amsterdam: Elsevier.

Yanenke, M. M. (1967). *The Method for Fractional Steps*. Berlin, Springer-Verlag.

Yuan, Y. R. (1993). The characteristic finite difference method for enhanced oil recovery simulation and L^2 estimates. *Science in China (Series A)*, *11*, 1296--1307.

Yuan, Y. R. (1993). The characteristic-mixed finite element method for enhanced oil recovery simulation and optimal order L^2 error estimate. *Chinese Science Bulletin, 21,* 1761--1766.

Yuan, Y. R. (1994). The characteristic mixed finite element method and analysis for two dimensional chemical-flooding reservoir simulation. *Acta Mathematicae Applicatae Sinica*, *1*, 118-131.

Yuan, Y. R. (1999). The characteristic finite difference fractional steps method for compressible two-phase displacement problem. *Science in China (Series A)*, *1,* 48-57. http://dx.doi.org/10.1007/BF02872049

Yuan, Y. R. (2000). Finite element method and analysis for chemical-flow simulation. *Systems Science and Mathematical Sciences*, *3*, 302--308

Yuan, Y. R. (2001). Characteristic finite difference fractional steps methods for three-dimensional compressible multi-component displacement problem. *Acta Mathematicae Applicatae Sinica*, *2*, 242-249.

Yuan, Y. R. (2002). The upwind difference method for compressible two-phase displacement problem. *Acta Mathematicae Applicatae Sinica*, *3*, 484-496.

Yuan, Y. R. (2003). The upwind finite difference fractional steps methods for two-phase compressible flow in porous media. *Numer Methods Partial Differential Eq*., *19*(1), 67-88. http://dx.doi.org/10.1002/num.10036

Yuan, Y. R. (2013). *Theory and application of numerical simulation of energy sources*, basis of numerical simulation of chemical production (tertiary oil recovery), Chapter 3, 257-304. Beijing: Science Press.

Yuan, Y. R., Yang, D. P., & Qi, L. Q. (1998). *Research on algorithms of applied software of the polymer. Qinlin Gang* (editor in chief), Proceedings on chemical flooding, Beijing: Petroleum Industry Press, 246-253.

International Journal of Chemistry; Vol. 6, No. 4; 2014
ISSN 1916-9698 E-ISSN 1916-9701
Published by Canadian Center of Science and Education

Synthesis of Pyrrolo[3, 4-d]Pyrimidine Thiono Derivatives via Aza Wittig Reaction

Hussain Ali Soleiman[1]

[1] Chemistry Department, Aswan Faculty of Science, Aswan University, Egypt

Correspondence: Hussain Ali Soleiman, Chemistry Department, Aswan Faculty of Science, Aswan University, Egypt. Tel: 2-97-344-7480. Fax: 2-97-344-7450. E-mail: hsoleiman2001@yahoo.com

Received: September 9, 2014 Accepted: October 16, 2014 Online Published: October 28, 2014

doi:10.5539/ijc.v6n4p55 URL: http://dx.doi.org/10.5539/ijc.v6n4p55

Abstract

New pyrolo [3,4-d] pyrimidine derivatives were obtained from the aza-Wittig reactions of iminophosphorane with phenylisocyanates via of amino compounds with triphenylphosphine, hexachloroethane and triethyl-amine produced iminophosphorane.

Keywords: amino compound,isocyanate, pyrrole, pyrimidine, aza-Wittig reaction, synthesis

1. Introduction

The aza-Wittig reactions of iminophosphoranes have received increased attention in view of their utility in the synthesis of nitrogen heterocyclic compounds (Palacios et al., 2006, 2007; Lopez et al., 2007; Lertpibulpanya et al., 2006; Marsden et al., 2008; Haraguchi et al., 2004; Cushman et al., 2004; Depecker et al., 2004; Wnuk et al., 2004). The reaction is useful in the synthesis of acyclic imines and heterocumulenes and in the intramolecular formation of carbon-nitrogen double bonds in heterocyclic synthesis. Stability, basicity, and nucleophilicity of iminophosphoranes are mainly determined by the substitutes at the nitrogen atom. Carbonyl groups of aldehydes, ketones, acid halides, and heterocumulenes are generally reactive (Daboun et al., 1983). Recently we have been interested in the synthesis of new pyrrolo [3,4-d] pyrimidine derivatives via aza-Wittig reaction by pyrimidines nuclei with phenylisocyanate (He et al., 2013, 2014). Pyrimidine derivatives play an important role in several biological and pharmacological active substances such as antibacterial and antitumor agents as well as agrochemical and veterinary products (Wright et al., 1977; Taylor et al., 1992; Traxler et al., 1997; Vicentini et al., 1989; Molina et al., 1994). The nucleophilicity at the nitrogen is a factor of essential mechanistic importance in the use of these iminophosphoranes as aza-Wittig reagents. Iminophosphoranes are important reagents in synthetic organic chemistry, especially in the synthesis of naturally occurring products, compounds with biological and pharmacological activity (Ramazani et al., 2008). Organophosphorus compounds have been extensively employed in organic synthesis as useful reagents, as well as legends, in a number of transition metal catalysts (Kaska, 1983; Ramazani et al., 2006; Stolzenberg et al., 2005).

2. Experimental

2.1 Synthesis of 6-Amino-4-Hydroxy-2-Thiouracil Sodium Salt Derivatives (1a-f)

To a solution of 4.6 mg (0.2 Mol) of metallic sodium in 75 ml of absolute ethanol was added 7.6 gm (0.1 Mol) of powdered thiourea and arylidenocyano-ethyl-acetate (cinnamonitrile) ylidenocyanoethylacetate. The reaction mixture was heated under reflux (0.1 mol) for two hours, then filtered while hot. The sodium salt of 6-amino-4-hydroxy-2-thiouracil thus obtained was washed alcohol and dried.

2.2 Synthesis of 6-Amino-4-Hydroxy-2-Thiouracil Derivatives (2a-f)

To a cold solution sodium salt of 6-amino-4-hydroxy-2-thiouracil derivatives (1a-f) in ice-water was added dilute HCl until the mixture was neutralized, whereby crystalline products separated out, and crystallized from the appropriate solvent (ethanol) to give 6-amino-4-hydroxy-2-thiouracil derivatives (2a-f). The results are listed in Table 1.

2.3 Synthesis of 4-Hydroxy-6-Aminotriphenylphosphorane-2-Thiouracil (3a-f)

To a mixture of 6-amino-4-hydroxy-2-thiouracil derivatives 2a-f (1.56, 1.71, 2.22, 2.332.62, 8 mmol), triphenylphosphine (3.14 g, 12 mmol) and hexachloroethan (2.84 g, 12 mmol) in dry acetonitrile (40 ml) was

Table 1. Characterization of compounds (1-5) a-f

Comp. No.	M.P. °C	Colour	Yield %	Cryst.	M.F (M. Wt.)	Analysis % calced (found) C	H	N	S	M.S.
1a	>300	Yellow	40	Ethanol	$C_5H_6N_3OSNa$ (179.17)	33.52 (33.50)	3.38 (3.38)	23.45 (23.48)	17.89 (17.85)	179
1b	>300	Pale yellow	50	Ethanol	$C_6H_9N_3OSNa$ (194.20)	37.11 (37.12)	4.67 (4.66)	21.64 (21.70)	16.51 (16.56)	194
1c	>300	Brown	80	Ethanol	$C_9H_8N_3O_2SNa$ (245.23)	44.08 (44.10)	3.29 (3.30)	17.13 (17.15)	13.07 (13.12)	245
1d	>300	White	70	Ethanol	$C_{11}H_{11}N_3OSNa$ (256.27)	51.55 (51.56)	4.33 (4.32)	16.40 (16.44)	12.51 (12.50)	256
1f	>300	Yellow	85	Ethanol	$C_{12}H_{12}N_3O_2SNa$ (285.29)	50.52 (50.48)	4.24 (4.22)	14.73 (14.75)	11.24 (11.30)	285
2a	218-220	Yellow	40	Ethanol	$C_5H_6N_3OS$ (156.18)	38.45 (38.45)	3.87 (3.88)	26.90 (26.86)	20.53 (20.48)	156
2b	200-202	Pale yellow	50	Ethanol	$C_6H_9N_3OS$ (171.21)	42.09 (42.12)	5.30 (5.30)	24.54 (24.50)	18.72 (18.75)	171
2c	244-246	White	80	Ethanol	$C_9H_8N_3O_2S$ (222.24)	48.64 (48.66)	3.63 (3.62)	18.91 (18.94)	14.43 (14.48)	222
2d	187-189	Yellow	70	Ethanol	$C_{11}H_{11}N_3OS$ (233.28)	56.63 (56.60)	4.75 (4.76)	18.01 (18.05)	13.74 (13.70)	233
2f	>300	Yellow	90	Ethanol	$C_{12}H_{12}N_3O_2S$ (262.30)	54.95 (54.90)	4.61 (4.60)	16.02 (16.06)	12.22 (12.28)	262
3a	123-125	Pale yellow	20	Ethanol	$C_{23}H_{20}N_3OSP$ (417.46)	66.17 (66.20)	4.83 (4.80)	10.07 (10.12)	7.68 (7.64)	417
3b	144-146	White	40	Ethanol	$C_{23}H_{22}N_3OSP$ (419.48)	65.86 (65.84)	5.29 (5.30)	10.02 (10.06)	7.64 (7.70)	419
3c	133-135	Brownish yellow	50	Ethanol	$C_{27}H_{22}N_3OSP$ (467.52)	69.36 (69.35)	4.74 (4.74)	8.99 (9.00)	6.86 (6.90)	467
3d	168-170	White	40	Ethanol	$C_{29}H_{23}N_3OSP$ (492.55)	70.42 (70.40)	4.71 (4.70)	8.53 (8.50)	6.51 (6.46)	492
3f	283-285	White	60	Ethanol	$C_{24}H_{22}N_3OSP$ (431.49)	66.81 (66.78)	5.14 (5.10)	9.74 (9.78)	7.43 (7.40)	431
4a	114-116	Pale yellow	60	Ethanol	$C_{12}H_{10}N_4OS$ (258.29)	55.80 (55.80)	3.90 (3.90)	21.69 (21.70)	12.41 (12.40)	258
4b	162-164	Pale yellow	20	Ethanol	$C_{13}H_{12}N_4OS$ (272.32)	57.34 (57.34)	4.44 (4.44)	20.57 (20.50)	11.77 (11.70)	272
4c	154-156	Pale yellow	45	Ethanol	$C_{16}H_{11}N_4O_2S$ (323.34)	59.43 (59.45)	3.43 (3.40)	17.33 (17.35)	9.91 (9.90)	324
4d	149-151	White	20	Ethanol	$C_{18}H_{14}N_4OS$ (334.39)	64.65 (64.68)	4.22 (4.20)	16.75 (16.70)	9.59 (9.65)	334
4f	259-261	Pale yellow	35	Ethanol	$C_{19}H_{16}N_4O_2S$ (364.42)	62.62 (62.60)	4.43 (4.44)	15.37 (15.40)	8.80 (8.86)	364

added dropwise of tiethylamine (2.42 g, 24 mmol) at room temperature. After for 6h, the solvent was removed under reduced pressure and the residue was recrystallized from EtOH to give iminophosphorane (3a-f).

2.4 Synthesis of Pyrrolo [3,4-D] Pyrimidine Derivatives (5a-f)

With a mixture of iminophosphorane derivatives (3a-f) (4.17, 4.19, 4.92, 4.92, 4.31 respectively). (10 mmol) in dry methylene dichloride (25 ml) was added phenyl isocyanate (10 mmol) under nitrogen at room temperature. After the reaction mixture was standing 8-10 hours at 0-5 °C, the solvent was removed off under reduce pressure and ether (petroleum ether (1: 2, 20 ml) was added to precipitate triphenylphosphine oxide. Filtered, the solvent was removed to give carbodiimide derivatives, which were directly cyclized to pyrrolo [3,4-d] pyrimide derivatives (4a-f).

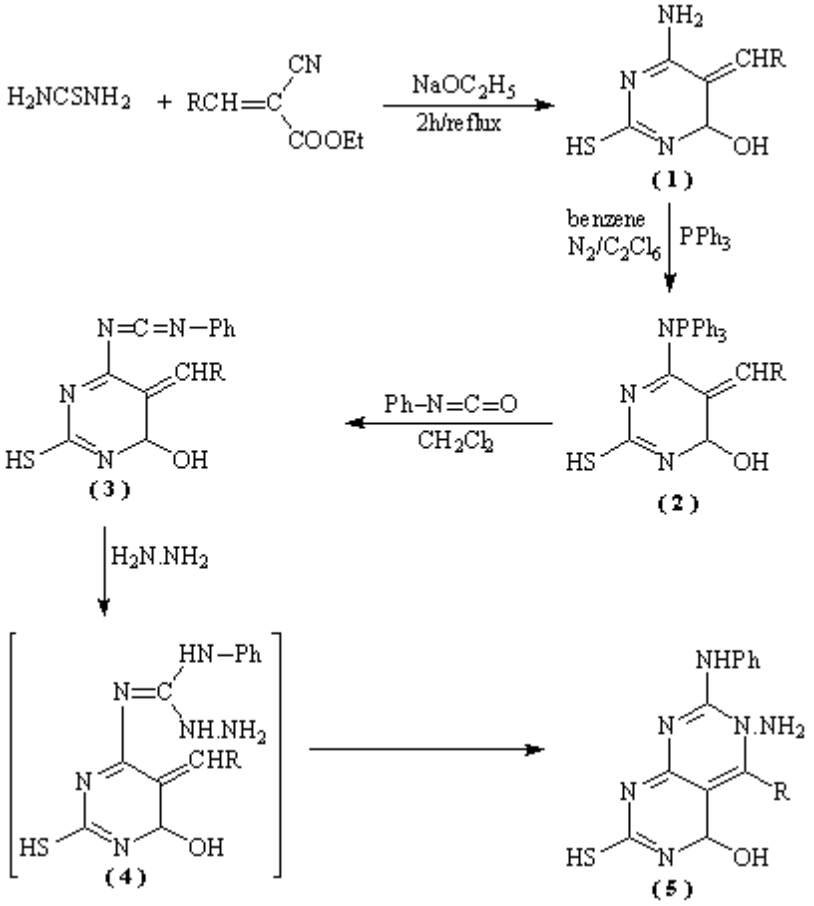

Where (1, 2, 3, 4) a-f: a, R = H; b, R = CH_3-; c, R = C_6H_5-; d, R=p-CH_3 O-C_6H_4 ; f, R=C_4H_3O.

3. Results and Discussion

The 6-amino-5-alkyl or/aryl-4-hydroxy-2-mercapto pyrimidine derivatives 1a-f was obtained by cyclization of alkylidine or/arylidine with thiourea under basic condition. The structure of compounds 1a-f were confirmed by elemental analysis (c.f. Table 1), and IR spectrum (γ KBr) showed general absorption bands at 3500 cm-1 (OH), and at 3370-3350 cm-1 (NH2). The 1H NMR spectrum (DMSO)[10] of compounds 1a-f showed signals. 1a: at 9.0 ppm(s, 1H, OH), 8.7 ppm(s, 1H, SH), at 8.5 ppm(s, 1H, Hpyrimidine), 6 ppm(s, 2H, CH2), at 5.2 ppm(br, 2H, NH2). 1b: at 9.0 ppm(s, 1H, OH), at 8.7 ppm(s, 1H, SH), at 8.5 ppm(s, 1H, Hpyrimidine), at 6 ppm(s, 1H, CH), at 5.2 ppm(br, 2H, NH2), at 2.3 ppm(s, 3H, CH3). 1c: at 9.0 ppm(s, 1H, OH), at 8.7 ppm(s, 1H, SH), at 8.5 ppm(s, 1H, Hpyrimidine), at 6 ppm(s, 2H, CH2), at 5.2 ppm(br, 2H, NH2), 1b: at 9.0 ppm(s, 1H, OH), at 8.7 ppm(s, 1H, SH), at 8.5 ppm(s, 1H, Hpyrimidine), at 8.3-7 ppm(m, 5H, Ar-H+), at 6 ppm(s, 1H, CH), at 5.2 ppm(br, 2H, NH2). Thinopyrimidine derivatives 1a-f were converted to iminophosphorane 2a-f via reaction with triphenylphosphine, hexachloroethane and triethylamine (Scheme). The structure of compounds 2a-f were

confirmed by elemental analysis (c.f. Table 1), and IR spectrum (KBr), general absorption band at 3500 cm^{-1} (OH). The 1H NMR spectrum (DMSO)[10] of compounds 2a-f showed signals, 2a: at 9.0 ppm(s, 1H, OH), at 8.7 ppm(s, 1H, SH), at 8.5 ppm(s, 1H, Hpyrimidine), 6 ppm(s, 2H, CH2), at 5.2 ppm(br, 2H, NH2), 2b: at 9.0 ppm(s, 1H, OH), at 8.7 ppm(s, 1H, SH), at 8.5 ppm(s, 1H, Hpyrimidine), at 6 ppm(s, 1H, CH), at 5.2 ppm(br, 2H, NH2), at 2.3 ppm(s, 3H, CH3), 2c: at 9.0 ppm(s, 1H, OH), at 8.7 ppm(s, 1H, SH), at 8.5 ppm(s, 1H, Hpyrimidine), 6 ppm(s, 2H, CH2), at 5.2 ppm(br, 2H, NH2), at 8.3-7(m, 10H, Ar-H+). Iminophosphorane 2a-f reacted with aromatic isocyanates to give carbodiimides 3a-f (Scheme 1). The structure of compounds 3a-f were confirmed by elemental analysis (c.f. Table 1), and IR spectrum (KBr), general absorption band at 3500 cm^{-1} (OH). The 1H NMR spectrum (DMSO)[10] of compounds 3a-f showed signals, 3a: at 9.0 ppm(s, 1H, OH), at 8.7 ppm(s, 1H, SH), at 8.5 ppm(s, 1H, Hpyrimidine), 6 ppm(s, 2H, CH2), at 5.2 ppm(br, 2H, NH2), 3b: at 9.0 ppm(s, 1H, OH), at at 8.7 ppm(s, 1H, SH), at 8.5 ppm(s, 1H, Hpyrimidine), at 6 ppm(s, 1H, CH), at 5.2 ppm(br, 2H, NH2), at 2.3 ppm(s, 3H, CH3), 3c: at 9.0 ppm(s, 1H, OH), at 8.7 ppm(s, 1H, SH), at 8.3-7(m, 10H, Ar-H+), at 8.5 ppm(s, 1H, Hpyrimidine), 6 ppm(s, 2H, CH2), at 5.2 ppm(br, 2H, NH2) . The carbodiimides 3a-f reacted with hydrazine to give the guanidine derivatives intermediate 4 via nucleophilic addition, which cyclizes to give compounds 5a-f (Scheme 1). The structure of compounds 5a-f were confirmed by elemental analysis (c.f. Table 1), and IR spectrum (KBr), general absorption band at 3500 cm^{-1} (OH), and 3370-3350 cm^{-1} (NH2, NH). The 1H NMR spectrum (DMSO)[10] of compounds 5a-f showed signals, 5a: at 9.5(s, 1H, NH), at 9.0 ppm(s, 1H, OH), at 8.7 ppm(s, 1H, SH) 8.5 ppm(s, 1H, Hpyrimidine), at 6 ppm(s, 2H, CH2), at 5.2 ppm(br, 2H, NH2), 5b : at 9.0 ppm(s, 1H, OH), at 8.7 ppm(s, 1H, SH), at 8.5 ppm(s, 1H, Hpyrimidine), at 6 ppm(s, 1H, CH), at 5.2 ppm(br, 2H, NH2), at 2.3 ppm(s, 3H, CH3), 5c: at 9.0 ppm(s, 1H, OH), 8.7 ppm(s, 1H, SH), at 8.3-7 ppm(m, 10H, Ar-H+), at 8.5 ppm(s, 1H, Hpyrimidine), at 6 ppm(s, 2H, CH2), at 5.8 ppm(br, 2H, NH2).

In conclusion, we have developed an efficient synthesis pyrimidinopyrimidine thione derivatives via aza-Wittig reactions. This method utilizes easily accessible starting materials and allows mild reaction conditions, straightforward product isolation and good yields.

References

Cushman, M., Sambaiah, T., Jin, G.., Illarionov, B., Fischer, M., & Bacher, A. (2004). Design, synthesis, and evaluation of 9-D-ribitylamino-1,3,7,9-tetrahydro-2,6,8-purinetriones bearing alkyl phosphate and alpha,alpha-difluorophosphonate substituents as inhibitors of tiboflavin synthase and lumazine synthase. *J. Org. Chem., 69*, 601.

Daboun, H. A., & El-Reedv, A. M. Z. (1983). Symposium on Malononitrile and Other Reactive Malono-Synthons, Cairo, 7 April 1983, 85. *Naturforsch, 38b*, 1686.

Depecker, G., Patino, N., Giorgio, C. D., Terreux, R., Cabrol-Bass, D., Bailly, C., … Condom, R. (2004). Cyclic PNA-based compound directed against HIV-1 TAR RNA: Modelling, liquid-phase synthesis and TAR binding Org. *Biomol. Chem., 2*, 74. http://dx.doi.org/10.1039/B311775H

Haraguchi, K., Kubota, Y., & Tanaka, H. (2004). Ring Opening of 1',2'-Epoxynucleosides with Aluminum Reagents: Stereoselective Entry to Ribonucleosides Substituted at the Anomeric Position. *J. Org. Chem., 69*, 1831.

He, P., Li, Z. F., Hou, Q. F., Wang, Y. L., & Zhao, K. (2013). An efficient synthesis of 2,3,6,7-tetrasubstituted 4,6-dihydro-4-oxo-3H-pyrrolo[3,4-d]pyrimidin-7-carbonitrilederivatives Arkivoc (iii), 199-209.

He, P., Wu, J., Hu, Y. G., Li, Z. F., Hou, Q. F., Wang, Y. L., … Zhang, E. (2014). Efficient and Selective Construction of Pyrrolo[3,2-d]pyrimidine Derivatives. *Bull. Korean Chem. Soc., 35*(2), 1.

Kaska, W. C. (1983). Phosphorus ylides are not only important synthons of the Wittig reaction but have also been used extensively as alkyl-ligands Coord. *Chem Rev, 48*, 1.

Lertpibulpanya, D., Marsden, S. P., Rodriguez-Garcia, I., & Kilner, C. A. (2006). Asymmetric Aza-Wittig Reactions: Enantioselective Synthesis of β-Quaternary Azacycles Angew. *Chem. Int. Ed., 45*, 5000. http://dx.doi.org/10.1002/ange.200601383

López, J. L., Tárraga, A., & Molina, P. (2007). Substitution and ring-opening reactions of an azasubstituted [5] ferrocenophane: preparation of 1,1'-unsymmetrically disubstituted ferrocenes. *Arkivoc, iv*, 39.

Marsden, S. P., Mc Gonagle, A. E., & Mckeever-Abbas, B. (2008). Catalytic aza-Wittig Cyclizations for Heteroaromatic Synthesis Org. *Lett., 10*, 2589. http://dx.doi.org/10.1021/o1800921n

Molina, P., & Vilaplana, M. J. (1994). Iminophosphoranes: Useful Building Blocks for the Preparation of

Nitrogen-Containing Heterocycles Synthesis, 1197. http://dx.doi.org/10.1055/s-1994-25672

Palacies, F., Herran, E., Alonso, C., Rubiales, G., Lecea, B., Ayerbe, M., & Cossio, F. P. (2006). Reaction of N -Vinylic Phosphazenes with α,β-Unsaturated Aldehydes. Azatriene-Mediated Synthesis of Dihydropyridines and Pyridines Derived from β-Amino Acids. *J. Org. CHem., 71*, 6020. http://dx.doi.org/10.1021%2fjo060775b

Palacios, F., Alonso, C., Aparicio, D., Rubiales, G., & Santos, J. M. (2007). The aza-Wittig reaction: An efficient tool for the construction of carbon-nitrogen double bonds Tetrahedron, 63, 523.

Palacios, F., Herran, E., Allonse, C., & Rubiales, G. (2007). Regioselective synthesis of dihydropyridines and pyridines derived from β-aminoacids from N-vinylic phosphazenes Arkivoc, (iv), 397.

Ramazani, A., Kazemizadeh, A. R., Ahmadi, E., Noshiranzadeh, N., & Souldozi, A. (2008). Synthesis and Reactions of Stabilized Phosphorus Ylides Curr. *Org. Chem., 12*, 59. http://dx.doi.org/10.1039/9781849730839-00001.

Ramazani, A., Kazemizadeh, A. R., Namadi, E., Slepokura, K., & Lis, T. (2006). Synthesis and X-Ray Single Crystal Structure of Dialkyl 2-[1-(2,2-Dimethylpropionyl)-3,3-dimethyl-2-oxobutyl]-3-(triphenylphosphoranylidene)succinates. *Z. Naturforsch, 616*, 1128.

Stolzenberg, H., Weinberger, B., Fehlhammer, W. P., Pühlhofer, F. G., & Weiss, R. (2005). Free and Metal-Coordinated (*N*-Isocyanimino)triphenylphosphorane: X-ray Structures and Selected Reactions. *Eur. J. Inorg. Chem., 21*, 4263. http://dx.doi.org/10.1002/ejic.200500196

Taylor, E. C., & Patel, H. H. (1992). Synthesis of pyrazolo[3,4,-d]pyrimidine analogues of the potent antitumor agent N-{4-[2-(2-amino-4(3H)-oxo-7H-pyrrolo[2,3-d]pyrimidin-5-yl)ethyl]benzoyl}-L-glutamic acid (LY231514). *Tetrahedron, 48*, 808.

Traxler, P., Bold, G., Frei, J., Lang, M., Lydon, N., Mett, H., …Furet, P. (1997). Use of a Pharmacophore Model for the Design of EGF-R Tyrosine Kinase Inhibitors: 4-(Phenylamino)pyrazolo[3,4-d]pyrimidines. *J. Med. Chem., 40*, 3601. http://dx.doi.org/10.1021/jm970124v

Vicentini, C.B., Bli, T., Veronese, A.C., Brandolini, V., Manfrini, M., & Guarneri, M. (1989). Synthesis and in-vitro antifungal activity of 6-trifluoromethyipyrazolo[3,4-6*d*]pyrimidin-4(5*H*)-thiones. *Pestic, Sci., 27*, 77. http://dx.doi.org/10.1002/ps.2780270108

Wnuk, S. F., Lewandowska, E., Companioni, D. R., Garcia, P. I., Jr., & Secrist, J. A. (2004). Synthesis and cytotoxicity of 9-(2-deoxy-2-alkyldithio-β-D-arabinofuranosyl)purine nucleosides which are stable precursors to potential mechanistic probes of ribonucleotide reductases. III *Org. Biomol. Chem., 2*, 120. http://dx.doi.org/10.1039/B311504F

Wright, G. E., & Brown, N. C. (1977). Inhibitors of Bacillus subtilis DNA polymerase III. Structure-activity relations of 6-(phenylhydrazino)uracils. *J. Med. Chem., 20*, 1181. http://dx.doi.org/10.1021/jm00219a014

International Journal of Chemistry; Vol. 6, No. 4; 2014
ISSN 1916-9698 E-ISSN 1916-9701
Published by Canadian Center of Science and Education

Cs-137 in Sand and Seawater Samples from Piraquara Beach, Brazil:

Discharge site of effluents from the Angra dos Reis Nuclear Power Plants

Maurilio F. Menezes[1,2], Cássia C. Turci[2], João A. Medeiros[2]

[1] Chemistry Division, Angra 2 Nuclear Power Plant, Eletrobrás Termonuclear S.A. – ELETRONUCLEAR, Angra dos Reis, Brazil

[2] Chemistry Institute, Rio de Janeiro Federal University, Rio de Janeiro, Brazil

Correspondence: Maurilio F. Menezes, Chemistry Division, Angra 2 Nuclear Power Plant, Eletrobrás Termonuclear S.A. – ELETRONUCLEAR, Rodovia Governador Mário Covas km 517, BR 101-SUL, CEP 23948-000, Angra dos Reis, Rio de Janeiro, Brazil. Tel: 55-24-3362-9224. E-mail: menezes@eletronuclear.gov.br

Received: September 10, 2014 Accepted: September 26, 2014 Online Published: October 29, 2014

doi:10.5539/ijc.v6n4p60 URL: http://dx.doi.org/10.5539/ijc.v6n4p60

Abstract

This study presents the Cs-137 radionuclide concentration and activity in sand profile and seawater samples from Piraquara Beach (PB) and from an adjacent small stretch of sand used as a beach. Both sites are located near the discharge point for cooling water and liquid effluents from the Almirante Álvaro Alberto Nuclear Power Station (CNAAA) in Brazil. The chemical composition of the sand samples was determined by granulometric analysis, elemental chemical characterization, and X-ray diffraction (XRD). Mineral sorbents for the Cs-137 radionuclide were found close to the discharge point. The presence of Cs-137 radionuclides in sand and seawater samples was determined by gamma spectrometry analysis, which was also used for seawater samples after absorption by ammonium phosphomolybdate (APM). The Cs-137 radionuclide activity measurements were lower than the minimum detectable activity (MDA): sand < 0.31 $Bq \cdot kg^{-1}$, direct analysis of seawater < 0.42 $Bq \cdot L^{-1}$, and seawater with APM < 0.004 $Bq \cdot L^{-1}$. The aim of this study was to measure the amount of the Cs-137 radionuclide in the deeper layers of PB. A determination of radioactive exposure to individuals was not performed because the result values were lower than the MDA values. Our results indicate that the study site shows no contamination by the Cs-137 radionuclide.

Keywords: beach sand, ^{137}Cs, radioactive pollution, seawater

1. Introduction

1.1 Cs-137 Radionuclide

Radioactive pollution comprises more than 200 active radionuclides, and effluents from nuclear power plants are one source of radionuclides in the seas and oceans (Aarkrog, 2003; International Atomic Energy Agency [IAEA], 1995, 2001, 2004). Other sources of radionuclide contamination in the seas and oceans are fallout (Collins, Jardim, & Collins, 1998; Aarkrog, 2003; IAEA, 1995, 2004), nuclear tests (Aarkrog, 2003; IAEA, 1995), nuclear submarine accidents (Aarkrog, 2003; IAEA, 2004), dumping (IAEA, 1999), effluents from reprocessing plants (Aarkrog, 2003; IAEA, 2001), radiochemical source losses (IAEA, 1988), nuclear accidents (Aarkrog, 2003; IAEA, 1995, 2004), and detonation of nuclear weapons (Aarkrog, 2003; IAEA, 2004).

In considering the environmental impact of radionuclides, the Cs-137 radionuclide is very important, not only because it has a relatively long half-life of 30 years, but also because of its chemical behavior, which causes Cs-137 to be disseminated in its ionic form by fluids in the human body, in a similar manner to that of sodium and potassium ions (Collins et al., 1998; IAEA, 1995; Agency for Toxic Substances and Disease Registry [ATSDR], 2004; Figueira & Cunha, 1998; National Research Council [NRC], 1961). Owing to this feature, the Cs-137 radionuclide is one of the main contributors to radiation from artificial sources in the environment, and is a fundamental indicator of radioactive pollution. Thus, Cs-137 is an important tool for the evaluation of disseminated radiation resulting from nuclear accidents and for monitoring radiation around nuclear power plants (IAEA, 2004, 2011; United Nations Scientific Committee on the Effects of Atomic Radiation [UNSCEAR]; International Union of Radioecology [IUR]). The severity of the effects of radiation exposure to the Cs-137

radionuclide on the human body depends on the absorbed energy per unit of mass and the parts of the body directly affected. Thus, aspects that should always be considered are what the dose absorbed by the body was and which organs received the highest doses (IAEA, 1988; National Nuclear Energy Commission [CNEN], 2005; CNEN; Haber & Rothstein, 1969). Such issues, associated with the "Law of Bergoni é and Tribondeau" (CNEN; Haber & Rothstein, 1969) indicate the danger of exposure to radiation doses for people, especially in infants and children. Radionuclides released into the marine environment may be dispersed, diluted, redistributed, and finally accumulated in specific ecosystem compartments. The processes of dispersion, accumulation, and transport of radionuclides in the marine environment are influenced by physical, chemical, and biological factors (Aarkrog, 2003; IAEA, 2001, 2004).

1.2 Angra dos Reis Nuclear Power Plants

The Almirante Álvaro Alberto Nuclear Power Station (CNAAA) is located on the southeastern coast of Brazil, in the city of Angra dos Reis, 100 km west of the city of Rio de Janeiro, and is the site of two nuclear power plants: Angra I and Angra II (Angra III is under construction), both operated by Eletrobras Termonuclear—ELETRONUCLEAR (ETN). The two plants, Angra I and Angra II, located on Itaorna Beach, began operations in 1985 and 2000, respectively. The water used for cooling in the plants is collected at Itaorna Beach and discharged, along with liquid effluents, through an underground channel in Saco da Piraquara de Fora Bay (SPF) (ETN), where Piraquara Beach (PB) is located (Figure 1).

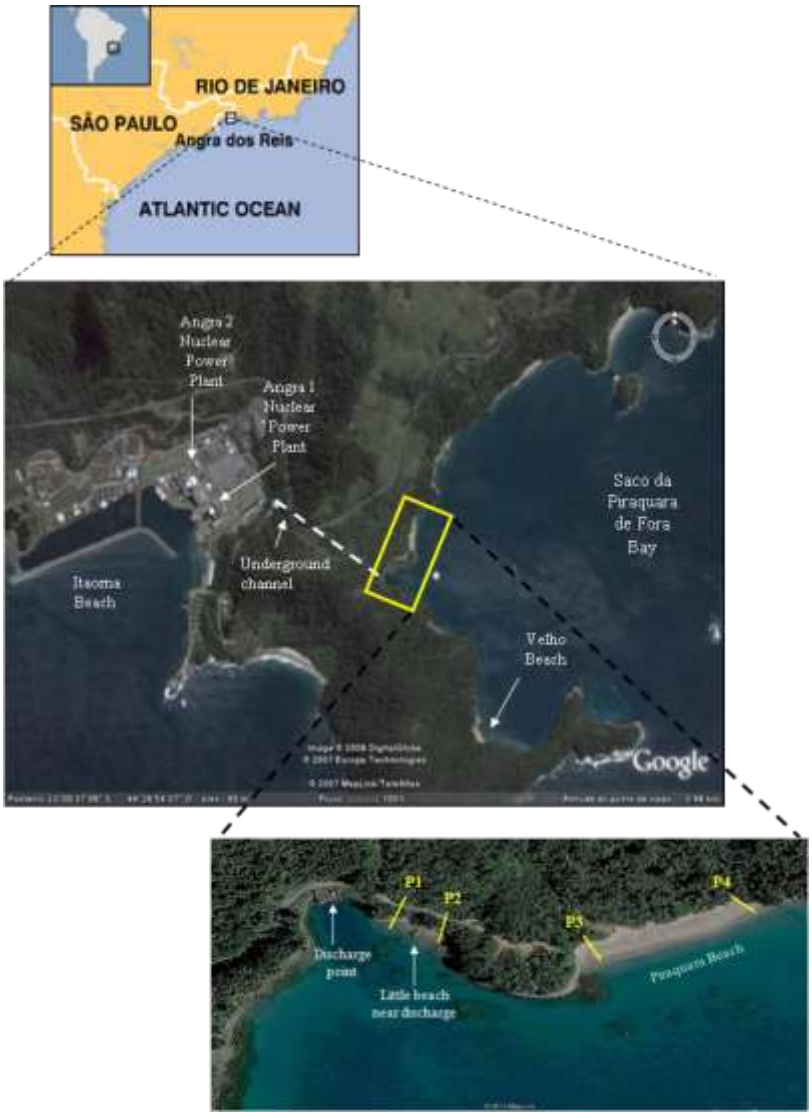

Figure 1. Location of the Angra 1 and 2 nuclear power plants on Itaorna Beach, Angra dos Reis, Brazil. The expanded view shows the underground channel, the discharge point, and Piraquara Beach in Saco da Piraquara de Fora Bay. The main sand sampling points (P1, P2, P3, and P4) are shown in yellow.

In 1985, a landslide, which occurred on PB, modified the composition of the sand at PB, and almost blocked the CNAAA discharge point (Figure 2). After restoration, land advancement separated a small stretch of sand, which is used as a beach and is located beside the CNAAA discharge point, from PB (Figure 1). Today, this small stretch of sand and PB are often used for leisure and recreation.

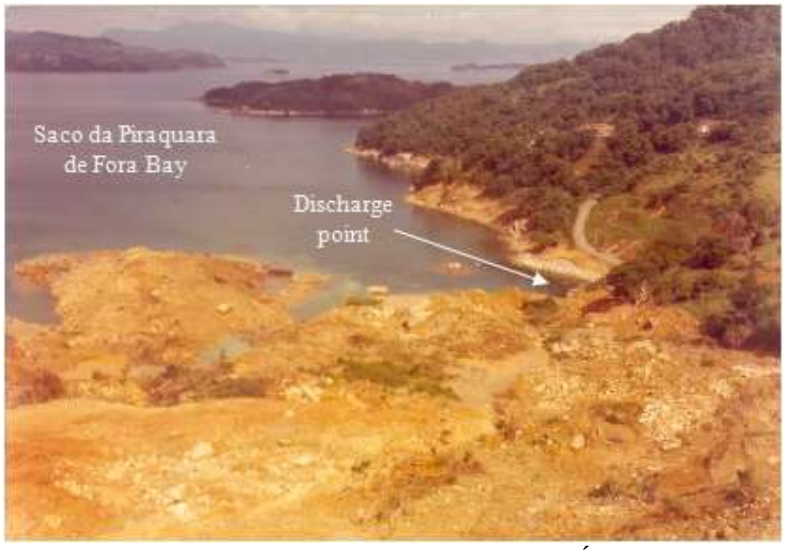

Figure 2. Photo of the 1985 landslide that almost blocked the Almirante Álvaro Alberto Nuclear Power Station (CNAAA) discharge point.

1.3 Cs-137 in Beach Sand

In comparing with the studies of Cs-137 in soils (Dion, Romanek, Hinton, & Bertsch, 2005; Bostick, Vairavamurthy, Karthikeyan, & Chorover, 2002; Flury, Mathison, & Harsh, 2002; Lujanienė, Vilimaitė-Šilobritienė, & Jokšas, 2005; McKinley et al., 2004; Todorović, Milonjić, & Čomor, 1992; Chowdhury, Kamal, Alam, Aftabuddin, & Zafar, 2004; Komarneni, 1985; Kanai et al, 2013; Rajec, Šucha, Eberl, Środoń, & Elsass, 1999; Sawhney, 1970; Environmental Protection Agency [EPA], 1999; Wahlberg & Fishman, 1962), the adsorption of the Cs-137 radionuclide in beach sand has not yet been well explored (Flury, Czigány, Chen, & Harsh, 2004; McKinley et al., 2001; Nyarko et al., 2011). The migration of the Cs-137 radionuclide through soil was observed in the Goiânia accident (IAEA, 1988), and also surrounding the Hanford plant (Flury et al., 2004) where high levels of Cs-137 caused by seepage were detected in sediments and in other studies (McKinley et al., 2001; Bostick et al., 2002; Flury et al., 2002; McKinley et al., 2004; Todorović et al., 1992; Chowdhury et al., 2004). Several studies have assessed the factors that cause adsorption of Cs-137, and the type and location of Cs^+ ion adsorption in the inner layers and the frayed edge sites (FES) of phyllosilicate minerals, such as vermiculite, illite, kaolinite, muscovite, and others (Figueira & Cunha, 1998; Flury et al., 2004; McKinley et al., 2001; Nyarko et al., 2011; Dion et al., 2005; Bostick et al., 2002; Flury et al., 2002; Lujanienė et al., 2005; McKinley et al., 2004; Todorović et al., 1992; Chowdhury et al., 2004; Komarneni, 1985; Kanai et al, 2013; Rajec et al., 1999; Sawhney, 1970; EPA, 1999; Wahlberg & Fishman, 1962).

McKinley et al. (2004) reported that the absorption of Cs^+ ions by phyllosilicate minerals, such as illite and kaolinite, is favorable. The exchange of K^+ ions for Cs^+ ions in the internal structural layers of tetrahedral-octahedral-tetrahedral (T-O-T) type structures results in a strong retention of Cs^+ ions within phyllosilicates. Another interesting study presented by the Environmental Protection Agency of the United States of America (EPA-USA) measured significant partition coefficient values for the Cs^+ ion in minerals composed of phyllosilicates, such as vermiculite and kaolinite, among others (EPA, 1999).

1.4 Study Site in Saco da Piraquara de Fora Bay

In our study area, the sand from the beach at PB was mixed with the soil from the landslide, which altered the mineralogical composition, and could possibly result in an increased adsorption of the Cs-137 radionuclide in the recreation areas of the beaches near the CNAAA liquid effluent discharge point. Liquid effluents from CNAAA are released in batches of cooling water into SPF. The geography of this inlet and the presence of islands at the entrance to the inlet, create a natural barrier against the entry of big currents and waves, and retard the dispersion of radionuclides out of SPF. Thus, the accumulation of the Cs-137 radionuclide in the sand is directly related to its concentration in the seawater. This release of effluents can lead to increased amounts of radionuclides in the

marine water, and may exceed the values recommended by the United States Nuclear Regulatory Commission [US-NRC] and the safe limit of radioactive dose exposure recommended by the National Nuclear Energy Commission (CNEN, 2005), which is the Brazilian regulator of ETN.

The current generated by the discharge of cooling water added to the liquid effluents from CNAAA mixed with the waters of SPF, prevents the formation of waves on PB and, particularly, on the small stretch of sand used as a beach close to discharge point. This lack of waves causes the sand morphology of the beach to not be significantly altered (Pilkey et al., 1993; Suguio, 1992), and this could possibly enhance the adsorption of the Cs-137 radionuclide by the sand because dispersion in SPF is slow and the grains that make up the sand layers are only slightly changed. This situation could lead to a localized concentration of Cs-137 with possible migration occurring mainly after the sand mixed with the soil from the 1985 landslide.

Franklin, Rosman, and Fernandes (2004) modeled the dispersion of Cs-137 and H-3 radionuclides in SPF and reported that CNAAA, according to its environmental licensing, can release up to 8×10^{11} Bq·year^{-1} of the Cs-137 radionuclide. The authors determined that SPF is not affected by wind or by external currents, and that the speed of the cooling water and disposal of effluents from CNAAA is the main current source in SPF.

Carvalho, Ferreira, Azevedo, Martins, and Lauria (2013) showed that the Cs-137 radionuclide was present in sediments that were in the direction of the mixing zone of SPF. The authors highlighted that the start of operations at the Angra 2 plant was responsible for increasing the flow of the discharge stream, which caused clay materials to be dragged from the bottom sediments to the discharge point, and increased the capacity for adsorption of the radionuclides released by CNAAA.

Lucca et al. (2005) studied the effect of the thermal plume from the CNAAA cooling water and discharged effluents in SPF using rhodamine. In their study, the dissemination of rhodamine in SPF mainly occurred along the short stretch used as a beach. This fact led us to study this area.

Therefore, considering the facts presented above, and because of the lack of studies performed on this short stretch, the determination of the concentration of the Cs-137 radionuclide in the SPF seawater, in the short stretch used as a beach, and in the PB leisure area is important because these are the first sites to receive the CNAAA cooling water and liquid effluents.

2. Method

2.1 Materials and Equipments

Materials used are nitric acid P.A. (Merck), cesium chloride P.A.(Fluka), APM (Aldrich) and 1% nitric acid solution. The equipments used are a Atomic Absorption Spectrometer VARIAN, model Spectr AA558, for chemical analyses; a Bruker-D4 Endeavor XRD for XRD analyses and the gamma-ray spectrometer manufactured by Canberra for the radiometric analysis (for energy efficiency of the detector used standard cocktail made by Eckert & Ziegler Analytics, traceable by the National Institute of Standards and Technology (NIST).

2.2 Sampling

Samples were collected from the recreation zone, where people (children, in particular) have contact with the wet sand on the beach (National Environment Council [CONAMA], 2000), and in the spreading zone, where morphological changes of the sand occur due to wave action (Pilkey et al., 1993; Suguio, 1992). Profile samplings were carried out using collecting tubes, with the goal of identifying the presence of Cs-137 radionuclides in deeper layers. Seawater was sampled from the surface in front of the profile sampling sites at a distance of approximately 5 m from each collection point in the sand. The sampling points were located on PB, which is used as a recreation zone near the CNAAA discharge point, the short stretch used as a beach next to the discharge point, and the spreading area. The main sampling points near the discharge point are shown in Figure 1 and the coordinates of each sampling point are presented in Table 1. Figure 1 shows Velho Beach, the location of point 5, which is also used for recreation. This beach is not highlighted because it is farther away from the CNAAA discharge point; however, Velho Beach is close to the sediment collection points where the presence of Cs-137 radionuclides was detected by Carvalho et al. (2013). The blank samples (sand and seawater) were collected at Mambucaba Beach (point 6), which is located 9 km southeast of CNAAA. The coordinates were determined using a Map 276C Global Positioning System (GPS) instrument manufactured by Garmin.

For sampling of the sand profiles, two iron cylindrical collectors were built, each with a transparent acrylic tube placed in its interior, similar to those used in previous studies (IAEA, 1989, 2003; Boyd, 1995; Boyd & Tucker, 1998). The sampling depth was about 20 cm at points 1 and 2 (next to the discharge point), 40 cm at points 3 and 4, and 60 cm at points 5 and 6.

The sand samples were collected in the recreation area in a location between the high and low tide, but where the water from the waves was always in contact with the sand. A circular sampling design was used, based on one central sample with eight further samples collected at a radius of 30 cm from the central sample, simulating a compass. About 5 kg of sand was collected, drained by gravity for 6 h, dried at 105 ℃ until a constant weight was reached, and stored in Marinelli beakers. The samples were subsequently sealed, stored under refrigeration, and analyzed by gamma spectrometry (IAEA, 2003; Vianna et al., 1995; Michael, 1998; Cunha & Fabra, 1995; Godoy et al., 2003; Cunha, Munita, Paiva, & Teixeira, 1993).

Table 1. Coordinates of sand and seawater* sampling points

Sampling points	Latitude	Longitude
Point 1	23 °00′42″ S	44 °26′46″ W
	23 °00′42″ S(*)	44 °26′46″ W(*)
Point 2	23 °00′41″ S	44 °26′45″ W
	23 °00′41″ S(*)	44 °26′44″ W(*)
Point 3 - Piraquara Beach	23 °00′38″ S	44 °26′41″ W
	23 °00′38″ S(*)	44 °26′40″ W(*)
Point 4 - Piraquara Beach	23 °00′33″ S	44 °26′40″ W
	23 °00′33″ S(*)	44 °26′39″ W(*)
Point 5 - Velho Beach	23 °01′12″ S	44 °26′26″ W
	23 °01′12″ S(*)	44 °26′25″ W(*)
Point 6 - Mambucaba Beach (blank samples)	23 °01′40″ S	44 °31′56″ W
	23 °01′42″ S(*)	44 °31′56″ W(*)

2.3 Chemical characterization

Chemical analyses were carried out in the laboratories of the Center for Mineral Technology (CETEM). Granulometric curves were constructed for each point according to the classification of the Brazilian Technical Standards Association (ABNT, 1995) and Vargas (1977) for identification of the sand profiles (Figure 3).

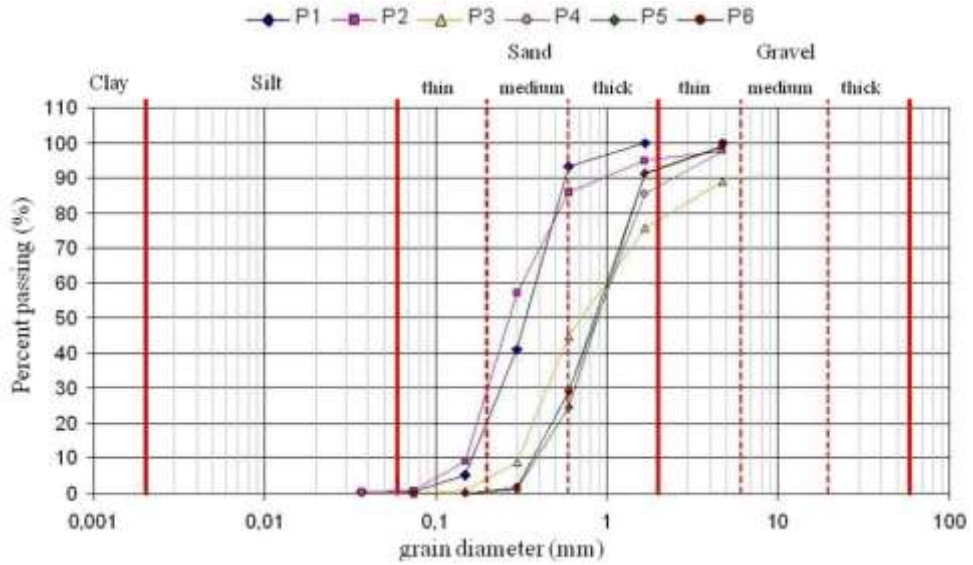

Figure 3. Granulometric curves for sampling points 1–6

The techniques employed for the elemental quantitative chemical analyses were: gravimetry for SiO_2 and ash; flame atomic absorption using acetylene/nitrous oxide for CaO, MgO, TiO_2, and Al_2O_3; flame atomic absorption using acetylene/air for Na_2O, K_2O, MnO, and Fe_2O_3. The measurements were performed in triplicate, and the results are presented in Table 2.

Table 2. Chemical characterization of sand samples from points 1–6

Parameters (%)	Point 1	Point 2	Point 3	Point 4	Point 5	Point 6
SiO_2	73.8	68.0	82.0	86.7	94.0	95.0
CaO	0.34	0.37	1.4	1.3	0.12	0.10
MgO	0.60	0.61	0.38	0.25	0.09	0.09
Na_2O	0.65	0.66	0.61	0.38	0.30	0.31
K_2O	1.6	1.5	1.4	1.3	0.70	0.64
TiO_2	3.9	4.3	0.81	0.35	0.20	0.18
MnO	0.14	0.19	441 $mg \cdot kg^{-1}$	185 $mg \cdot kg^{-1}$	66.8 $mg \cdot kg^{-1}$	40.2 $mg \cdot kg^{-1}$
Al_2O_3	4.9	4.3	4.2	3.5	2.1	2.0
Fe_2O_3	11.7	18.8	3.9	1.0	0.55	0.15
ash	0.94	0.86	2.0	1.7	0.53	0.33

X-ray diffraction (XRD) analysis of each sample was also performed at the laboratories of the CETEM, to complement the chemical profiling of the sand samples. The diffractograms obtained for points 1–5 are presented in Figures 4–8, respectively. The XRD powder diffractograms were obtained using a Bruker-D4 Endeavor system. The qualitative interpretation of the spectra was performed by a comparison with standards using the Bruker DiffracPlus software. The XRD results are discussed in section 3.2.

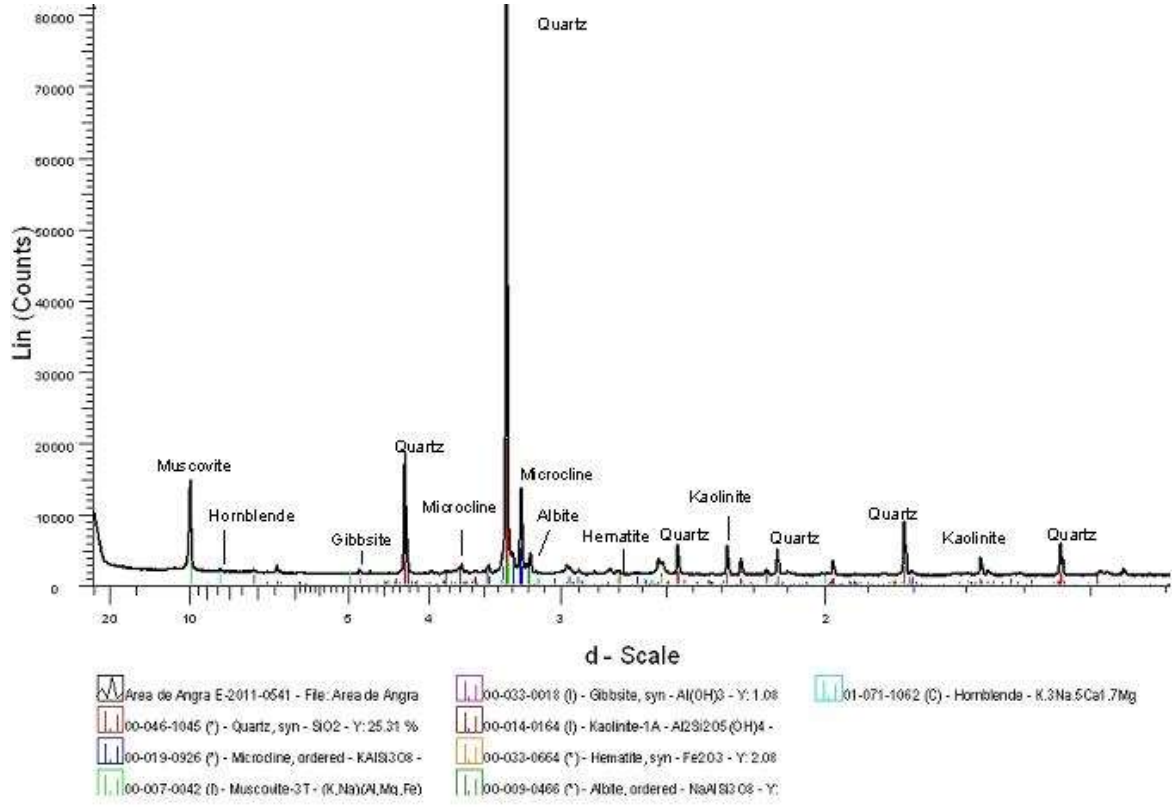

Figure 4. X-ray diffractogram of the point 1 sample

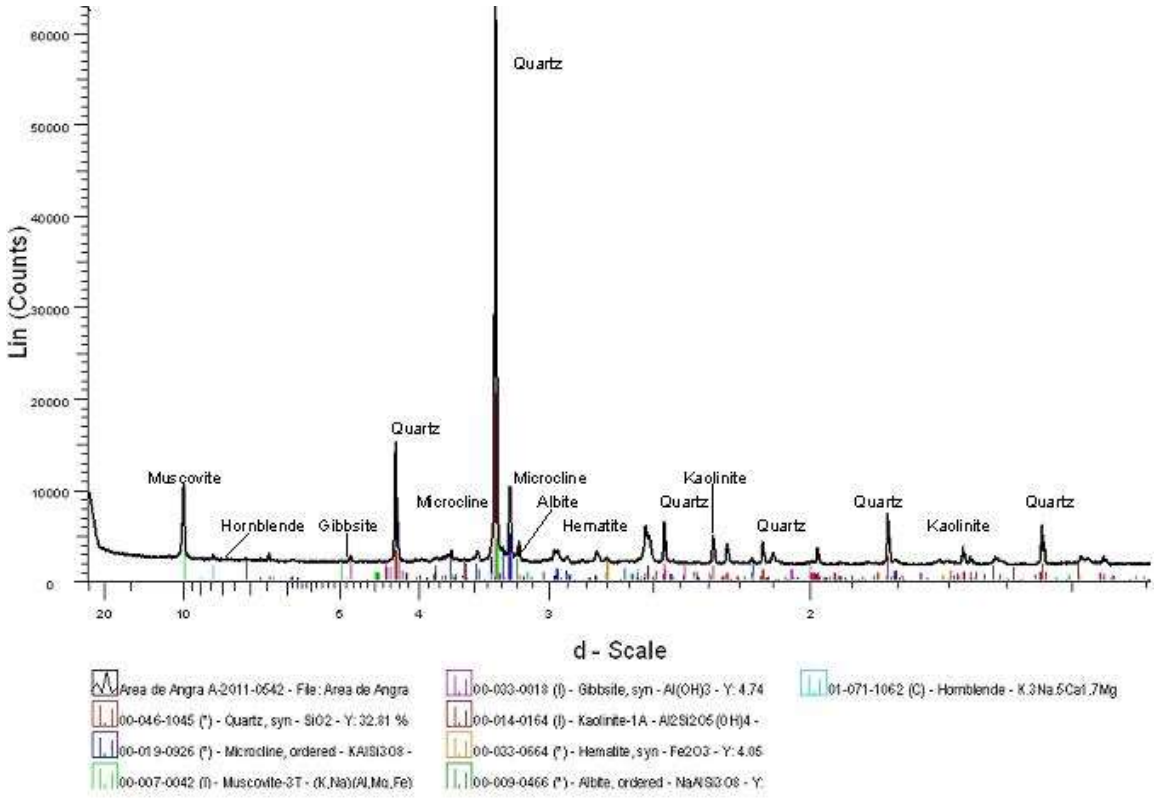

Figure 5. X-ray diffractogram of the point 2 sample

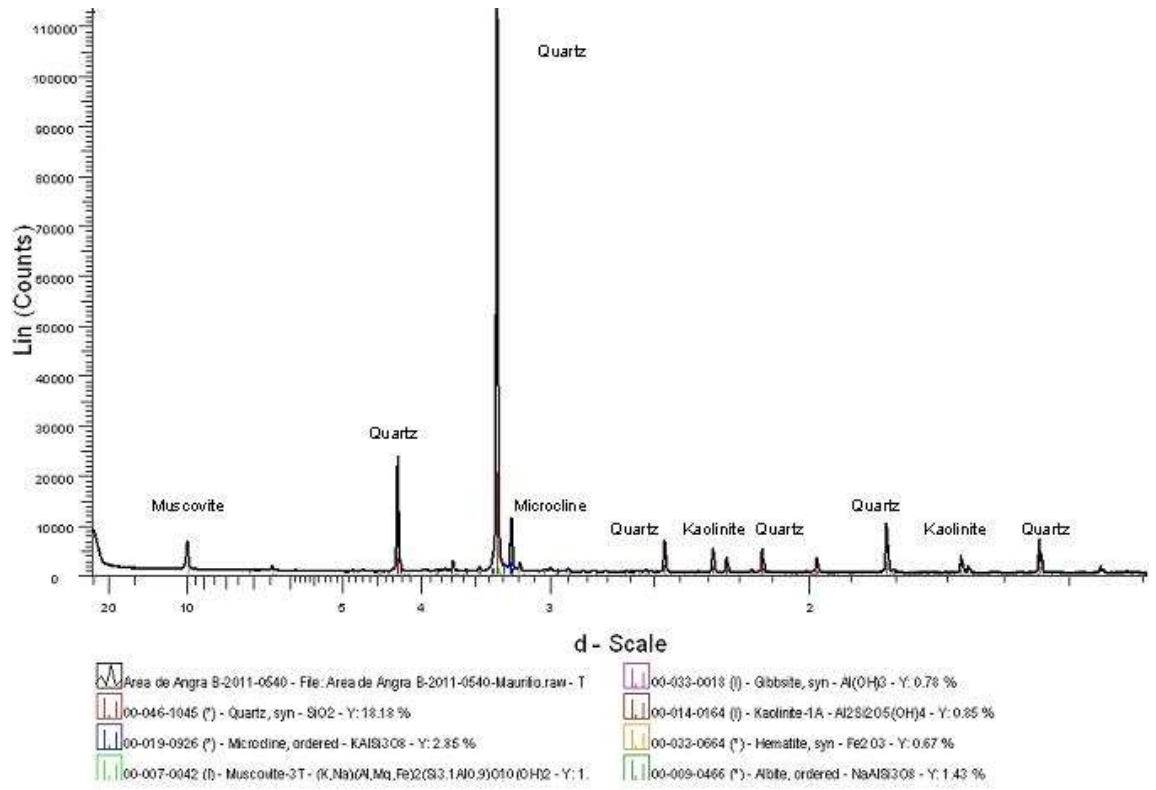

Figure 6. X-ray diffractogram of the point 3 sample

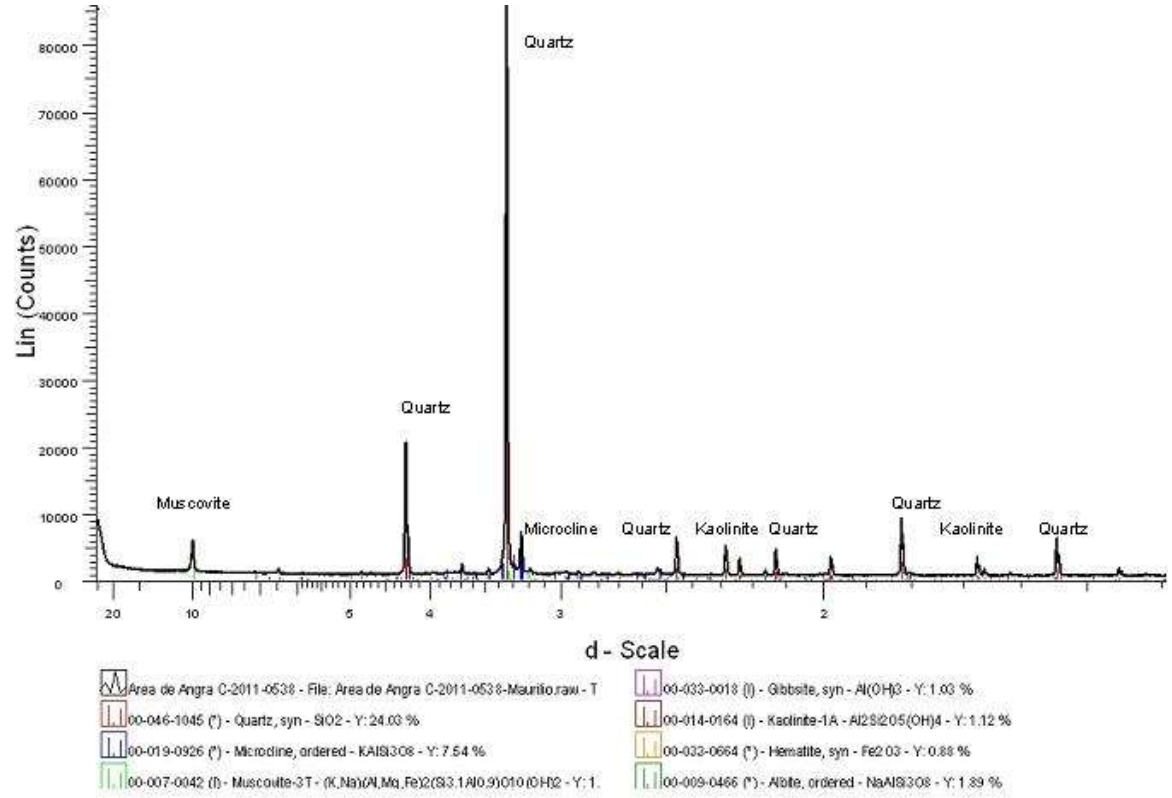

Figure 7. X-ray diffractogram of the point 4 sample

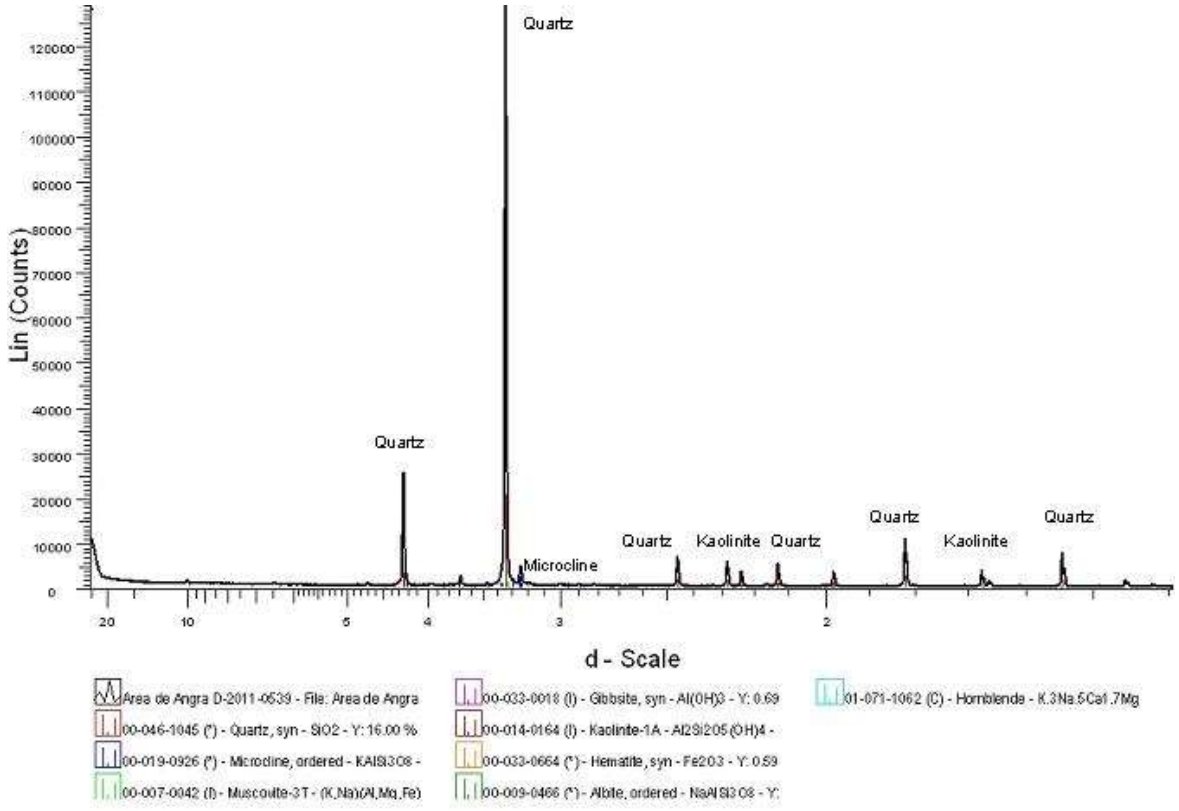

Figure 8. X-ray diffractogram of the point 5 sample

2.4 Gamma Spectrometry Analysis

The radiochemical analyses were performed in the ETN laboratory that regularly participates in inter-laboratory exercises promoted by the CNEN. Gamma spectrometry was used for direct analysis of the sand samples. Two methods were used for gamma spectrometry analysis of the seawater samples: direct analysis and analysis of the precipitate resulting from adsorption of the Cs-137 radionuclide by ammonium phosphomolybdate (APM).

Method 1: About 5 L of seawater was collected from the surface, filtered with a 0.45 mm filter, and placed in polyethylene bottles. These samples were transferred to Marinelli beakers, sealed, and stored under refrigeration until the radiochemical analysis was performed (IAEA, 2003; Vianna et al., 1995; Michael, 1998; Cunha & Fabra, 1995; Godoy et al., 2003; Cunha et al., 1993).

Method 2: About 20 L of seawater was collected from the surface, filtered with a 0.45 mm filter, and the pH was adjusted to 1.6 using nitric acid. Cesium chloride P.A. (0.26 g) was added, and the liquid was agitated for 10 min. Subsequently, APM (4.0 g) was added, the liquid was agitated for 1 h, and then left to rest for 24 h. The sample was then filtered with a 0.45 mm filter and washed with a 1% nitric acid solution. After drying at 60–70 ℃ for 48 h, the filters were counted for 60 000 s using the same geometry as the certified standard (Nyarko et al., 2011; Buesseler, Aoyama, & Fukasawa, 2011; Honda et al., 2012; Aoyama, Tsumune, Uematsu, Kondo, & Hamajima, 2012; Kaeriyama et al., 2013; Cunha, Figueira, & Saito, 1999; Aoyama, Hirose, Miyao, & Igarashi, 2000; Figueira, Saraiva, & Cunha, 2001; Inoue et al., 2012). The recovery of added cesium was around 98%.

The gamma-ray spectrometer was equipped with a high purity germanium detector. This system has a 20% relative efficiency and an energy resolution of 1.8 keV for the Co-60 radionuclide at the reference energy of 1.33 MeV. The coaxial germanium detector was mounted vertically and coupled to a digital 3 keV high voltage source. The detector was placed inside a thick lead shielding with an inner layer of cast copper to reduce background radiation. The output signal of the detector was directed to a computer equipped with a Model 9660 multichannel analyzer (Canberra). The Genie-2000 software package from Canberra was used for data acquisition, and in the scanning and nuclide identification modules. The system was calibrated for energy and efficiency in the same geometry as that of the samples. The energy calibration was performed using a certified calibration source with known energies: Co-60, $E\gamma = 1332.5$ keV and Cs-137, $E\gamma = 661.6$ keV. The energy efficiency of the detector was determined using a standard cocktail made by Eckert & Ziegler Analytics, traceable by the National Institute of Standards and Technology (NIST) in the same geometry as that of the samples.

The Marinelli beakers containing the samples (sand and seawater) were placed in direct contact with the detector. Each sample was counted for 60 000 s. The decays were corrected to July 2012 for both the sand and seawater samples. Measurements were also carried out with an empty Marinelli beaker, under identical conditions, to determine the background count. The background count was subtracted from each sample measurement to obtain the actual activity of the radionuclides.

To obtain gamma spectrometry measurements for the Cs-137 radionuclide adsorbed by APM, the seawater samples were filtered using a filter of the same dimensions as the standard filter cocktail of radionuclides manufactured by Eckert & Ziegler Analytics. The concentration of the Cs-137 radionuclide was measured directly at 661.6 keV (Vianna et al., 1995; Cunha & Fabra, 1995; Buesseler et al., 2011; Honda et al., 2012; Aoyama et al., 2000, 2012; Kaeriyama et al., 2013; Figueira et al., 2001; Inoue et al., 2012; da Silveira, Schmidt, Campos, de Godoi, & Ikeda, 2000).

3. Results and Discussion

3.1 Sampling

We observed that the mixture of soils from the landslide affected the sampling locations differently, because the points that did not experience effects from the landslide had greater depth values in the sampling. The new composition of the beach sand, especially in points 1 and 2, generated greater resistance to the entrance of the profile sampler at the collection points. The points that were moderately or weakly affected by the landslide, points 3 and 4, had greater depth with the profile sampler compared with points 1 and 2. The results of the elemental analysis (Table 2) are in agreement with this view, as higher concentrations of Fe_2O_3, TiO_2, and Al_2O_3 were observed in points 1 and 2, which were most affected by the landslide (see Section 3.2).

3.2 Chemical Analyses

The granulometric curves (Figure 3) show that there is little difference in the sample composition at points 1 and 2. These locations were mostly composed of particles smaller than 0.04 mm, i.e., silt(0.6 and 0.8%, respectively), whereas points 3–6 were mostly fine granulated sand according to the ABNT 6502/95 standard (ABNT, 1995) and Vargas (1977). Figure 2 shows that the landslide occurred predominately in the area where points 1 and 2 are

located; this explains the differentiated composition observed (Table 2) and the different grain sizes observed (Figure 3). Using this reasoning, points 3 and 4 were moderately affected by the landslide; compared with points 1 and 2, points 3 and 4 have a higher concentration of SiO_2 and a similar concentration of Al_2O_3, whereas the highest concentration of CaO is observed for points 3 and 4 (Table 2). Points 5 and 6 have similar compositions and are characterized by a reduction in Fe_2O_3 concentration when compared with the other points.

The chemical characterization of the samples (Table 2), supported by the granulometric curves, shows the differences in the chemical compositions of the samples collected at the different points. The XRD analyses of points 1 and 2 (Figures 4 and 5, respectively) complement these experiments, as the presence of phyllosilicate minerals is observed. These minerals, such as microcline, muscovite, gibbsite, kaolinite, hematite, albite, and hornblende, are Cs^+ cation exchangers. The XRD analyses of points 3 and 4 (Figures 6 and 7, respectively) also show the presence of microcline, muscovite, gibbsite, kaolinite, hematite, albite, and hornblende, but with lower intensities. This result confirms that the main area affected by the landslide was where points 1 and 2 are located. The XRD analysis of point 5 (Figure 8) shows the predominant presence of quartz, with an insignificant presence of phyllosilicates, which indicates that the beach sand at this point is less prone to contamination by the Cs-137 radionuclide.

3.3 Cs-137 Gamma Spectrometry Analysis

The measured concentration of the Cs-137 radionuclide in the seawater samples for all sampled points by both methods (<0.42 $Bq \cdot L^{-1}$ for direct analysis by gamma spectrometry and <0.004 $Bq \cdot L^{-1}$ for analysis using pre-concentration with APM) was below the minimum detectable activity (MDA) values for gamma spectrometry analysis. The measured concentration of the Cs-137 radionuclide in the sand for all sampled points was below the MDA value of 0.31 $Bq \cdot kg^{-1}$.

The amount of radionuclides from nuclear tests, nuclear accidents, effluents from nuclear fuel reprocessing plants and nuclear power plants, and nuclear weapons detonations are linked to fallout and ocean currents and have distinctive values around the world (Table 3). A factor that could have contributed to the low concentrations of Cs-137 found in this study is the dilution effect that occurs when creeks, streams, and rivers, which are commonly present in the southern region of the State of Rio de Janeiro, are present next to coastal waters.

Table 3. Cs-137 radionuclide activity in seawater from Piraquara Beach and other regions in Brazil and the world

Region	Reference	Cs-137 ($Bq \cdot m^{-3}$)
Brazilian Coast	Figueira & Cunha, 1998	1.4
Brazilian Southeastern Shelf	Godoy et al., 2003	0.9–4.0
São Paulo Coast (Brazil)	Cunha et al., 1993	1.7–1.9
Whole Brazilian Coast	Cunha et al., 1999	0.8–1.7
Brazilian Southern Coast	Figueira et al., 2001	1.0–4.7
Around the Japanese archipelago	Inoue et al., 2012	0.93–52.53
Mediterranean Sea	IAEA, 1995	5.0–11.8
Northeastern Atlantic	IAEA, 1995	2.8–125
Pacific Ocean	IAEA, 2005	1.4–2.0[1]
South and Southeastern Atlantic	IAEA, 2005	1.4
Piraquara Beach (PB)	This study*	<4.0
Small stretch of beach next to the CNAAA discharge point	This study*	<4.0
Velho Beach	This study*	<4.0

* results from the methodology using ammonium phosphomolybdate (APM)

With respect to the results presented in Table 3, it is important to note that the seawater samples were collected in the open sea, far from the coast, where there is significant mixing with ocean currents along the Brazilian coast. The position of the southern coast of Rio de Janeiro, in relation to marine currents, is somewhat north of the region of convergence of two major ocean currents (the warm Brazil current and the cold Falklands current), and this region is not influenced by the northern hemisphere ocean currents (da Silveira et al., 2000). Lower values are detected for the Cs-137 radionuclide along the coast of Brazil (Table 3) because accidents, nuclear testing, and the discharge of radioactive waste in the oceans are more concentrated in the northern hemisphere, according to reports from the IAEA (IAEA, 1995, 1999, 2001, 2004).

This study comprised sampling of water in bathing beaches and recreational areas. The current created by the discharge of effluents and cooling water in the opposite direction of the waves creates a resistance to the arrival of waves on the sands of PB. This fact retards the dispersion of the Cs-137 radionuclide and promotes its deposition on the beach sands next to the CNAAA discharge point. Thus, it can be assumed that the values

determined at these sampling points were not affected by the influence of the concentration of the Cs-137 radionuclide in the oceanic currents.

The importance of correlating the values of Cs-137 found in the sand with the radiation to which humans will be exposed was highlighted in Section 1.1. However, such a correlation can only be validated by calculating the amount of radiation to which the public is exposed (Alencar & Freitas, 2005; Freitas & Alencar, 2004; UNESCAR, 1988, 2000). The calculation of the radioactive dose exposure to the public at PB is important to verify the proper functioning of the CNAAA liquid effluent discharge. However, this study shows that the Cs-137 radionuclide values found are below the MDA values and are within the limit of release for effluents, which is 37 $Bq \cdot L^{-1}$, recommended by NRC-USA for the Cs-137 radionuclide (Wahlberg & Fishman, 1962). Therefore, the values obtained in this study are not harmful to the public. This data is important to local beachgoers and to the general population.

4. Conclusion

The measurements of the Cs-137 radionuclide in sand samples from PB, the small stretch of sand used as a beach next to the discharge point, and Mambucaba and Velho Beaches confirm that these locations do not contain detectable radioactive contamination by the Cs-137 radionuclide. Granulometric and chemical composition analyses showed that the landslide at PB introduced minerals composed of phyllosilicates, which are known as Cs^{+} cation exchangers, into the sand composition, especially close to the discharge point of effluents from CNAAA (points 1 and 2). However, the amount of phyllosilicates found in the beach sands was not enough to adsorb significant amounts of the Cs-137 radionuclide. The profile samples show that migration of the Cs-137 radionuclide did not occur to the deeper layers that were sampled because all the results were below the MDA values. The values of Cs-137 found in the seawater samples were similar to those found by other researchers who conducted studies in Brazilian waters at points farther away from the coast, where a dilution effect by ocean currents is present.

The values of the Cs-137 radionuclide measured in the samples collected in this study were below the MDA values and did not allow the radiation dose exposure of the public to be calculated. Therefore, we conclude that the beaches studied do not contain detectable amounts of the Cs-137 radionuclide. Thus, the public can enjoy the peace, tranquility, and beauty of these locations without the risk of exposure to the Cs-137 radionuclide. Conversely, we must increase our concern and radiochemical monitoring of oceans to acquire further knowledge about the extent of the effects along the Brazilian coast from the Fukushima radioactive accident. This incident compels us to continue with new radiological monitoring studies because of the large quantity of radionuclides being released into the atmosphere, seas, and oceans.

Acknowledgments

The authors express their thanks to Eletrobrás Termonuclear S.A.—ELETRONUCLEAR for supporting this study and granting permission for the spectrometric analyses performed in the Laboratory at Angra 2 Nuclear Power Plant. We would also like to thank the CETEM for performing the granulometric analysis, elementary chemical composition, and XRD analysis.

References

Aarkrog, A. (2003). Input of anthropogenic radionuclides into the World Ocean. *Deep-Sea Research Part II: Topical Studies in Oceanography, 50*, 2597-2603. http://dx.doi.org/10.1016/S0967-0645(03)00137-1

Agency for Toxic Substances and Disease Registry. (2004, April). Department of Health and Human Services, *Public Health Statement, Cesium*, CAS#: 7440-46-20. Retrieved January 2, 2012, from http://www.atsdr.cdc.gov/phs/phs.asp?id=575&tid=107

Alencar, A. S., & Freitas, A. C. (2005). Reference levels of natural radioactivity for the beach sands in a Brazilian southeastern coastal region. *Radiation Measurements*, *40*, 76-83. http://dx.doi.org/10.1016/j.radmeas.2004.08.003

Aoyama, M., Hirose, K., Miyao, T., & Igarashi, Y. (2000). Low level ^{137}Cs measurements in deep seawater samples. *Applied Radiation and Isotopes*, *53*, 159-62. http://dx.doi.org/10.1016/S0969-8043(00)00128-7

Aoyama, M., Tsumune, D., Uematsu, M., Kondo, F., & Hamajima, Y. (2012). Temporal variation of ^{134}Cs and ^{137}Cs activities in surface water at stations along the coastline near the Fukushima Dai-ichi Nuclear Power Plant accident site, Japan. *Geochemical Journal*, *46*, 321-325. http://dx.doi.org/10.2343/geochemj.2.0211

Bostick, B. C., Vairavamurthy, M. A., Karthikeyan, K. G., & Chorover, J. (2002). Cesium adsorption on clay minerals: An EXAFS spectroscopic investigation. *Environmental Science & Technology*, *36*, 2670-2676. http://dx.doi.org/10.1021/es0156892

Boyd, C. E. (1995). *Bottom soils, sediment, and pond aquaculture*. New York, NY: Chapman and Hall.

Boyd, C. E., & Tucker, C. S. (1998). *Pond aquaculture water quality management*. Boston: Kluwer Academic Publishers.

Brazilian Technical Standards Association. (1995). *Rochas e Solos–Terminologia, Technical Standard, ABNT-NBR 6502/95 Brazil*. Retrieved May 11, 2012, from https://intranet.ifs.ifsuldeminas.edu.br/~eder.clementino/GEST%C3%83O%20AMBIENTAL/LEGISLA%C3%87%C3%83O%20AMBIENTAL/NORMAS%20BRASILEIRAS%20REGULAMENTADORAS/NBR/NBR%2006502%20-%201995%20-%20Rochas%20e%20Solos.pdf

Buesseler, K, Aoyama, M., & Fukasawa, M. (2011). Impacts of the Fukushima Nuclear Power Plants on marine radioactivity. *Environmental Science & Technology, 45*, 9931-9935. http://dx.doi.org/10.1021/es202816c

Carvalho, F. M., Ferreira, I. M., Azevedo, I. M. A., Martins, N. S. F., & Lauria, D. D. (2013). Sorção de ^{60}Co e ^{137}Cs em sedimentos do Saco da Piraquara de Fora – Angra dos Reis. *IX Latin American IRPA Regional Congress on Radiation Protection and Safety – IRPA 2013*. Rio de Janeiro, Brazil. Retrieved August 21, 2013, from http://www.sbpr.org.br/irpa13/AnaisdoIRPA2013/Radioprotecciondelpacientetrabajadoresmiembros delpublicoymedioambiente/3523.pdf

Chowdhury, M.I., Kamal, M., Alam, M. N., Aftabuddin, S., & Zafar, M. (2004). Environmental radioactivity of the St. Martin's island of Bangladesh. *Radioprotection, 39*, 13-21. http://dx.doi.org/10.1051/radiopro:2003018

Collins, K. E., Jardim, I. C. S. F., & Collins, C. H. (1988). O que é Césio-137? *Química Nova, 11*, 169-178.

Cunha, I. I. L., Munita, C. S., Paiva, R. P., & Teixeira, A. (1993). Levels of cesium-137 in seawater and fish from the Brazilian coast. *Science of The Total Environment, 139-140*, 431-435. http://dx.doi.org/10.1016/0048-9697(93)90040-D

Cunha, I. I. L., & Fabra, E. L. (1995). ^{137}Cs radioactivity data in Brazil. *Fresenius Environmental Bulletin, 4*, 19-24.

Cunha, I. I. L., Figueira, R. C. L., & Saito, R. T. (1999). Application of radiochemical methods and dispersion model in the study of environmental pollution in Brazil. *Journal of Radioanalytical and Nuclear Chemistry, 239*, 477-82. http://dx.doi.org/10.1007/BF02349054

da Silveira, I. C. A., Schmidt, A. C. K., Campos, E. J. D., de Godoi, S. S., & Ikeda, Y. (2000). Corrente do Brasil ao largo da Costa Leste Brasileira. *Revista Brasileira de Oceanografia, 48*, 171-183. http://dx.doi.org/10.1590/S1413-77392000000200008

Dion, H. M.; Romanek, C. S., Hinton, T. G.; Bertsch, P. M. (2005). Cesium-137 in floodplain sediments of the Lower Three Runs Creek on the DOE Savannah River Site. *Journal of Radioanalytical and Nuclear Chemistry, 264*, 481-488. http://dx.doi.org/ 10.1007/s10967-005-0741-6

Eletrobras Termonuclear S.A.—ELETRONUCLEAR. *Estudo do Impacto Ambiental da Unidade 3 da Central Nuclear Almirante Álvaro Alberto, volume 2, item 6.5.3.4*. Retrieved December 11, 2013, from http://www.eletronuclear.gov.br/hotsites/eia/v02_06_diagnostico.html#6534

Environmental Protection Agency. (1999). *Understanding variation in partition coefficient, K_d, values. Volume II: Review of geochemistry and available K_d values for cadmium, cesium, chromium, lead, plutonium, radon, strontium, thorium, tritium (^{3}H), and uranium*. Appendix D; EPA, USA.

Figueira, R. C. L., & Cunha, I. I. L. (1998). A contaminação dos oceanos por radionuclídeos antropogênicos. *Química Nova, 21*, 73-77. http://dx.doi.org/10.1590/S0100-40421998000100012

Figueira, R. C. L., Saraiva, E. S. B. G., & Cunha, I. I. L. (2001). Simultaneous analysis of ^{137}Cs, ^{90}Sr, ^{238}Pu and $^{239+240}$Pu in Brazilian seawater. *Journal of Radioanalytical Nuclear Chemistry, 248*, 801-804. http://dx.doi.org/10.1023/A:1010673602722

Flury, M., Mathison, J. B., & Harsh, J. B. (2002). In situ mobilization of colloids and transport of cesium in Hanford sediments. *Environmental Science & Technology, 36*, 5335-5341. http://dx.doi.org/10.1021/es025638k

Flury, M., Czigány, S., Chen, G., & Harsh, J. B. (2004). Cesium migration in saturated silica sand and Hanford sediments as impacted by ionic strength. *Journal of Contaminant Hydrology, 71*, 111-126. http://dx.doi.org/10.1016/j.jconhyd.2003.09.005

Franklin, M. R., Rosman, P. C. C., & Fernandes, H. M. (2004). Modelling of the transport of ^{3}H and ^{137}Cs

released with the liquid effluents of Angra dos Reis Nuclear Power Plants into Ilha Grande Bay – Rio de Janeiro – Brazil. *Aquatic forum 2004: International conference on isotopes in environmental studies* (pp. 88-89). Monte Carlo.

Freitas, A. C., & Alencar, A. S. (2004). Gamma dose rates and distribution of natural radionuclides in sand beaches—Ilha Grande, Southeastern Brazil. *Journal of Environmental Radioactivity*, *75*, 211-223. http://dx.doi.org/10.1016/j.jenvrad.2004.01.002

Godoy, J. M., Carvalho, Z. L., da Costa Fernandes, F., Danelon, O. M., Ferreira, A. C. M., & Roldão, L. A. (2003). ^{137}Cs in marine samples from the Brazilian southeastern coastal region. *Journal of Environmental Radioactivity*, *70*, 193-98. http://dx.doi.org/10.1016/S0265-931X(03)00103-6

Haber, A. H., & Rothstein, B. E. (1969). Radiosensitivity and rate of cell division: "Law of Bergonié and Tribondeau". *Science*, *163*, 1338-1339. http://dx.doi.org/10.1126/science.163.3873.1338

Honda, M. C., Aono, T., Aoyama, M., Hamajima, Y., Kawakami, H., Kitamura, M., … Saino, T. (2012). Dispersion of artificial caesium-134 and -137 in the western North Pacific one month after the Fukushima accident. *Geochemical Journal*, *46*, e1-e9. http://dx.doi.org/10.2343/geochemj.1.0152

Inoue, M., Kofuji, H., Nagao, S., Yamamoto, M., Hamajima, Y., Fujimoto, K., … Minakawa, M. (2012). Low levels of ^{134}Cs and ^{137}Cs in surface seawaters around the Japanese Archipelago after the Fukushima Dai-ichi Nuclear Power Plant accident in 2011. *Geochemistry Journal*, *46*, 311-320. http://dx.doi.org/10.2343/geochemj.2.0218

International Atomic Energy Agency. (1988). *The Radiological Accident in Goiânia*. Retrieved January 10, 2012, from http://www.pub.iaea.org/books/iaeabooks/3684/The-Radiological-Accidente-in-Goinia

International Atomic Energy Agency. (1989). Measurement of radionuclides in food and the environment, *Technical Reports Series, 295*, Vienna.

International Atomic Energy Agency. (1995). Sources of radioactivity in the marine environment and their relative contributions to overall dose assessment from marine radioactivity (MARDOS). *IAEA TECDOC, 838*, Vienna.

International Atomic Energy Agency. (1999). Inventory of radioactive waste disposals at sea. *IAEA TECDOC, 1105*, Vienna.

International Atomic Energy Agency. (2001). Generic models for use in assessing the impact of discharges of radioactive substances to the environment. *Safety Report Series, 19*, Vienna.

International Atomic Energy Agency. (2003). Collection and preparation of bottom sediment samples for analysis of radionuclides and trace elements. *IAEA TECDOC, 1360*, Vienna.

International Atomic Energy Agency. (2004). Worldwide Marine Radioactivity Studies (WOMARS) Radionuclide levels in Oceans and Seas. *IAEA TECDOC, 1429*, Vienna.

International Atomic Energy Agency. (2011). *Fukushima Nuclear Accident Update Log*. Retrieved June 20, 2012, from http://www.iaea.org/newscenter/news/2011/fukushima200511.html

International Atomic Energy Agency. *INES*. Retrieved June 12, 2012, from http://www.iaea.org/Publications/Factsheets/English/ines.pdf

International Union of Radioecology. Retrieved June 6, 2012, from http://www.iur-uir.org/upload/fukushima-godoy_1_.pdf

Kaeriyama, H., Ambe, D., Shimizu, Y., Fujimoto, K., Ono, T., Yonezaki, S., … Watanabe, T. (2013). Direct observation of ^{134}Cs and ^{137}Cs in surface seawater in the western and central North Pacific after the Fukushima Dai-ichi nuclear power plant accident. *Biogeosciences*, *10*, 4287-4295. http://dx.doi.org/10.5194/bg-10-4287-2013

Kanai, Y., Saito, Y., Tamura, T., Nguyen, V. L., Ta, T. K. O., & Sato, A. (2013). Sediment erosion revealed by study of Cs isotopes derived from the Fukushima Dai-ichi nuclear power plant accident. *Geochemical Journal*, *47*, 79-82. http://dx.doi.org/10.2343/geochemj.2.0234

Komarneni, S. (1985). Phillipsite in Cs decontamination and immobilization. *Clays and Clay Minerals*, *33*, 145-151. http://dx.doi.org/10.1346/CCMN.1985.0330209

Lucca, E. V. D., Bandeira, J. V., Lorenzzetti, J. A., da Costa Moreira, R., de Castro, R. M., Salim, L. H., … Esposito, E. S. C. (2005). Uso de sensor hiperespectral aerotransportado no monitoramento da pluma termal oceânica decorrente da descarga de refrigeração da central nuclear de Angra dos Reis. *Revista Brasileira de Cartografia*, *50*, 48-55.

Lujanienė, G., Vilimaitė-Šilobritienė, B., & Jokšas, K. (2005). Accumulation of ^{137}Cs in bottom sediments of the Curonian Lagoon. *Nukleonika, 50*, 23-29.

McKinley, J. P., Zeissler, C. J., Zachara, J. M., Serne, R. J., Lindstrom, R. M., Schaef, H. T., & Orr, R. D. (2001). Distribution and retention of ^{137}Cs in sediments at the Hanford site, Washington. *Environmental Science & Technology, 35*, 3433-3441. http://dx.doi.org/10.1021/es0018116

McKinley, J. P., Zachara, J. M., Heald, S. M., Dohnalkova, A., Newville, M. G., & Suttom, S. R. (2004). Microscale distribution of cesium sorbed to biotite and muscovite, *Environ. Sci. Technol., 38*, 1017-1023.

Michael F. L. (1998). *Handbook of radioactivity analysis*. San Diego: Academic Press.

National Environment Council (2000). Revisa os critérios de Balneabilidade em Águas Brasileiras, no 274/2000. Brazil. Retrieved May 11, 2012, from http://www.mma.gov.br/port/conama/legiabre.cfm?codlegi=272

National Nuclear Energy Commission. (2005). *Diretrizes Básicas de Proteção Radiológica*. CNEN-NN-3.01. Retrieved February 21, 2012, from http://www.cnen.gov.br/seguranca/normas/pdf/Nrm301.pdf

National Nuclear Energy Commission. *Apostila educativa-Radiação Ionizante*. Retrieved May 11, 2012, from http://www.cnen.gov.br/ensino/apostilas/rad_ion.pdf

National Research Council. (1961). Atomic Energy Commission, National Academy of Sciences. *The Radiochemistry of Cesium*, NAS-NS 3035. Retrieved January 6, 2012, from http://www.radiochemistry.org/periodictable/pdf_books/pdf/rc000032.pdf

Nyarko, E., Botwe, B. O., Ansong, J. E., Delfanti, R., Barsanti, M., Schirone, A., & Delbono, I. (2011). Determination of ^{210}Pb, ^{226}Ra and ^{137}Cs in beach sands along the coastline of Ghana. *African Journal of Environmental Pollution and Health, 9*, 17-23.

Pilkey, O. H., Young, R. S., Riggs, S. R., Smith, A. W. S., Wu, H., & Pilkey, W. D. (1993). The concept of shoreface profile of equilibrium: A critical review. *Journal of Coastal Research, 9*, 255-278.

Rajec, P., Šucha, V., Eberl, D. D., Środoń, J., & Elsass, F. (1999). Effect of illite particle shape on cesium sorption. *Clays and Clay Minerals, 47*, 755-760. http://dx.doi.org/10.1346/CCMN.1999.0470610

Sawhney, B. L. (1970). Potassium and cesium ion selectivity in relation to clay mineral structure. *Clays and Clay Minerals, 18*, 47-52. http://dx.doi.org/10.1346/CCMN.1970.0180106

Suguio, K. (1992). In T. A. Queiroz (ed.), *Dicionário de Geologia Marinha*, São Paulo, Brazil.

Todorović, M., Milonjić, S. K., & Čomor, J. J. (1992). Adsorption of radioactive ions $^{137}Cs^{+}$, $^{85}Sr^{2+}$, and $^{60}Co^{2+}$ on natural magnetite and hematite. *Separation Science and Technology, 27*, 671-679. http://dx.doi.org/10.1080/01496399208018910

United Nations Scientific Committee on the Effects of Atomic Radiation. (1988). *Sources and effects of ionizing radiation*, New York.

United Nations Scientific Committee on the Effects of Atomic Radiation. (2000). *Sources and effects of ionizing radiation*, New York.

United Nations Scientific Committee on the Effects of Atomic Radiation. *The Chernobyl accident*. Retrieved June 6, 2012, from http://www.unscear.org/unscear/en/chernobyl.html

United States Nuclear Regulatory Commission. Retrieved July 10, 2013, from http://www.nrc.gov/reading-rm/doc-collections/cfr/part020/appb/Cesium-137.html

Vargas, M. (1977). *Introdução à Mecânica dos Solos*. São Paulo, Brazil: McGraw–Hill do Brasil.

Vianna, M. E., Tauhata, L., Oliveira, J. P., Oliveira, A. E., Garcia, L. C., da Conceição, C. S., & Clain, A. F. (1995). Quality of radionuclide analysis in environmental samples. *Science of The Total Environment, 173-174*, 15-18. http://dx.doi.org/10.1016/0048-9697(95)04745-X

Wahlberg, J. S., & Fishman, M. J. (1962). Adsorption of cesium on clay minerals. *USGS Bull 1140-A*, 771.

International Journal of Chemistry; Vol. 6, No. 4; 2014
ISSN 1916-9698 E-ISSN 1916-9701
Published by Canadian Center of Science and Education

Reviewer Acknowledgements

International Journal of Chemistry wishes to acknowledge the following individuals for their assistance with peer review of manuscripts for this issue. Their help and contributions in maintaining the quality of the journal is greatly appreciated.

Many authors, regardless of whether *International Journal of Chemistry* publishes their work, appreciate the helpful feedback provided by the reviewers.

Reviewers for Volume 6, Number 4

Adel F. Shoukry

Ahmad Galadima

Ahmad Sazali Hamzah

Ahmet Ozan Gezerman

Greg Peters

Haidong Huang

Hiren Chandrakant Mandalia

Jalal Isaad

Liang Yang

Maria Rambla-Alegre

Patricia Costa

R. K. Dey

Rabia Rehman

Rizvi Syed

Saroj Kumar Panda

Sudheer Chava

Valter Aragao do Nascimento

Weimin Chen

Albert John

On behalf of,

The Editorial Board of *International Journal of Chemistry*

Canadian Center of Science and Education

Call for Manuscripts

International Journal of Chemistry (IJC) is an international, double-blind peer-reviewed, open-access journal published by the Canadian Center of Science and Education. The journal focuses on the following topics: analytical, inorganic, organic, materials, nuclear and physical chemistry as well as neurochemistry and biochemistry. It provides an academic platform for professionals and researchers to contribute innovative work in the field. IJC carries original and full-length articles that reflect the latest research and developments in both theoretical and practical aspects of chemistry.

The journal is published in both print and online versions. The online version is free access and download.

We are seeking submissions for forthcoming issues. All manuscripts should be written in English. Manuscripts from 3000–8000 words in length are preferred. All manuscripts should be prepared in MS-Word format, and submitted online, or sent to: ijc@ccsenet.org

Paper Selection and Publishing Process

a) Upon receipt of a submission, the editor sends an e-mail of confirmation to the submission's author within one to three working days. If you fail to receive this confirmation, your submission e-mail may have been missed.

b) Peer review. We use a double-blind system for peer review; both reviewers' and authors' identities remain anonymous. The paper will be reviewed by at least two experts: one editorial staff member and at least one external reviewer. The review process may take two to three weeks.

c) Notification of the result of review by e-mail.

d) If the submission is accepted, the authors revise paper and pay the publication fee.

e) After publication, the corresponding author will receive two hard copies of the journal, free of charge. If you want to keep more copies, please contact the editor before making an order.

f) A PDF version of the journal is available for download on the journal's website, free of charge.

Requirements and Copyrights

Submission of an article implies that the work described has not been published previously (except in the form of an abstract or as part of a published lecture or academic thesis), that it is not under consideration for publication elsewhere, that its publication is approved by all authors and tacitly or explicitly by the authorities responsible where the work was carried out, and that, if accepted, the article will not be published elsewhere in the same form, in English or in any other language, without the written consent of the publisher. The editors reserve the right to edit or otherwise alter all contributions, but authors will receive proofs for approval before publication.

Copyrights for articles are retained by the authors, with first publication rights granted to the journal. The journal/publisher is not responsible for subsequent uses of the work. It is the author's responsibility to bring an infringement action if so desired by the author.

More Information

E-mail: ijc@ccsenet.org

Website: www.ccsenet.org/ijc

Paper Submission Guide: www.ccsenet.org/submission

Recruitment for Reviewers: www.ccsenet.org/reviewer

The journal is peer-reviewed
The journal is open-access to the full text
The journal is included in:

Bibliography and Index of Geology
CAS
DOAJ
EBSCOhost
Google Scholar
LOCKSS
JournalTOCs
Open J-Gate
PKP Open Archives Harvester
ProQuest
Standard Periodical Directory
Ulrich's
Universe Digital Library
WorldCat

International Journal of Chemistry
Quarterly

Publisher Canadian Center of Science and Education
Address 1120 Finch Avenue West, Suite 701-309, Toronto, ON., M3J 3H7, Canada
Telephone 1-416-642-2606
Fax 1-416-642-2608
E-mail ijc@ccsenet.org
Website www.ccsenet.org/ijc

ISSN 1916-9698